

NEUROMECHANICAL ACTIVITY OF THE WRIST MUSCLES DURING STABILIZATION TASKS

A Dissertation
Presented to
The Academic Faculty

by

Ellenor Janice Brown

In Partial Fulfillment
of the Requirements for the Degree
Doctor of Philosophy in the
School of Biological Sciences

Georgia Institute of Technology
December 2017

COPYRIGHT © 2017 BY ELLENOR JANICE BROWN

NEUROMECHANICAL ACTIVITY OF THE WRIST MUSCLES DURING STABILIZATION TASKS

Approved by:

Dr. Jun Ueda, Advisor
School of Mechanical Engineering
Georgia Institute of Technology

Dr. Boris Prilutsky
School of Biological Sciences
Georgia Institute of Technology

Dr. Minoru Shinohara, Co-Advisor
School of Biological Sciences
Georgia Institute of Technology

Dr. Lena Ting
Department of Biomedical Engineering
Georgia Institute of Technology
Emory University

Dr. Thomas Burkholder
School of Biological Sciences
Georgia Institute of Technology

Date Approved: August 25, 2017

ACKNOWLEDGEMENTS

I would like to thank my advisors and committee members for their continued guidance and encouragement throughout this PhD process. I would also like to thank the National Institutes of Health, the National Science Foundation, the Japan Society for the Promotion of Science, the Georgia Space Grant Consortium, and the School of Biological Sciences for funding me and my research. For this dissertation, I collected data from more than 60 subjects. I would like to thank them all for being so generous with their time and hanging out with a stranger in a strange laboratory while said stranger experimented on them for 3-5hrs. Last but certainly not least, I need to thank my family and friends for continuing to be whatever I need whenever I need it.

TABLE OF CONTENTS

ACKNOWLEDGEMENTS	iii
LIST OF TABLES	vii
LIST OF FIGURES	viii
LIST OF SYMBOLS AND ABBREVIATIONS	x
SUMMARY	xi
CHAPTER 1. Background	1
1.1 Introduction	1
1.2 Joint-Stabilizing Co-Contraction of Antagonist Muscles	3
1.3 Methods of Assessing Muscle Activation	3
1.4 Joint-Dependent Spinal Mechanisms	5
1.4.1 Reciprocal Inhibition	5
1.4.2 Recurrent Inhibition	6
1.5 Task-Dependent Control of Spinal Mechanisms	7
1.5.1 Reciprocal Inhibition	7
1.5.2 Recurrent Inhibition	9
1.6 Correlation of Cortical and Spinal Neural Oscillations	15
1.7 Specific Aims	22
1.7.1 Specific Aim 1	24
1.7.2 Specific Aim 2	25
1.7.3 Specific Aim 3	27
CHAPTER 2. Amplitudes of Muscle Mechanical Activity -- Automatic Analysis of Ultrasound Shear-wave Elastography in Skeletal Muscle Without Non-Contraction Tissue Contamination	29
2.1 Introduction	29
2.2 Methods	32
2.2.1 Subjects	32
2.2.2 Motor task	32
2.2.3 Ultrasound data recording	36
2.2.4 Data analysis	37
2.2.5 Image processing for NCT identification	38
2.2.6 Image processing for shear modulus assessment	43
2.2.7 Statistical analysis	45
2.3 Results	45
2.3.1 Algorithm Optimization	45
2.3.2 Spatial SD and mean of shear modulus	46
2.3.3 Depth-related distribution of NCT removal	47
2.3.4 Total area of NCT	48
2.3.5 Linearity of elastography with loading	49

2.3.6 Rank order of tasks	50
2.4 Discussion	51
2.4.1 Image processing algorithm	52
2.4.2 Elastography data	53
2.5 Conclusion	58
 CHAPTER 3. Effects of Vibration and Co-Contraction on Neuromotor Oscillations and Steady Muscle Activation	 60
3.1 Introduction	60
3.2 Methods	63
3.2.1 Subjects	63
3.2.2 Motor task	64
3.2.3 Vibration	67
3.2.4 Recordings	67
3.2.5 Data analysis	68
3.2.6 Statistical analysis	71
3.3 Results	72
3.3.1 EMG amplitudes during vibration	72
3.3.2 Beta-band oscillations and coherence	75
3.3.3 Effects of vibration and co-contraction on beta-band CMC	83
3.3.4 Beta-band oscillations and low-frequency oscillations in motor output	85
3.4 Discussion	85
3.4.1 Muscle activation level	86
3.4.2 Effects of vibration and co-contraction on beta-band CMC	88
3.4.3 Beta-band oscillations and low-frequency oscillations in motor output	90
3.5 Conclusion	92
 CHAPTER 4. Recurrent Inhibition in Multi-Axial Wrist Activity	 94
4.1 Introduction	94
4.2 Methods	96
4.2.1 Subjects	97
4.2.2 Motor tasks	97
4.2.3 Electrical Stimulation	98
4.2.4 Recordings	99
4.2.5 Data Analysis	100
4.3 Results and discussion	100
4.3.1 Experiment 1: Recurrent Inhibition during FCR-ECR Co-contraction	101
4.3.2 Experiment 2: Exclusion of H-reflex Influence	103
4.4 Conclusion	105
 CHAPTER 5. Discussion	 106
5.1 Integration	106
5.1.1 Implications for wrist stability	106
5.1.2 Beta-band CMC and Spinal Mechanisms	108
5.1.3 Beta-band neural oscillations and motor output	109
5.1.4 Contributions	110
5.2 Significance	111

5.3	Future Directions	113
CHAPTER 6.	Conclusion	115
REFERENCES		116

LIST OF TABLES

Table 1: A list of forces (F_x , F_y , F_z) and torques (M_x , M_y , M_z) applied by the robot for each loading condition.	35
Table 2: Effect of NCT removal on the linearity of muscle elasticity across linear loading conditions.....	50
Table 3: Total z-transformed total beta-band coherence for each subject	82
Table 4: Correlation coefficient between beta-band neuromotor oscillations and delta-band power in rectified EMG.	85

LIST OF FIGURES

Figure 1: Schematic of neural mechanisms controlling antagonist muscles	8
Figure 2: Schematic of neural mechanisms controlling recurrent inhibition.....	11
Figure 3: Schematic of intensity-dependent recurrent inhibition	12
Figure 4: Schematic of task-dependent mutual recurrent inhibition.....	15
Figure 5: Summary schematic model of dissertation.....	23
Figure 6: Aim 1 experimental arrangement	34
Figure 7: Aim 1 representative ultrasound elastography images.....	37
Figure 8: Aim 1 image processing algorithm	41
Figure 9: Aim 1 standard deviation and mean of shear modulus	48
Figure 10: Aim 1 distribution of NCT removal by depth.	49
Figure 11: Aim 1 histogram of task rank errors.....	51
Figure 12: Aim 2 representative recordings of EEG and EMG.....	69
Figure 13: Aim 2 representative FCR amplitude.....	73
Figure 14: Aim 2 mean EMG amplitude of FCR	74
Figure 15: Aim 2 mean EMG amplitude of ECR	75
Figure 16: Aim 2 representative FCR power, C3 power and CMC.....	76
Figure 17: Aim 2 representative FCR power at the peak frequency of CMC during vibration	77
Figure 18: Aim 2 representative C3 power at the peak frequency of CMC during vibration	78

Figure 19: Aim 2 representative CMC during vibration.....	79
Figure 20: Aim 2 representative FCR power at the peak frequency of CMC after vibration	80
Figure 21: Aim 2 representative C3 power at the peak frequency of CMC after vibration	81
Figure 22: Aim 2 representative CMC after vibration.....	82
Figure 23: Aim 2 total beta-band CMC for each subject.....	84
Figure 24: Aim 3 averaged stimulations of the median nerve during radial deviation..	102
Figure 25: Aim 3 recurrent inhibition during FCR-ECR co-activation tasks.....	103
Figure 26: Aim 3 recurrent inhibition at two stimulation intensities.....	105

LIST OF SYMBOLS AND ABBREVIATIONS

CMC	Corticomuscular Coherence
ECR	Extensor Carpi Radialis
ECU	Extensor Carpi Ulnaris
EEG	Electroencephalogram
EMG	Electromyogram
EOG	Electrooculogram
FCR	Flexor Carpi Radialis
H-reflex	Hoffman Reflex
IN	Interneuron
MVC	Maximum Voluntary Contraction
M-wave	Compound Muscle Action Potential
PAD	Primary Afferent Depolarization
RC	Renshaw Cell
TRI	Triceps Longus
USSWE	Ultrasound Shear-Wave Elastography

SUMMARY

Wrist joint stability is vital to hand function and thus overall upper limb function. The overarching goal of the study is to understand the neuromuscular control and mechanical properties of the wrist muscles for wrist stabilization. Aim 1 focuses on development of an analysis method for ultrasound elastography images toward estimating individual muscle force changes in a wrist muscle. The application of multiple forces and torques at the hand and the activity of several forearm muscles to maintain stability necessitated the development of a new method of capturing and analyzing individual muscle activity. Aim 2 focuses on neural oscillations and amplitudes of muscle activity during co-contraction (i.e. simultaneous contraction for joint stability) of a wrist flexor and extensor for wrist flexion-extension stabilization and when extra afferent input is applied to the muscles. Aim 3 addresses modulation of the amplitudes of motor output via recurrent inhibition during co-activation (i.e. simultaneous activation for movement, joint stability, etc.) of a wrist flexor and extensor muscle working as synergists or antagonists for wrist stabilization. The contributions of this dissertation include new insights into the spinal and cortical control of wrist stabilization and an analysis method for capturing the activity and mechanical properties of the wrist muscles during complex wrist stabilization.

CHAPTER 1. BACKGROUND

1.1 Introduction

Wrist joint stability is vital to hand function and overall upper limb function. A strategy for adjusting the stability of a joint is co-contraction of antagonist muscles. The overarching goals of this dissertation are to 1) understand the neural mechanisms of wrist stability, given the unique neural mechanisms involved, and 2) quantify the amplitudes and oscillations of wrist muscle neural and mechanical activity during wrist stabilization.

The neural mechanisms controlling motor output cause coordinated muscle activation and contractions. The most common way to measure muscle activation is through electromyography (EMG). EMG captures changes in the voltage of aggregate neural activity of a muscle via electrodes on the overlying skin or electrodes embedded into the muscle. However, both types of EMG have limitations that make it difficult to accurately measure the neural activity of wrist muscles. When multiple, small muscles are positioned close to each other and have redundant function (e.g. the muscles of the forearm) such that they cannot or will not be activated in isolation for a given task, surface EMG recordings over one muscle will be contaminated by “crosstalk” from the surrounding muscles. The use of intramuscular electrodes reduces crosstalk, but is invasive and limits the range of muscle activity allowed as the electrodes are dislodged by strong muscle contractions. For these reasons, alternative methods are needed to measure wrist muscle activity non-invasively with adequate spatial resolution. One such method is ultrasound elastography. The ultrasound image provides the spatial resolution needed to target superficial and deep muscles while elastography provides mechanical

data that correlates linearly with muscle force. The ability to measure muscle elasticity can also enhance the understanding of how individual muscle stiffness contributes to overall joint stiffness. In Aim 1, an improved method for analyzing muscle ultrasound shear-wave elastography (USSWE) is presented with application to data from a wrist muscle during stabilization of the wrist and proximal upper limb joints against complex loading.

After examining the mechanical properties related to muscle activation, the neural control of muscle activation amplitudes and oscillations are examined. For simpler wrist stability tasks (i.e. co-contraction without handgrip or complex loading), EMG is reintroduced for its ability to capture frequency and amplitude content or neural activity. The neural control of antagonistic wrist muscle activity is interesting due to the deviation from classical models of “true antagonist” intermuscular spinal mechanisms and coordinated muscle activity. “True antagonists,” such as the biceps and triceps brachii at the elbow and the tibialis anterior and soleus at the ankle, generate opposing torques about an axis of movement and the involved spinal mechanisms support antagonistic out-of-phase activity. However, the wrist has two defined axes of movement (i.e. flexion/extension and radial/ulnar deviation) about which pairs of muscles are controlled as antagonists or synergists depending on the movement. This flexibility in the muscles’ functional relationships is reflected in the involved spinal mechanisms. Aims 2 and 3 focus on the functional consequences of these unique spinal mechanisms during voluntary agonist contractions and co-contractions at the wrist in humans.

1.2 Joint-Stabilizing Co-Contraction of Antagonist Muscles

As mentioned above, co-contraction of antagonist muscles is a strategy for increasing joint stability. Co-contraction occurs naturally during interaction with unstable environments,^{1,2} the initial stages of motor learning³⁻⁵, anticipation of perturbations⁶, and utilization and modulation of afferent input that is compromised (e.g. during aging^{7,8}).

Several spinal mechanisms are involved in regulating how the activity and sensory feedback from one muscle influences other muscles. Between true antagonists, Ia afferent input to an agonist muscle causes both facilitation of the agonist and synergists and inhibition of antagonists through a spinal mechanism called reciprocal inhibition^{9,10}. Co-contraction presents a unique situation where both agonists and antagonists are intended to be active simultaneously, which makes spinal mechanisms that facilitate agonist activity and inhibit antagonist activity appear counterproductive. There is evidence that the control of neural mechanisms related to Ia afferent feedback differs between agonist contraction and co-contraction of true antagonists^{11,12}. However, there has been little attention paid to understanding how the control of these spinal mechanisms and related motor output is modified for co-contraction of muscles with flexible functional relationships such as those acting at the wrist.

1.3 Methods of Assessing Muscle Activation

EMG is a popular and accessible method for measuring muscle activity, is generally reliable, and has high sampling frequencies for spectral analysis and capturing short duration neural features. For these reasons, EMG was used to examine neural oscillations and amplitudes of the wrist muscles in this dissertation (Aims 2 and 3). However, EMG has limitations. Intramuscular EMG is prone to electrode displacement at higher contraction intensities while surface EMG is susceptible to cross-talk^{13,14}. It has been shown in previous studies that as muscle activation increases, muscle elasticity increases, thus coupling muscle activity with the mechanical properties of the muscle¹⁵⁻¹⁷. Therefore, muscle elasticity data can be used to monitor muscle activity. Muscle shear modulus measured with Ultrasound Shear-Wave Elastography (USSWE) is a recently established measure of muscle elasticity. USSWE measures the speed of soundwave propagation through the tissues to estimate shear modulus. This method appears to be advantageous in assessing mechanical activity of an individual muscle because it provides measurements with better spatial resolution and allows for direct assessment of mechanical properties.

The current method for analysis of USSWE videos to quantify muscle shear modulus is to calculate the spatial average of shear modulus across a manually selected region of interest in each frame, including connective tissues. As connective tissue stiffnesses are distinct from the stiffness of the surrounding muscle tissues, the inclusion of connective tissue areas in an image is expected to skew mean elasticity values for a given measurement. To assess the effect of connective tissue inclusion on comparisons of muscle activity, comparisons of muscle activity across several loading conditions are completed with and without connective tissue.

1.4 Joint-Dependent Spinal Mechanisms

The spinal mechanisms influencing pairs of true antagonist muscles differ from those influencing flexor carpi radialis (FCR) and extensor carpi radialis (ECR) at the wrist.¹⁸⁻²⁰ FCR and ECR act as synergists for radial deviation and antagonists for flexion and extension. The spinal mechanisms of focus in this dissertation are reciprocal inhibition and recurrent inhibition.

1.4.1 Reciprocal Inhibition

Reciprocal inhibition refers to the inhibition of an antagonist muscle due to Ia afferent input from an agonist muscle. Stimulation of Ia afferents via electrical stimulation of a sensory nerve or as a downstream effect of stimulating muscle spindles via muscle stretch or tendon tap causes excitation of the homonymous alpha motor neuron (i.e. monosynaptic facilitation) and group I interneurons. Between true antagonists, the group I interneurons are Ia interneurons that synapse onto antagonist alpha motor neurons to complete a disynaptic inhibition pathway.^{9,10} Ia interneurons to the antagonist receive recurrent inhibition from the agonist.

The disynaptic inhibition between FCR and ECR at the wrist follows a similar pathway to between antagonists and has similar net effects for agonist contraction, but with some important changes. The most pertinent for this dissertation is that the involved interneurons may not be Ia interneurons. Ia interneurons are inhibited by Renshaw cells,

while the group I interneurons between FCR and ECR are not ¹⁹. The absence of this inhibition of group I interneurons may reduce the ability of spinal mechanisms to diminish antagonist inhibition when needed (e.g. during co-contraction of FCR and ECR).

1.4.2 Recurrent Inhibition

Recurrent inhibition refers to Renshaw cell mediated inhibition of the homonymous motor neurons and motor neurons of synergist muscles. Renshaw cells are activated by collaterals of alpha motor neurons and cause homonymous and heteronymous inhibition of synergists ²¹. This negative feedback loop is thought to regulate the gains of muscle activation²². For true antagonists, Renshaw cells inhibit both the homonymous motor neuron and Ia interneurons to the antagonist, thus disinhibiting the antagonist. In other words, Renshaw cell activity inhibits the agonist and causes relative facilitation of the antagonist, a pattern that is opposite to that of reciprocal inhibition.

At the wrist, recurrent inhibition does not influence group I interneurons between FCR and ECR ¹⁹. Instead, FCR and ECR share mutual recurrent inhibition²⁰, wherein the Renshaw cells activated by the alpha motor neurons of one muscle inhibit the motor neuron pools of both muscles, as is seen between synergist muscles at a joint ²¹ or between task-level synergists cross joints in the lower limb^{22,23}. Mutual recurrent inhibition is thought to allow for parallel control of gain across synergists. For FCR and ECR, mutual recurrent inhibition is expected to contribute to control of radial deviation.^{19,20}

1.5 Task-Dependent Control of Spinal Mechanisms

1.5.1 *Reciprocal Inhibition*

During voluntary co-contraction of true antagonistic pairs (Figure 1a), spinal reciprocal inhibition originating from Ia afferents of the antagonist and inhibiting the agonist is reduced or abolished relative to single agonist contraction¹¹. This maintains the excitability of both muscles. Mechanisms to reduce reciprocal inhibition include activation of Renshaw cells to inhibit Ia inhibitory interneurons directly^{19,24} (Figure 1a at 2) and presynaptic inhibition of Ia terminals onto Ia interneurons via excitation of primary afferent depolarization interneurons (PAD INs,^{12,25}; Figure 1a at 1). Due to this Renshaw cell configuration, reduction of presynaptic inhibition on Ia terminals synapsing onto antagonist motor neurons (relative to the relaxed state,¹²; Figure 1a at 3) causes both disinhibition of Ia afferent inputs that serve as positive feedback to the motor neuron and, indirectly, increased recurrent inhibition of Ia interneurons to the agonist. In other words, both monosynaptic facilitation and disinhibition of the opposing muscle occur, which still maintains the excitability of the muscles.

In the FCR and ECR pair (Figure 1b) that work as antagonists for flexion and extension of the wrist joint, Renshaw cell inhibition to group I inhibitory interneurons is absent^{19,20} (Figure 1b at 2), replaced by inhibitory connections to the agonist motor neuron (Figure 1b at 4). With mutual recurrent inhibition, increasing motor output of the antagonist directly inhibits agonist motor output. In this situation, lack of presynaptic inhibition of Ia terminals onto the antagonist motor neuron (Figure 1b at 3) facilitates the

antagonist while indirectly inhibiting the agonist via recurrent inhibition. It has been shown that presynaptic inhibition of this Ia pathway is controlled differently in the wrist than between antagonists at the ankle and is not altered between agonist contraction or co-contraction.^{18,26}

Figure 1: Neural mechanisms controlling motor output between true antagonist muscles (left) and between FCR and ECR (right). Between antagonists (left), Ia input from the antagonist muscle spindles sent via primary afferent neuron excite the antagonist motor neuron and group I interneurons. As a result, the antagonist is excited while the agonist is inhibited. To reduce inhibition of the agonist, the primary afferent depolarization interneuron is excited to cause presynaptic inhibition of the primary afferent neuron (1). The group I interneuron can also be directly inhibited by the Renshaw cell (2). Between FCR and ECR (right), presynaptic inhibition still occurs (1), but Renshaw cells from the antagonist (ECR) do not inhibit the group I interneurons to the agonist (FCR). Excitation is shown as open triangles, inhibition as closed circles. Connections that are absent in the depicted configuration but are present in the other configuration are shown as gray, dotted lines. Abbreviations: FCR = flexor carpi radialis; ECR = extensor carpi radialis; AG = agonist; ANT = antagonist; MN = motor neuron; RC = Renshaw cell; IN = interneuron; PAD = primary afferent depolarization.

With the modified configuration of recurrent inhibition, presynaptic inhibition of group I interneurons and motor neurons^{11,12,18} may not function large enough to abolish the Ia-originated inhibition during antagonist co-contraction of FCR and ECR. This would compromise the excitability of the co-contracted wrist muscles. Evidence suggests that reciprocal inhibition is reduced or abolished at the wrist¹¹. However, this evidence is limited by the number of subjects and methodology used.

1.5.2 Recurrent Inhibition

During simple contraction of one muscle in a pair of true antagonists (Figure 2a), agonist motor neuron collaterals excite Renshaw cells (Figure 2a-b at 6) and cause recurrent inhibition of the homonymous motor neuron (Figure 2a at 4) and of the IaIN to the antagonists (Figure 2a at 2). The former (Figure 2a at 4) causes direct inhibition of agonist motor neurons. The latter (Figure 2a at 2) causes relative facilitation of the antagonist by inhibiting the IaIN²⁷, and thus reduces IaIN inhibition of the antagonist (Figure 2a at 7). Increased activation of the agonist motor neurons should facilitate recurrent inhibition of the agonist and of the IaIN, thus causing reduction in antagonist inhibition (Figure 2a at 7), unless other neural input modulates Renshaw cell activity. However, the opposite is true – recurrent inhibition is proportionally diminished. This reduced recurrent inhibition is likely caused by inhibition of Renshaw cell activity via descending control (Figure 2a at 5²²). This intensity dependence is depicted in Figure 3.

In contrast to simple agonist contraction, increasing intensity of co-contraction showed no decreases in homonymous recurrent inhibition (Figure 2a at 4), likely due to

the lack of net inhibition of Renshaw cells via descending control (Figure 2a at 5²⁴). Greater Renshaw cell activity during co-contraction causes inhibition of IaIN (Figure 2a at 2), and thus disinhibition/facilitation of the antagonist muscle (Figure 2a at 7). This maintains excitability of the antagonist, which is beneficial for co-contraction of antagonist muscles. However, maintenance of the antagonist is accomplished at the expense of greater homonymous recurrent inhibition (Figure 2a at 4). Taken together, the control of Renshaw cells between antagonists favors antagonistic activity by reducing recurrent inhibition only during increasing agonist contraction, and serves as an indicator for the relationship between muscles within the current motor control scheme.

Between FCR and ECR, Renshaw cell activity works to inhibit/reduce the gain of both motor pools in parallel (Figure 2b at 3 and 4) and has no direct influence on group I non-reciprocal inhibition (Figure 2b at 2). In this configuration, recurrent inhibition has the same inhibitory effect on the homonymous motor pool as seen for true antagonists (Figure 2a and Figure 2b at 4), but the opposite effect on the antagonist motor pool (inhibition, Figure 2b at 3) compared with true antagonists (facilitation, Figure 2a at 2 and 7). Because of this, it is unclear how recurrent inhibition between synergistic wrist muscles will be controlled in comparison to known patterns of control in true antagonists across task intensities. When only one of the observed muscles is active in a pair of muscles with mutual recurrent inhibition, recurrent inhibition may not decrease with intensity, as this would disinhibit the inactive muscle. Instead, recurrent inhibition may only be reduced when both muscles are active and working as synergists, thus facilitating activity in both muscles.

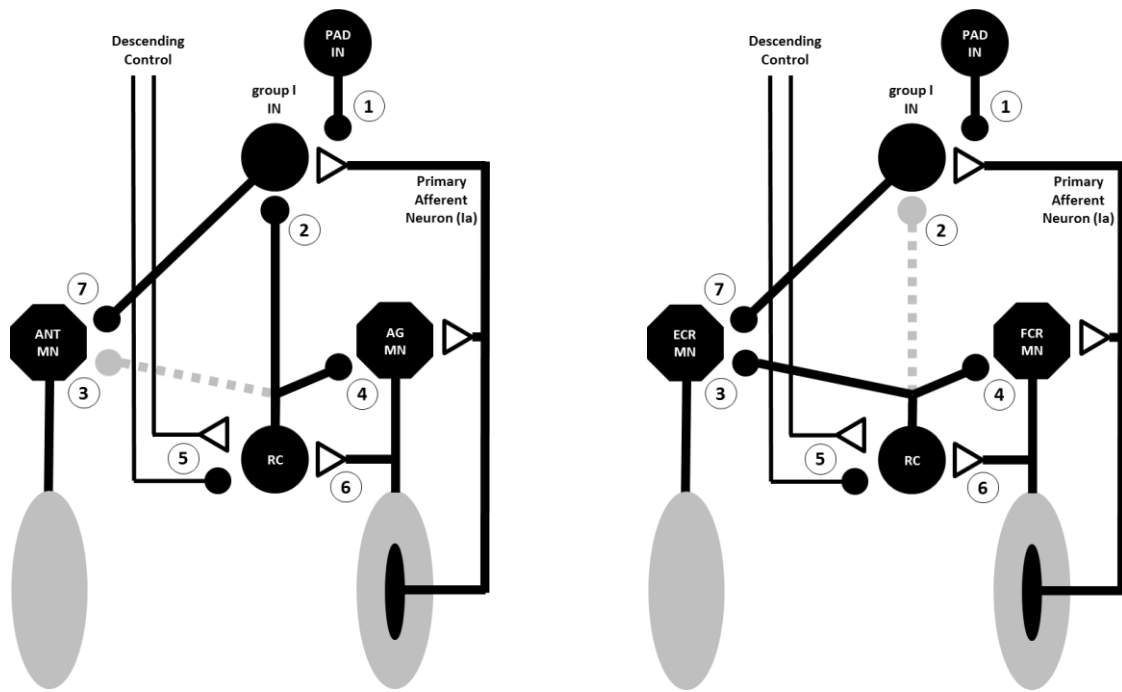


Figure 2: Neural mechanisms controlling recurrent inhibition impacting antagonist muscles (left) and FCR and ECR (right). For true antagonists (left), agonist-coupled Renshaw cells inhibit both the agonist (4) and group I inhibitory interneurons (2) to the antagonist. At the wrist, agonist-coupled Renshaw cells inhibit both the agonist (FCR at 4) and the antagonist (ECR at 3). The amount of Renshaw cell activity, or recurrent inhibition, in both configurations is regulated via descending control (5). Excitation is shown as open triangles, inhibition as closed circles. Connections that are absent in the depicted configuration but are present in the other configuration are shown as gray, dotted lines. Abbreviations: FCR = flexor carpi radialis; ECR = extensor carpi radialis; AG = agonist; ANT = antagonist; MN = motor neuron; RC = Renshaw cell; IN = interneuron; PAD = primary afferent depolarization. Note: AG/ANT switched from Figure 1.

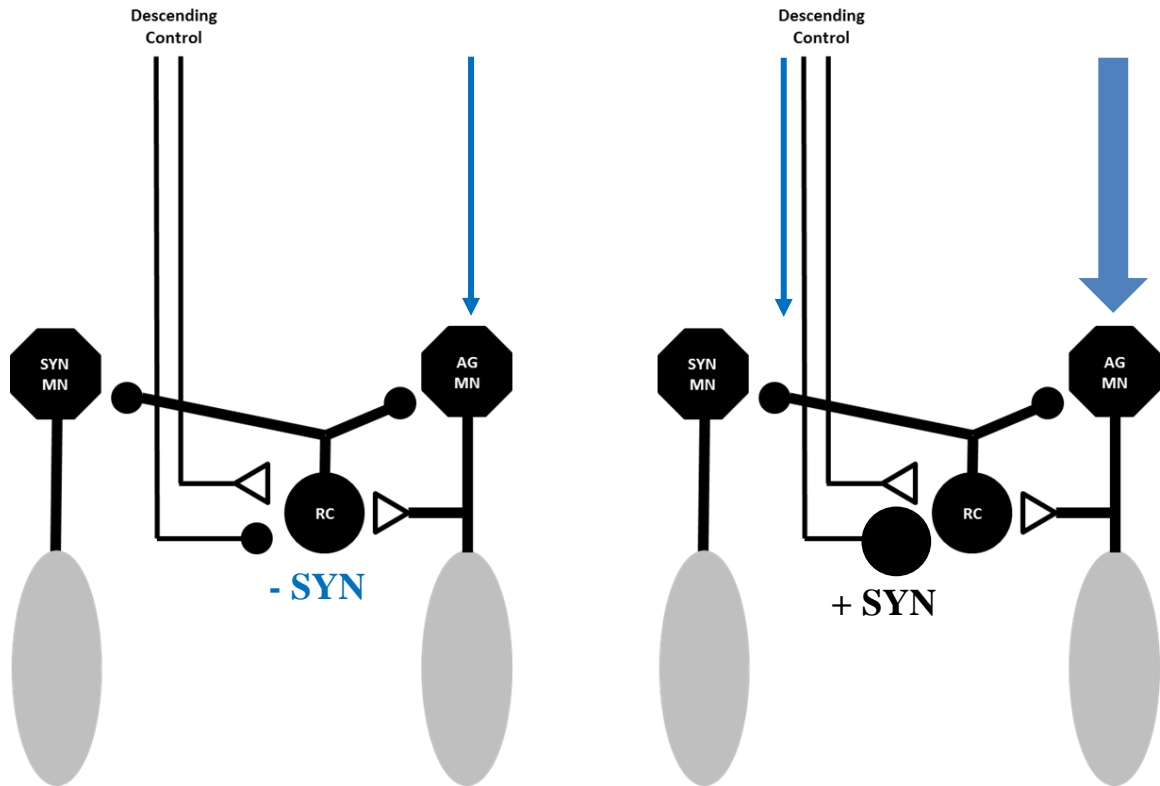


Figure 3: Intensity-dependent recurrent inhibition. Increased agonist activation causes relative decreased in recurrent inhibition, possibly due to centrally controlled inhibition of Renshaw cells. This would cause relative facilitation of agonist activity and synergist activity. Synergist activity via mutual inhibition is the focus of Aim 3.

During radial deviation, concurrent activation of both FCR and ECR is considered synergistic activity. However, when FCR and ECR are concurrently active during wrist stabilization, they have traditionally been treated only as antagonists in a flexion/extension co-contraction. This limited view does not consider co-contraction about the radial/ulnar deviation axis, nor how the FCR and ECR are controlled in relation to each other during wrist stabilization tasks, whether as synergists, antagonists, or some other possibility. Previous research on other muscle pairs that share mutual recurrent inhibition may provide fundamental principles toward our understanding of wrist

stabilization. It is known that recurrent inhibition between muscles can be modulated by task-relevant concurrent contraction of remote muscles in the lower limb. Recurrent inhibition from quadriceps (knee extensors) to soleus (ankle extensor) was only reduced in tasks where these muscles were synergistically activated for extending the limb during stance, compared to the non-synergistic condition where both were activated without a synergistic function during sitting ²³. The authors argued that descending control of Renshaw cells contributes to selection of the appropriate synergistic relationships for various postural tasks in the lower limb. It is unknown whether these principles of recurrent inhibition for posture control apply to the upper limb and, further, to a pair of muscles working at the same joint. These principles may provide a new perspective on how recurrent inhibition contributes to the posture/stabilization control of the wrist. If the synergistic activity of the quadriceps and soleus is analogous to the synergistic activity of FCR and ECR in radial deviation, and the non-synergistic activation of the quadriceps and soleus during sitting is analogous to the non-synergistic (antagonistic, in this case) activation of FCR and ECR during flexion/extension co-contraction, then recurrent inhibition between the concurrently active FCR and ECR can be modulated in a task-dependent manner. The task dependence of recurrent inhibition is depicted in Figure 4.

In radial deviation and flexion/extension co-contraction, FCR and ECR have a different functional relationship (synergist and antagonist, respectively). Flexion/extension co-contraction also activates antagonists to FCR and ECR. In the lower limb, the relationship between the quadriceps and the inactive tibialis anterior (ankle flexor, antagonist to soleus, and shares mutual recurrent inhibition with the

quadriceps) was unchanged during the seated and postural concurrent activation of the quadriceps and soleus²³, while the quadriceps-soleus inhibition was reduced as explained above. The same patterns of quadriceps-soleus recurrent inhibition held true in one subject who exhibited activation of the tibialis anterior during the knee and ankle extension task²³. This implies that the status of an antagonist muscle, active or inactive, does not influence the recurrent inhibition relationships for the agonist. Applying this to the wrist, the involvement of additional wrist muscles is not expected to influence the control of FCR-ECR recurrent inhibition as long it does not influence the FCR-ECR functional relationship. Lastly, if levels of recurrent inhibition between FCR and ECR differ for flexion/extension co-contraction and radial/ulnar co-contraction, this would suggest that the wrist axes can be controlled separately for stability.

Because the FCR and ECR exchange recurrent inhibition, it is likely that co-activation will reduce the activity of both. They also exchange reciprocal inhibition, so it is likely that vibration of one muscle increases activity in the homonymous muscle and decreases activity in the other. Without recurrent inhibition of the Ia INs, it is likely that co-contraction will not alter this pattern.

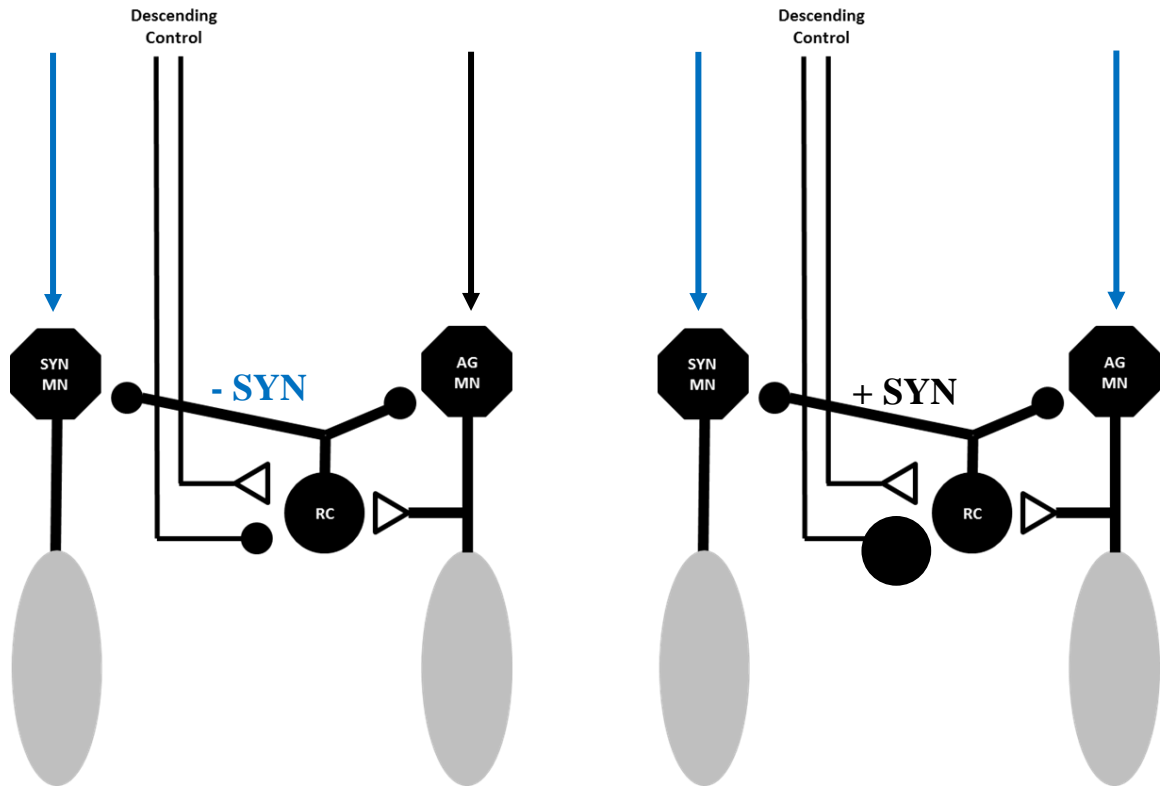


Figure 4: Task-dependent mutual recurrent inhibition. Here, both the agonist and synergist are active. On the left, both are active but not working as functional synergists. Activity of the agonist causes recurrent inhibition of the synergist. On the right, both muscles are active as functional synergists. Due to changes in descending control of the Renshaw cell, recurrent inhibition is reduced, causing a relative increase in synergist activity.

1.6 Correlation of Cortical and Spinal Neural Oscillations

In this dissertation, oscillations in the electroencephalogram (EEG) of the primary motor cortex and EMG from the contracting wrist muscles are quantified and correlated to gain insight into the motor control and performance of wrist muscles during wrist stabilization. In Aim 2, corticomuscular coherence will serve as the main EEG-EMG correlation variable. Corticomuscular coherence (CMC) is the linear correlation between

cortical and muscular neural signals in the frequency domain. Values of CMC range from 0-1, with 0 representing no correlation and 1 representing a perfectly linear relationship. The strength of CMC is thought to reflect the strength of coupling between the motor cortex and muscle neural activity²⁸. This viewpoint is supported by comparing the muscle-dependent strength of CMC to the distribution of corticomotor neurons (i.e. cortical neurons that directly synapse onto motor neurons). CMC is strongest in the distal limb segments related to fine motor tasks where the involved muscles have a greater number of corticomotor neurons.²⁹⁻³¹ There is also a task dependence of corticomotor connectivity which may influence the strength of CMC. Studies of primates have shown that specific populations of corticomotor neurons are active during agonist tasks but are inactive during co-contraction.^{30,32}

The frequencies of CMC also vary with the task parameters and state of sensory input. CMC in beta-band (14-35 Hz) is prominent during isometric tasks of moderate intensity force matching tasks^{33,34}, during interaction with a compliant load³⁵, and during tasks where movement is stopped or suppressed³⁶, and is studied primarily in visuomotor target matching tasks. Beta-band CMC is also known to be influenced by the state of afferent input.³⁷⁻⁴¹ Beta-band CMC is reduced with the loss of afferent input due to anesthesia,³⁷ cooling,⁴¹ and deafferentation.⁴⁰ Conversely, the introduction of extraneous afferent input by brief electrical or mechanical stimulation of peripheral motor or sensory nerves also causes a reduction of beta-band CMC. In the latter case, the reduction is transient, followed by a rebound beyond pre-stimulus values after the stimulation of either the agonist or antagonist muscle.^{38,39}

In addition, beta-band CMC is correlated with motor output and performance. Beta-band cortical oscillations and CMC have been linked to greater or undivided attention^{42,43} and better precision task performance.⁴⁴ At the ankle, interindividual differences in beta-band CMC have been positively correlated to an increased proportion of low frequency (<5Hz) oscillations in motor output.⁴⁵ Other studies have noted a negative relationship between low frequency oscillations and performance precision when visual feedback resolution is altered.^{46,47} In any case, low frequency oscillations in motor output have a large impact on the overall steadiness of motor performance because they constitute the vast majority of power in the frequency domain and are correlated with motor performance when higher frequencies are not.

While beta-band CMC has been characterized across motor tasks and sensory conditions, the sources of beta-band neural oscillations and coherence are still not clear. The general idea is that beta-band CMC is generated in the motor cortex, transmitted to the spinal level, and appears in the motor output. Both beta-band and alpha-band (~10Hz) peaks are prominent in EEG during steady tasks. However, alpha-band CMC is generally absent, suggesting that these frequencies are “filtered” out, possibly at the central (cerebellum) and spinal (Renshaw cell) level, while beta-band oscillations are transmitted. To complicate things further, coherence, which was initially thought to be a purely efferent process, has been revealed to be bidirectional (efferent and afferent), suggesting that varying afferent feedback reinforces the rhythm of central oscillations. This may underpin the significant impact that afferent input, or lack thereof, has on the amplitudes and frequencies of coherence.

Regarding cortical beta-band oscillations, short latency intracortical inhibition (SICI), often modeled as a negative feedback loop, is the putative source. During static tasks involving the first dorsal interosseous muscle (FDI), augmentation of SICI via administration of diazepam, a medication that enhances GABA_A-ergic inhibitory postsynaptic potentials, increased cortical beta-band activity, suggesting that SICI is in fact the source of cortical beta-band activity. Further, the strength of SICI has been positively correlated with amounts of cortical beta-band activity when analyzed across subjects. However, beta-band CMC did not show similar responses to the diazepam, nor was there a correlation with SICI and CMC across subjects. Therefore, while SICI may generate cortical beta-band oscillations, the transmission of these beta-band oscillations to the spinal cord may depend upon intervening neural mechanisms.

The strong influence of “downstream” neural mechanisms for CMC may explain why other interventions that do not augment SICI can still increase beta-band CMC. For example, administration of carbamazepine (CBZ), an anti-seizure medication, increased beta-band CMC without altering cortical beta-band activity. One possible mechanism for reduction of beta-band CMC by CBZ use is alteration of cerebellar activity, which may include “filtering” of neural oscillations. CBZ also depresses static, but not dynamic, muscle spindle activity, which may disrupt the entrainment of muscle activity to cortical activity. This static muscle spindle activity may act as “neural noise” among the transmitted cortical signal.⁴⁸

In addition to the central (cerebellum) and peripheral (muscle spindle) mechanisms mentioned above, there are additional spinal mechanisms that may influence beta-band CMC. Recurrent inhibition, for example, is thought to desynchronize motor

unit activity toward tremor reduction. This desynchronization would introduce noise in the cortical drive to the muscles and reduce coherence. This idea was supported by modeling data suggesting that recurrent inhibition can reduce or shift motor pool coherence with descending drive. The role of recurrent inhibition in reducing CMC was further illustrated by the recent finding that the strength of recurrent inhibition across subjects was negatively correlated with beta-band CMC in the soleus ⁴⁹. Conversely, modeling data suggests that recurrent inhibition can also generate beta-band oscillations in motor pool activity ⁵⁰, providing a peripheral source of beta-band oscillations that may be independent of those transmitted from the cortex.

As mentioned above, Ia afferent input can cause fluctuations in beta-band CMC, whether afferent input is introduced from the agonist or antagonist. Immediately after stimulation or perturbation, beta-band CMC is disrupted. The disruption is followed by a rebound in beta-band CMC beyond pre-stimulus values and a return to pre-stimulus values after three to seven seconds. The amplitude of these fluctuations increases with the intensity of stimulation.³⁹ The immediate reduction could be due to activation of afferent feedback loops that cause interference with or cancelation of on-going beta-band oscillations transmitted from the cortex or generated in the spinal cord. Both cortical and spinal (EMG) signals in the beta-band show desynchronization during and immediately after sensory inputs. The reappearance of beta-band CMC may be due to the reduction of spinal afferent loops back to baseline levels. The presence of a rebound and augmentation of beta-band CMC may be due to resetting of beta-band oscillation generators, much like increases in beta-band CMC after halting movement or application of TMS.³⁸

During the disruption of beta-band CMC, other frequencies of CMC appear briefly. Alpha-band (8-14Hz) and theta-band (4-7Hz) CMC have emerged in previous studies. These frequency bands have been associated with tremor and may be driven by afferent activity. Alpha-band CMC in particular is thought to involve the sensorimotor cortex and result from activation of afferent pathways as supported by the following: 1) EMG leading EEG in phase analysis for CMC studies ⁵¹, 2) the evocation of tremor in alpha-band EMG activity during muscle vibration ⁵², 3) the evocation of alpha-band CMC during tasks requiring enhanced sensory feedback ⁵³, and 4) the presence of out-of-phase alpha-band intermuscular coherence between antagonist muscles, suggesting a connection to reciprocal inhibition ⁵⁴.

While increased afferent input shows consistent reduction of coherence across subjects, the removal of afferent input has variable effects. In Riddle et al ⁴¹, six of fifteen subjects showed reduced coherence during cooling, with no effect in the other subjects. Similarly in Pohja et al ⁴⁰, ischaemia reduced coherence in three of six subjects. Fisher et al ³⁷ looked at beta-band intermuscular coherence with the assumption that beta-band activity was cortically driven, but did show reductions in this coherence during anaesthesia. Taken together, it seems that the presence of afferent feedback is important for coherence, but only in a subset of subjects. Riddle et al. ⁴¹ and Witham et al ⁵⁵ established that subjects fell into three groups based on the relationship between the phase and frequency of coherence, a relationship that appears to reflect varying ratios of ascending and descending CMC. In the latter study, the group of six out of fifteen subjects had phase-frequency relationships indicative of strong efferent drive. Witham et al. ⁵⁵ clarified that subjects in this actually have similar levels of descending and ascending

coherence, while the other groups have greater ascending coherence. This study also found that across a set of subjects with representatives from each group, the average coherence (non-directional) and descending coherence were increased by cooling while ascending coherence was unchanged if not slightly reduced. Unfortunately, the analysis did not include directional analysis of cooling for each group separately to clarify how group differences impacted overall averaged coherence, nor was there analysis of changes in beta-band for EEG or EMG. Still, these studies clarify the importance of afferent feedback for coherence by showing the consistent presence and strength of ascending coherence in beta-band relative to descending coherence. The mechanisms behind the increase in beta-band coherence after cooling are unknown, but may rely on which frequencies of afferent feedback are being preserved or removed. Cooling would reduce inputs from sensory organs that could otherwise create “noise”, while preserving any beta-band oscillations generated in the cortex and spinal cord, as may be occurring during the CBZ treatments mentioned above.

Because beta-band CMC is transiently reduced by a brief stimulation of the peripheral nerves ^{38,39}, it is likely that sustained stimulation of the afferent pathways via vibration leads to a net reduction in the beta-band CMC throughout the vibration period, but this has not been demonstrated. Likewise, Renshaw mediated mutual recurrent inhibition has been shown to reduce beta-band CMC in the homonymous muscle ⁴⁹, and is predicted to do so during co-contraction of muscles that exchange recurrent inhibition ⁵⁰ but this has not been demonstrated. The FCR and ECR muscles are unique in that they exchange both reciprocal inhibition, like antagonists, and recurrent inhibition, like synergists. They are easily accessible to vibration, and their relative activity easily

manipulated by torque direction. They are ideal for examining the influence and accommodation of reciprocal inhibition and recurrent inhibition on beta-band CMC.

1.7 Specific Aims

In this dissertation, I analyzed mechanical aspects of wrist control and stabilization and the underlying neural mechanisms. For the mechanical aspect, I analyzed muscle stiffness and task steadiness during wrist stabilization tasks. To capture muscle stiffness and analyze muscle activation, I developed an analysis method for USSWE data collected from extensor carpi ulnaris (ECU) and triceps longus (TRI). Identification and removal of non-contraction tissue data from the contractile muscle tissue data influenced the mean and variability of elasticity measurements, and improved the use of USSWE as an alternative to EMG for measurement of the amplitude of forearm muscle activity. Task steadiness was assessed during co-contraction of flexor carpi radialis (FCR) and extensor carpi radialis (ECR).

To clarify neural pathways and their effects on motor output during wrist stabilization, spinal mechanisms between FCR and ECR were stimulated via mechanical and electrical stimulation protocols. FCR and ECR share both synergistic and antagonistic spinal mechanisms. This hybrid spinal configuration may be necessary for versatility of control about a multiaxial joint, particularly with muscles that have flexible functional relationships. However, this unique configuration has certain functional differences when compared to control of true antagonists. The differences in

neuromuscular activity and consequences for function are not well understood in either agonist contraction or co-contraction of the wrist muscles.

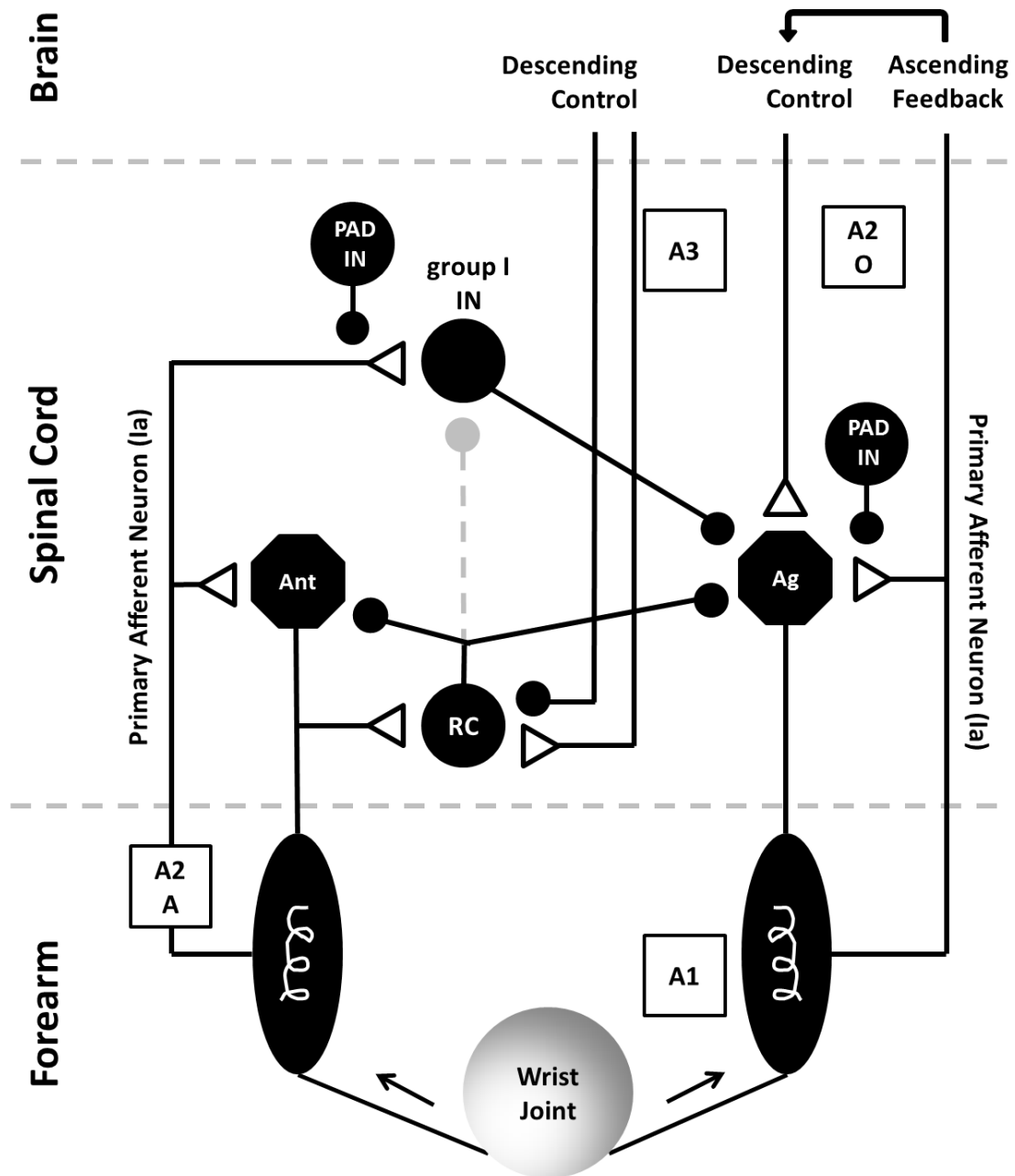


Figure 5: Summary schematic model of neural pathways and motor output of FCR and ECR. Labels for each Specific Aim are included near the mechanisms

addressed. A1 = Aim 1; A2-O = Aim 2 - Oscillations; A2-A = Aim 2 – Amplitudes; A3 = Aim 3; FCR = flexor carpi radialis, ECR = extensor carpi radialis; MN = motor neuron; RC = Renshaw cell, PAD = primary afferent depolarization; IN = interneuron

1.7.1 Specific Aim 1

Purpose: To quantify the mechanical activity of individual muscles by developing an automatic image-processing algorithm for obtaining shear modulus of contractile muscle tissues without the contamination of non-contractile connective tissues from elastography videos, and to examine the effect of this removal on the assessment of muscle elasticity, particularly for a wrist muscle during a wrist stabilization task (Figure 5 at A1).

Hypotheses: 1) Automatic removal of non-contractile connective tissues from ultrasound shear-wave elastography (USSWE) data is possible with the use of an image processing algorithm. 2) With this developed algorithm, quantified mechanical activity of individual muscles that excludes non-contractile tissue data would be lower, less variable, and have greater linearity with loading than data that includes non-contractile tissue. 3) Comparisons of mechanical activity across various loading tasks would be altered.

Rationale: USSWE, a newly developed tool, was used to estimate changes in individual muscle force as subjects grasped a robotic manipulator and resist multiaxial loads. This methodology is better suited for more complex tasks such as handgrip and multiaxial loading at the hand, where EMG over wrist muscles becomes less reliable. USSWE provides spatial resolution of muscle activation and there is no evidence of crosstalk or other sources of noise. An automatic image processing algorithm was developed to

analyze USSWE data, recorded as videos for each loading task trial. A major contribution of the algorithm is the identification of non-contractile tissue (NCT) within and around the contractile muscle tissue. NCT is often avoided in elastography measurements when possible, but the impact of its removal or exclusion from muscle elasticity measurements has not been formally assessed. In this study, the impact of removal of NCT elasticity data was examined by comparing mean muscle elasticity across tasks with linearly increasing loads and across various other loading conditions. The impact of NCT was also quantified as errors in ranking muscle elasticity across tasks with or without NCT data included. This analysis is important for assessment of wrist muscle activity and stiffness given the small size and increased density of NCT in the forearm muscles compared with larger proximal muscles observed in previous studies.

1.7.2 Specific Aim 2

Purpose: To understand the effect of co-contraction and applied Ia afferent input on correlated neural oscillations, steady motor output, and their relationships during wrist stabilization (Figure 5 at A2-A and A2-O).

Hypotheses: 1) Renshaw cell inhibition of group I interneurons is necessary for completely abolishing the Ia-originated inhibition during antagonist co-contraction. 2) Beta-band CMC is reduced with vibration and co-contraction. 3) Beta-band CMC is correlated with low-frequency power in rectified EMG (i.e. unsteadiness).

Rationale: The classical model of antagonist muscle activity involves pairs of muscles that share reciprocal inhibition via Ia pathways that cause monosynaptic excitation of the agonist muscles and Ia interneurons that inhibit the antagonist ^{56,57}. Suppression of reciprocal inhibition between muscles at the ankle that follow this classical model appears to be accomplished by presynaptic inhibition ¹² of Ia afferent synapses and inhibition of Ia interneurons via facilitation of Renshaw cells ²⁴. In contrast, the findings of Aymard et al. ¹⁹ show that Ia pathways between FCR and ECR involve group I interneurons that are not inhibited by Renshaw cells. This suggests that suppression of reciprocal inhibition is hindered during co-contraction. Previous studies have shown suppression of group I antagonist inhibition, but in a limited number of subjects and only with electrical stimulation using a paired pulse protocol ¹¹. The quantification and comparison of reciprocal inhibition between FCR and ECR during co-contraction and wrist flexion with functionally relevant Ia stimulation is the first goal of this study.

The experimental protocol for this study was designed to maximize functional relevance. For example, vibration was used in place of electrical stimulation of Ia pathways. Vibration provides advantages over electrical stimulation. First, vibration allows for the task-dependent dynamics of muscle spindle activity to be captured in the data. Second, it allows for sustained Ia input and involvement of various spinal mechanisms and reflexes (e.g. presynaptic inhibition, Ia pathways, Ib pathways, recurrent inhibition, presynaptic inhibition) to give a holistic view of motor output during steady state perturbations. Third, the timing and strength of these spinal mechanisms may be altered by sustained mechanical stimulation relative to electrical stimulation and/or brief perturbation. Additional measures taken to maximize functional relevance include

observing reciprocal inhibition in ongoing EMG and during voluntary contraction instead of using electrical stimulation test reflexes.

During a stability task, cortical activity in the beta-band is often correlated with spinal level beta-band activity expressed in EMG. Beta-band neural oscillations and corticomuscular coherence have been studied extensively during force matching and position tasks in various states of sensory involvement and have been correlated with task performance. Similar studies have not been conducted during co-contraction. As co-contraction is a stability task, beta-band activity and coherence are expected to have similar functional correlates and sensory modulation during co-contraction as have been shown in agonist contraction. The unique spinal mechanisms at the wrist may alter expected sensory modulation patterns, particularly with the preservation of reciprocal inhibition during co-contraction. The results from this study clarify the correlations and modulations of neural oscillations during co-contraction and sensory input.

EMG is used in this study to capture oscillations and amplitudes of muscle activity. In consideration of the limitations of EMG and for greater control of FCR and ECR muscle activation, a wrist co-contraction task is utilized without handgrip to reduce task complexity of finger involvement, and reduce the risk of EMG crosstalk.

1.7.3 Specific Aim 3

Purpose: To clarify the role of mutual recurrent inhibition between the active FCR and active ECR during wrist stabilization tasks where FCR and ECR are expected to function as agonists or antagonists (Figure 5 at A3).

Hypotheses: 1) Mutual recurrent inhibition between active FCR and active ECR, quantified by heteronymous inhibition, will be reduced only when FCR and ECR are acting as synergists (i.e. radial deviation and radial/ulnar co-contraction), not as antagonists (i.e. flexion/extension co-contraction). 2) There will be contraction intensity dependent changes in the relative amounts of inhibition, with possible task and intensity interaction.

Rationale: In Aim 2, amplitudes of flexor muscle activity were reduced by extensor vibration with no significant differences between tasks. This suggests that the ability to reduce or abolish group I inhibition was compromised by the unique configuration of recurrent inhibition at the wrist. While recurrent inhibition may not contribute to control of antagonistic reciprocal activity, it instead contributes to control of FCR and ECR in parallel. The modulation of this parallel control during antagonistic and synergistic activity of FCR and ECR has not been clarified. As the modulation of recurrent inhibition is thought to be centrally controlled, patterns of recurrent inhibition modulation would reflect centrally defined motor control schemes. Knowledge of these modulation patterns would enhance our understanding of multi-axial wrist control and stability. The feasibility study presented here outlines the exploration of mutual recurrent inhibition during stabilization for each axis of wrist movement.

CHAPTER 2. AMPLITUDES OF MUSCLE MECHANICAL ACTIVITY -- AUTOMATIC ANALYSIS OF ULTRASOUND SHEAR-WAVE ELASTOGRAPHY IN SKELETAL MUSCLE WITHOUT NON-CONTRACTION TISSUE CONTAMINATION

2.1 Introduction

Quantitative and qualitative assessment of joint torques (e.g., manual muscle testing, grip strength) is routinely used in clinical settings as a diagnostic tool for and as a means to monitor rehabilitation from neuromuscular disease and injury (e.g., stroke, spinal cord injury). Assessment of mechanical activity in individual contracting muscles would also be informative for diagnosis because the relative contributions of individual muscles to produce joint torque combinations (i.e. muscle coordination) often appear to be abnormal in the above-mentioned clinical populations according to the electrical activity of the muscles.^{58,59} In humans *in vivo*, however, mechanical output of contracting muscles cannot be quantified by direct measurement of individual muscle forces noninvasively.

As alternatives, surface electromyography, mechanomyography, and laser shear-wave elastography have been studied for estimating muscle force, but they all have various fundamental limitations. Surface electromyography measures electrical activity of muscles from skin surface, but its amplitude is not always linearly related to mechanical output of muscle (i.e. force)⁶⁰, or the linear relationship is reduced by task

conditions.¹⁵ Mechanomyography measures small lateral vibration of muscles from skin surface, but its amplitude is not always linearly related to muscle force especially at higher contraction levels.⁶¹⁻⁶³ Laser shear-wave elastography has recently been developed to measure propagation velocity of shear wave at skin surface overlaying an upper arm muscle⁶⁴, but its applicability to other muscles is yet to be examined. All of these recordings from the skin surface have common fundamental limitations including difficulty in obtaining reliable signals from deep muscles, variability across subjects, and susceptibility to crosstalk from neighboring muscles, particularly on body segments like the forearm where there are multiple small, closely packed, muscles (e.g. wrist muscles) with overlapping (i.e. redundant) function.^{13,14} To overcome these limitations, the potential of recently developed ultrasound shear-wave elastography (USSWE) has been demonstrated for assessing individual muscle contraction levels.⁶⁵ This work is motivated by the need to develop alternatives for EMG measurement over body segments prone to crosstalk and solve essential problems of the current use of USSWE in contracting muscles.

In USSWE, shear modulus is calculated from the propagation velocity of shear wave inside tissues, which can be spatially variable when tissues are made of different elasticities.^{66,67} In its current application to muscles, the spatial average of shear modulus distribution across a circular region of interest (ROI) of a muscle has been determined using a commercially available ultrasound device with included software (e.g. AixPlorer system Real-time ShearWave Elastography with Q-BOX software, Supersonic Imagine, Aix-en-Provence, France)^{17,68-70}. The obtained mean shear modulus of a large muscle is shown to be more linearly related to joint torque over a wide range of

contraction levels with less variability compared with surface electromyography^{15,17} and is not susceptible to crosstalk.⁷¹ The problem is that the simple spatial average of shear modulus distribution across a circular ROI in a muscle is not appropriate for assessing contraction level because it can include not only shear modulus of contractile tissues (i.e. muscle fibers) that produce force but also non-contractile tissues (NCT, i.e., skin, adipose tissue, and connective tissue) that can be distributed within the contractile tissue region. However, the impact of NCT inclusion in the image analysis on the assessment of muscle contraction intensity is unknown. Additionally, the above-mentioned determination of mean shear modulus is manually operated image by image with multiple steps, which is time consuming and prone to error and variability due to subjective placement of ROI in examining multiple images across trials, tasks, and individuals. Automated image processing algorithms have been developed for medical images, but many are specialized for tissues or organs other than skeletal muscle, employ methods that are not appropriate for NCT detection, or introduce more complexity than this study requires. These problems will need to be resolved for enhancing the accuracy and convenience of using ultrasound shear-wave elastography for assessing contracting muscles.

The purposes of this study were 1) to quantify the mechanical activity of individual muscles by developing an automated analysis method for determining mean shear modulus of muscles without the contamination of NCT in ultrasound shear-wave elastography and 2) to understand the effect of NCT on comparison of mean shear modulus of muscles across arm stabilization tasks with linear and variable muscle loadings. For the first purpose, an optimized clustering and thresholding algorithm was implemented for ultrasound B-mode images to identify NCT and remove shear modulus

values of NCT from spatial averaging of muscle shear modulus. Since elasticity of NCT is distinct from contractile tissues^{70,72}, the successful removal of these “outliers” is expected to reduce the variability of shear modulus value within ROI. The efficacy of removal of NCT contamination was tested by measuring the linearity and rank order of estimated muscle mechanical activity across motor tasks.

2.2 Methods

2.2.1 Subjects

Eleven male subjects (age: 21.3 ± 0.9 years (mean \pm SD)) provided informed consent according to the procedures approved by the ethics committees of the National Institute of Fitness and Sports in Japan, the Nara Institute of Science and Technology in Japan, and the Georgia Institute of Technology in Atlanta, GA, USA. All subjects were college athletes. Male athletes were chosen for their low subcutaneous fat and for their expected ability to control and stabilize their muscle activity. These attributes were expected to allow for optimal ultrasound image acquisition. All subjects were physically and cognitively healthy with no history of neuromuscular disorder.

2.2.2 Motor task

The motor task for the subjects was to maintain their upper limb posture against various combinations of force and torque loads applied by a robot. A task against various

forces and torques was utilized to obtain data in which healthy individuals may use various “non-standard” combinations of muscle activation as in clinical populations. Subjects were seated and grasped the handle of a robotic manipulator (PA10, Mitsubishi Heavy Industries Ltd., Tokyo, Japan) with the right hand. The starting position of the robotic manipulator handle was adjusted for each subject such that the shoulder joint was abducted to approximately 10° , the elbow joint was flexed to 90° , and the wrist joint was in a neutral position (i.e. standard posture). The elbow joint angle was monitored with an electro-goniometer (SG110, Biometrics Ltd, Newport, UK) and displayed on an analogue output unit (ADU301, Biometrics Ltd, Newport, UK) to maintain the right angle throughout the measurements. The robotic arm was programmed to apply complex force and torque loads up to six degrees of freedom (3 forces and 3 torques) at the handgrip. Torque about the longitudinal axis of the handle was excluded due to subjects having difficulty resisting this rotation without the handgrip sliding in the palm. While watching their hand and arm, subjects were instructed to contract their upper-limb muscles to maintain the standard posture against the complex force and torque loads applied by the robot manipulator. This experimental setup can be found in a picture that was taken during a pilot study (Figure 6).



Figure 6: A photo that includes the current experimental setup, taken during a pilot experiment. Axes of loading for robotic manipulator are: positive x , y and z axes point toward the subject, to the right of the subject, and upward, respectively. Note that the subject is being prepared for an upcoming trial, thus the elbow has not yet been adjusted to 90° of flexion. In addition, pilot EMG signals were explored for a purpose not addressed in this dissertation but were deemed unreliable due to motor noise from the robot.

The target muscles in this study were extensor carpi ulnaris (ECU) and triceps brachii longus (TRI). ECU was chosen as a representative forearm muscle to illustrate the use of elastography in a body segment prone to EMG crosstalk. TRI was chosen to represent larger muscles where reliability of EMG may often be degraded with relatively

thick subcutaneous adipose tissue. ECU plays a role in wrist extension and ulnar deviation while TRI plays a role in elbow and shoulder extension. Thirteen different types of muscle loadings were configured for the robotic manipulator so that the expected force/torque production (i.e. contraction level) with ECU and TRI would vary substantially in the same posture. The forces and torques for each loading condition are listed in Table 1. Tasks 1, 2 and 3 are linear loading conditions and were used to test linearity of muscle activity captured with elasticity data. Details of the loadings were determined by modifying a computational muscle model that contains 51 muscles across 12 joints of the human right arm and torso^{73,74} for the robotic device. Nonetheless, with the abundance of muscle contraction patterns for accomplishing the same end-point task performance^{75,76}, substantial variability of contraction level was anticipated in ECU and TRI across subjects. Each subject performed three 15-s trials of each loading task for each muscle. Subjects were instructed to use the same muscle activation strategies across trials for the same loading configuration. All subjects were able to resist the applied loads with minimal displacement of the arm and hand.

Table 1: A list of forces (Fx, Fy, Fz) and torques (Mx, My, Mz) applied by the robot for each loading condition.

Task #	Fx (N)	Fy (N)	Fz (N)	Mx (N·m)	My (N·m)	Mz (N·m)
1	0	0	20	0	-0.5	0
2	0	0	10	0	-0.25	0
3	0	0	30	0	-0.75	0
4	0	0	22.5	-0.9	0.1	0
5	0	0	10.8	2.3	-3	0
6	0	0	8.3	0.8	-0.9	0
7	0	0	42.7	-2.9	0.3	0
8	0	0	1.7	1.7	-3.3	0

9	-5.7	3.6	2.4	1.5	-3.4	0
10	30.7	-2.6	31.7	-0.6	0	0
11	-0.8	0	8.6	0.7	-0.9	0
12	-4.2	2.8	11.2	2.1	-3.1	0
13	-7.8	0.6	-19.7	0.3	-0.1	0

2.2.3 *Ultrasound data recording*

Ultrasound B-mode and elastography videos were obtained concurrently using the AixPlorer Ver. 4.0 ultrasound shear-wave elastography system with the musculoskeletal preset. The ultrasound system provides a repeatable and reliable method of quantifying mean shear modulus of muscles at various contraction levels, showing linear increases in mean shear modulus with increasing muscle activity^{16,17}. In this system, shear modulus is calculated from the shear-wave propagation velocity in the direction of the longitudinal axis of a probe (4-15 MHz, SL15-4, linear-array, 50-mm wide, Supersonic Imagine, Aix-en-Provence, France). In this experiment, the probe was held over the target muscle belly and aligned with the longitudinal axis of the muscle. Care was taken not to press or deform the muscle with the probe during measurements. ECU and TRI could not be monitored simultaneously as only one ultrasound probe was available. Therefore, loading configurations were performed to record one muscle and later repeated to record the other. B-mode and elastography data from each trial and muscle were saved as video (1 frame/s). Representative B-mode and elastography images of ECU and TRI are shown in Figure 7a and b, respectively, to show the differing architectures of the muscles. A rectangular area within the muscle, outlined in the B-mode images, was selected as the recording area for shear modulus data during the experiment. The recording area for

shear modulus was chosen to span the thickness of the muscle belly in ECU or to capture data from a central location in the muscle belly of TRI.

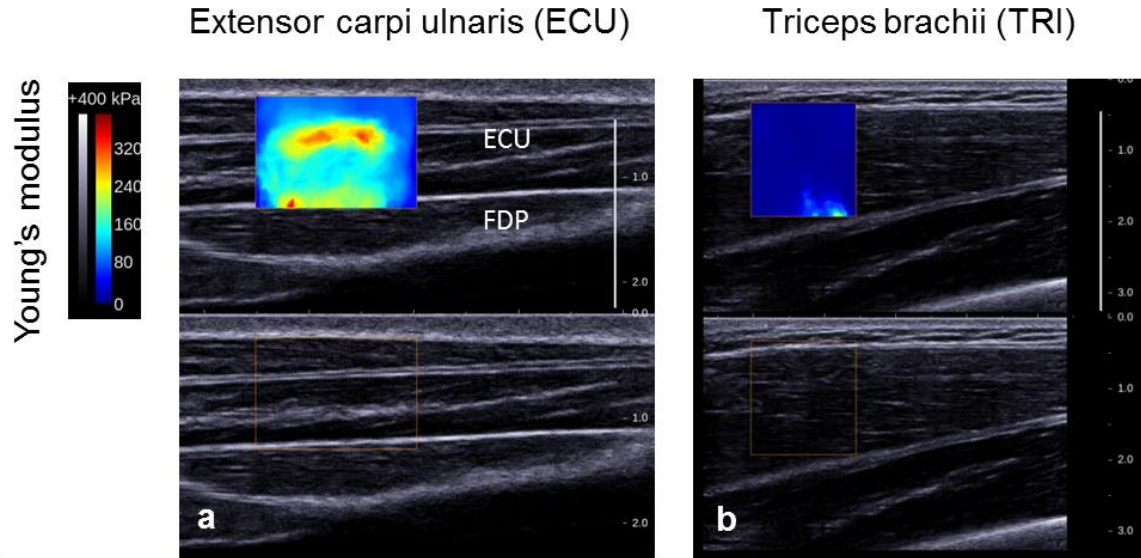


Figure 7: Representative ultrasound images of the extensor carpi ulnaris (ECU) (a) and the triceps brachii (TRI) (b). A colored box over the B-mode image (*top*) shows the region of interest (ROI) selected for the elastography recording. The long white bands of tissue across the middle of each image are connective tissue. The flexor digitorum profundus (FDP) is shown deep to ECU.

2.2.4 Data analysis

Ultrasound B-mode and elastography data were processed offline in MATLAB (Mathworks, Natick, MA, USA). In each trial, approximately 12 s of continuous video with consistent images were extracted for data analysis. Each video frame included two grayscale (B-mode) images of the underlying arm anatomy. One featured elastography, showing a color-coded rectangular overlay representing the calculated Young's modulus (Figure 7, upper images). The other was a copy of the B-mode image with only a colored rectangular outline corresponding to where Young's modulus was calculated (Figure 7,

lower images). The entire rectangular measurement area was used as the ROI from which data were processed. The dimension of the ROI was approximately 1.0×1.5 cm for ECU and 1.5×1.5 cm for TRI. The system calculated Young's modulus from measured shear wave velocity with the assumption that the measured substrate was isotropic. As muscle is anisotropic, the calculated Young's modulus data were transformed to shear modulus by dividing the Young's modulus values by 3 as in previous studies^{17,77,78}. For each trial, the scale of the color mapping for the modulus was adjusted to provide optimal visual resolution, i.e., large visual change of color without saturation to either end of the color scale. No trials reached the maximum measurable limit (266 kPa for shear modulus) of the ultrasound device.

2.2.5 Image processing for NCT identification

The greatest challenges of the automated ultrasound image processing were successful detection of NCT across muscles and subjects without excessive removal of contractile tissue data. A method was needed that was robust to differing NCT configurations and locations and occasional image quality issues. Several algorithms for analysis of ultrasound images exist with various applications from medical imaging⁷⁹⁻⁸³ to food quality assessments.⁸⁴⁻⁸⁶ These algorithms employ edge detection or image segmentation using pixel intensities, textures, or developed templates within a single image or tracked across several images in a video. The established edge detection algorithms were not appropriate for this study, as the main objective was to identify the full area of objects, i.e. non-contractile tissue segments. Further, the NCT within the

ultrasound images did not have enough sharp, continuous edges for sufficient edge detection. For segmentation of the image into areas of interest, intensity values⁸³ and visual texture⁸⁶ have been used to distinguish between tissues. For the analysis of ultrasound images of muscle for NCT removal, the tissues of interest were distinguishable by their differing intensities, which obviated the need for the more complex texture analysis. With distinct intensity values, methods of pixel clustering by intensity for tissue identification were most appropriate. For the above-mentioned reasons, an image processing algorithm was developed that identified bands of NCT based on intensities in the B-mode ultrasound image captured along the longitudinal axis of the muscle (Figure 8). Building upon established methods of intensity value clustering, intensity threshold and cluster shapes were modified to best suit the band-like nature of most NCT segments.

The initial part of the algorithm included determination of intensity threshold and clustering variables for identifying continuous NCT areas from distributed echo intensities. To start, each ultrasound video was converted into its constituent frames for processing in MATLAB. In each frame, the B-mode ultrasound image without the color-coded ROI (Figure 8a) was converted into a black and white image using the built-in MATLAB functions (“im2bw” and “graythresh”). One of these functions used Otsu’s method to choose an intensity threshold that minimizes the intraclass variance of the grouped pixels. For the output, ultrasound image pixels with intensities below the threshold were shown as black and assigned the intensity value 0, while all other pixels were shown as white with intensity value 1. For this analysis, the intensity threshold was

multiplied by X to bias the algorithm toward detecting more or less NCT in the initial stage (Figure 8b).

The white pixels were further examined to find major segments of NCT. Ideally, segments of NCT would appear as long, thick lines of white pixels spanning the length of the frame. Hence, a length threshold was applied: segments that were below the Y^{th} percentile of major axis length across all segments in the image were discarded (Figure 8c). Next, segments with eccentricity above the Z^{th} percentile were lengthened by $W\%$ on each end along the major axis (Figure 8d). This lengthening was implemented for cases where long bands of NCT were artificially broken up due to inadequate image quality, low contrast, or limitations of the intensity thresholding. It was expected to unite broken segments or at least cover more of the NCT band. All remaining clusters were transferred to a final NCT binary mask.

This NCT detection algorithm was trained on 88 images (four from each muscle and subject) randomly selected from the obtained images by the authors to determine values for X , Y , Z , and W . Each resulting binary mask was compared to a “solution”, a manually segmented version of the test image created by the authors beforehand. Results were scored based on the percentage of true positive pixels (correctly identified as NCT out of all NCT) and a combined score of the true positives and true negative pixels (correctly identified as contractile tissues out of all contractile tissue). For a given set of variable values, the true positive, true negative, and combined score were averaged across all 88 images.

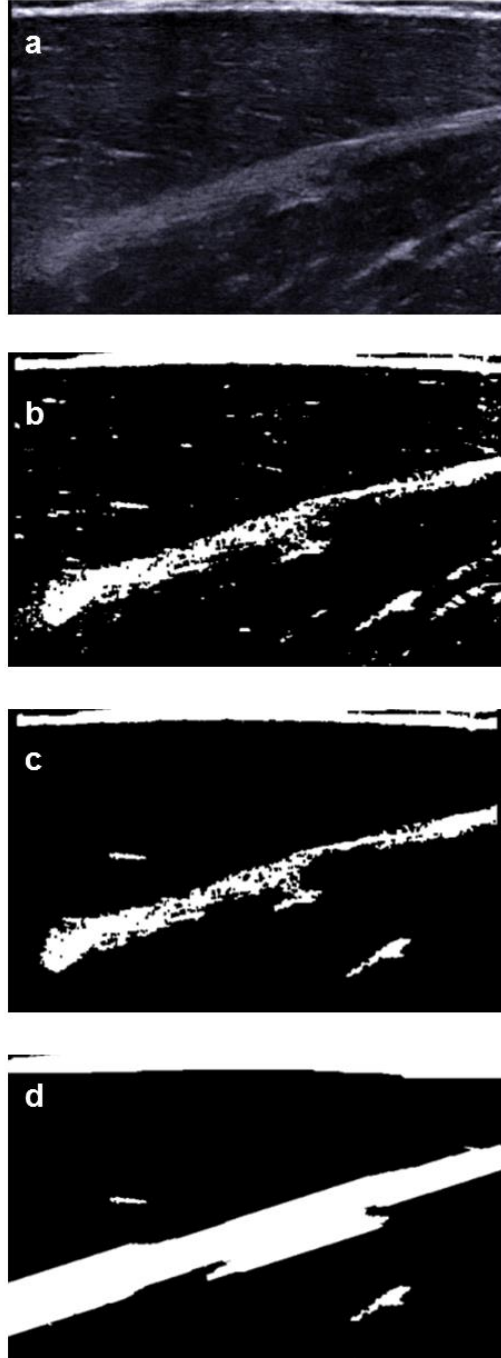


Figure 8: Progression of ultrasound B-mode images via image processing algorithm using an example of TRI. *a)* Original B-mode image. *b)* Transformed to black and white image using Otsu's intensity threshold multiplied by X . *c)* Segments with length below the Y^{th} percentile removed. *d)* Segments with eccentricity above the Z^{th} percentile were lengthened by $W\%$. See text for details of W , X , Y , and Z .

To optimize the variable set, a greedy algorithm was used to maximize the combined score while preferentially selecting variable sets with true positive values above 90%. To start, a random set of values was used as a seed. The random initial seed values for each variable were from 0.5 to 1.5 for *X*, 50% to 100% for *Y* and *Z*, and from 0 to 100% for *W*. From this seed, eight variable sets were generated by increasing and decreasing each of the four variable values separately by a small increment of 0.05, 2.5%, 2.5%, and 10% for *X*, *Y*, *Z*, and *W*, respectively. Thus, a total list of nine variable sets was tested initially. The next seed was determined by first finding the variable set with the highest combined score among those with true positive scores above 90%. If none of the true positive scores was above 90%, the algorithm selected the variable set with the highest combined score. If the true positive score was above 90% but the combined score was less than 5% lower than the highest combined score in the list, the variable set with the highest combined score was selected instead. To avoid infinite loops resulting from a repeated seed, a randomized process selected one value in the repeated seed, incremented or decremented the value, and then used the resulting variable set as the next seed. The algorithm continued until a seed had a true positive score above 90% and had either the highest combined score or was within 5% of the highest combined score in the current list. This greedy algorithm was used in order to explore the variable set space without having to run every possible option within an arbitrarily limited range of values. There was not expected to be a straightforward global maximum for the combined scores, so the variable set search was repeated 10 times to give a selection of variable sets and give insights on optimal ranges for each variable. Of the 10 variable sets [*X Y Z W*], the set with the highest combined score while having a true positive score about 90% was

selected for analysis of the video data. This optimized value set was used to identify NCT in each frame of the ultrasound videos, producing a binary mask (d) used to remove NCT data values from the ultrasound images.

2.2.6 Image processing for shear modulus assessment

Shear modulus values were read from each frame with and without inclusion of areas of NCT. Detection of color-coded shear modulus data was based on finding image pixels with high variability among RGB components, given that the rest of the image is essentially in grayscale with low variability. For each colored pixel detected, the algorithm found the closest matching pixel in the color scale displayed on the screen, and this color was translated into a shear modulus value based on the maximum value listed above the color scale. The maximum value was user selected in the user interface of the ultrasound system. The scale had 220 colors, signifying values from 0 to the maximum shear modulus value for each video.

Once shear modulus was quantified for each pixel in a given frame, the spatial mean value of shear modulus data in the ROI was calculated for each frame in a trial video with NCT. The frames with the least variability (i.e. SD of the mean values) for a 3s window were extracted from the video for further analysis, assuming the window indicated when muscle activity had settled. The spatial mean and SD of shear modulus in the ROI of these frames were determined with and without NCT for a given video. In addition, the relative amount of detected NCT area within the ROI was determined in

percentage of the total ROI area. These data were averaged across the extracted frames in each trial and then across trials for each loading configuration in each muscle.

It is possible that the identified NCT contains both adipose tissue with low shear modulus and connective tissue with high shear modulus. Adipose tissue appears primarily at the subcutaneous level and connective tissue appears deeper and within the muscle. To examine the depth-related distribution of NCT removal in the ROI, the amount of NCT removed at each 10% of equally-distributed levels of depth in the image (~1.5 mm/level) was calculated as a percentage of all NCT removed in the ROI. Thus obtained NCT removal at each depth level was averaged across all frames, trials, and loading configurations for each subject and muscle. This analysis was performed to obtain information that may help infer the relative amount of the superficial (adipose) tissue in the NCT removal compared with deeper (intramuscular) connective tissue.

To determine the impact of NCT removal, the linearity of mean shear modulus across the linear loading conditions was quantified as Pearson's coefficient and compared with and without NCT. In addition to analyzing linear loading, the rank order of tasks by increasing mean shear modulus was compared with and without NCT removal for each subject and muscle. Rank order was used as a means to express relative amounts of muscle activity under the complex loading configurations unique to this study. Differences in task ranking, or rank errors, were tabulated across subjects at each rank with NCT removal. For example, if a task is ranked at 1 (i.e. lowest mean shear modulus) with NCT removal for a given subject but is not ranked at 1 without NCT removal, this is counted as one rank error at rank 1. The total number of rank errors was

also determined for each muscle. For each muscle, there were 13 ranks in each subject, and thus 143 rank error possibilities across 11 subjects (i.e. 11×13).

2.2.7 *Statistical analysis*

Spatial mean and SD of shear modulus in the ROI were tested with a two-way analysis of variance (ANOVA) with repeated measures with factors being NCT and muscle. The distribution of NCT removal in reference to depth was also tested with a two-way ANOVA with repeated measures with factors being depth and muscle. When appropriate, post hoc comparisons were performed using Bonferroni correction. The amount of NCT area was compared between muscles using a dependent *t*-test. Pearson's correlation analyses were performed between the NCT area and changes in spatial mean and SD of shear modulus in the ROI for each muscle independently and also for both muscles together across subjects. The alpha value was set to 0.05. $P < 0.05$ and $P < 0.01$ are noted when significant. Values are reported as mean \pm SD in the text mean and mean and standard error in the figures.

2.3 **Results**

2.3.1 *Algorithm Optimization*

The determination of variable sets of [*X Y Z W*] was crucial for identifying NCT. When only Otsu's method was used for thresholding of the intensity values for

identifying NCT in the original B-mode image, the variable set of [1.0 0% 0% 0%] for [X Y Z W] had true positive score of 66.58%, far less than 90% required for NCT, and true negative score of 95.04%. In contrast, of the 10 variable sets [X Y Z W] found in the optimization search, the set [0.80 95% 90% 10%] had the highest combined score while having a true positive score above 90% (true positive score: 90.01%; true negative score: 81.46%). Hence, the true positive score with the uses of Otsu's method only was less than the method with additional optimization by 23.43% (i.e. 90.01%-66.58%). The combined score was 161.62 with Otsu's method only and 171.47 with the optimized value set [0.80 95% 90% 10%]. This optimized value set was used for the subsequent analysis of the video data in assessing the effects of NCT.

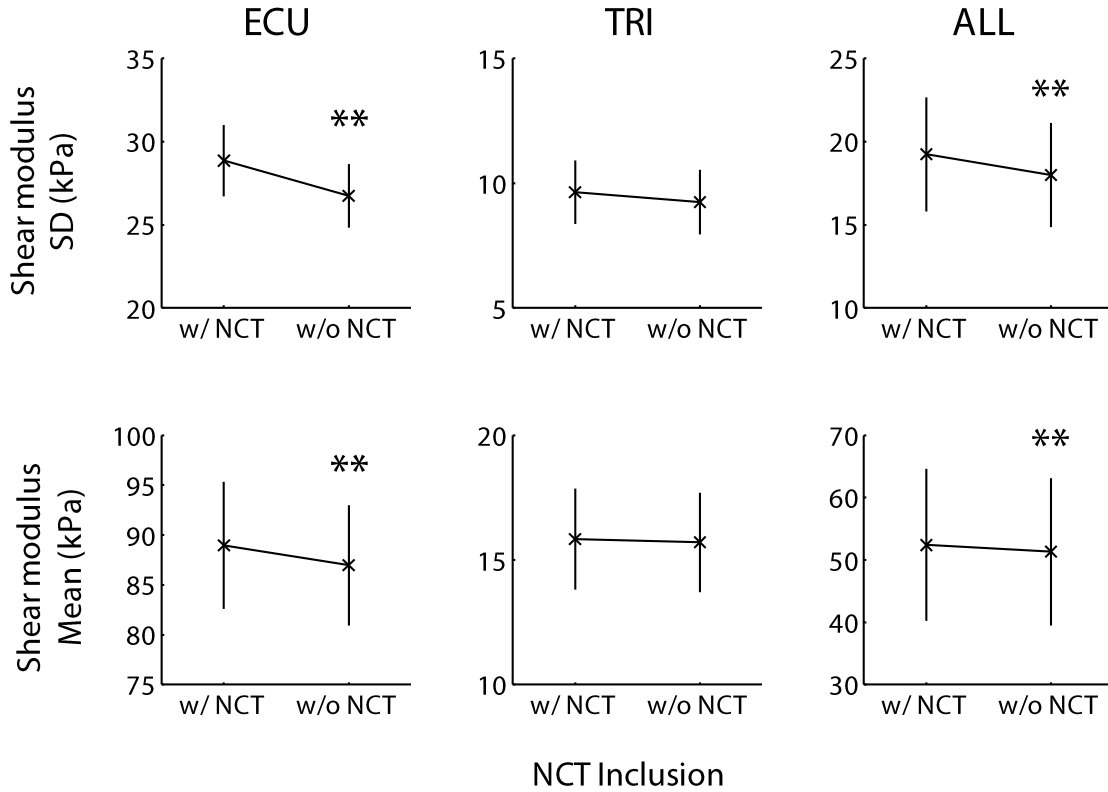
2.3.2 *Spatial SD and mean of shear modulus*

There were main effects of NCT and muscle on both spatial SD and mean of shear modulus in the ROI ($P < 0.01$ for all the main effects) (Figure 9). With the removal of NCT, SD and mean of shear modulus were reduced by 6.6% and 2.0%, respectively. SD and mean of shear modulus in ECU were about 2 and 4.5 times of values in TRI, respectively. There was also an interaction of NCT and muscle on shear modulus for both SD ($P < 0.01$) and mean ($P < 0.05$). In ECU, all subjects had reductions in SD, and all but one subject had reductions in mean when NCT was removed. The effects of NCT were more variable in TRI compared with ECU. With the removal of NCT, SD and mean were reduced by 7.3% ($P < 0.01$) and 2.3% ($P < 0.01$) in ECU, respectively, but the

smaller and more variable reductions in TRI (by 4.1% in SD and 0.8% in mean) did not reach statistical significance ($P > 0.05$).

2.3.3 *Depth-related distribution of NCT removal*

There was a significant interaction of depth and muscle on NCT removal ($P < 0.01$) (Figure 10). In TRI, more than half of NCT removal occurred at the shallowest depth whereas only 10% or less of NCT removal occurred at other depth levels, on average. The NCT removal from the shallowest level was greater than all but the 2 deepest levels ($P < 0.05$) where variability was large in TRI. In ECU, NCT removal was 5-14% across depth levels, on average. NCT removal from the shallowest depth was not significantly different from any other depth level except for the next shallowest depth level ($P < 0.05$) in ECU. At the shallowest level, NCT removal in TRI was more than four times compared with ECU ($P < 0.05$). Conversely, NCT removal from TRI was less at the deepest 7 levels compared with ECU ($P < 0.05$).



2.3.4 Total area of NCT

The total area of NCT was expressed as a percentage area relative to the whole area in the ROI (NCT area) of the B-mode images in each muscle. On average, NCT area in TRI ($13.5 \pm 9.78\%$) was less than one-third of that in ECU ($44.87 \pm 12.2\%$, $P < 0.001$). There was no significant correlation across subjects between NCT area and the change in mean or SD of shear modulus due to the removal of NCT when data for ECU and TRI were analyzed together or independently.

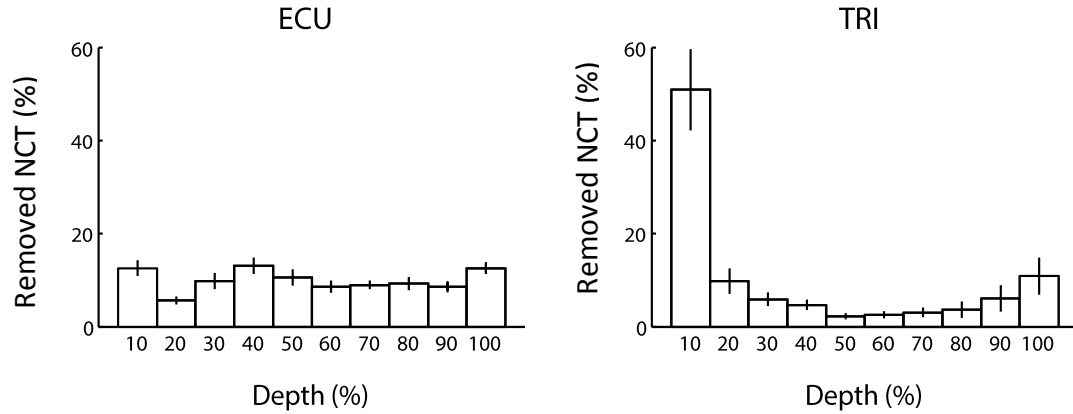


Figure 10: Distribution of NCT data removal in ROI by depth. Each graph shows the percentage of all removed pixels that were removed from a given depth in ROI.

2.3.5 *Linearity of elastography with loading*

Across the three linear loading conditions, removal of NCT increased the Pearson coefficient of mean muscle elasticity in 7 or 11 subjects for both ECU and TRI. In subject-muscle conditions for which the linearity was already moderate or low, the removal of NCT had varying effects on linearity. Muscle elasticity values for each subject, muscle, and task with and without NCT, and the Pearson coefficients for elasticity across the linear loading conditions are displayed in Table 2.

Table 2: Effect of NCT removal on the linearity of muscle elasticity across linear loading conditions

Data	Task #	Subjects										
		S1	S2	S3	S4	S5	S6	S7	S8	S9	S10	S11
ECU All	2	164.92	237.42	173.58	85.84	155.03	180.33	182.60	217.10	183.85	181.23	342.44
	1	252.91	273.03	314.37	118.29	312.04	278.27	334.10	232.93	265.79	202.05	391.83
	3	279.50	312.87	339.67	100.69	324.25	298.04	324.92	221.80	284.15	272.76	359.26
	<i>r</i>	0.955	0.999	0.928	0.457	0.897	0.934	0.838	0.289	0.939	0.954	0.335
ECU noNCT	2	163.42	226.91	161.40	112.49	143.36	160.50	168.76	218.31	171.92	171.97	340.08
	1	248.79	280.68	298.15	144.18	311.70	269.92	323.64	244.01	245.75	177.58	377.33
	3	278.25	328.26	355.84	106.51	326.06	280.10	321.38	230.43	268.93	261.87	354.63
	<i>r</i>	0.963	0.999	0.974	-0.148	0.899	0.902	0.860	0.471	0.957	0.893	0.387
TRI All	2	18.67	12.21	30.51	7.61	16.25	15.06	68.42	17.12	4.44	5.98	35.98
	1	57.69	113.05	51.92	7.36	68.49	19.06	86.85	52.65	12.01	40.25	76.39
	3	55.64	113.14	54.41	33.27	94.62	64.76	79.07	57.62	28.99	72.57	87.75
	<i>r</i>	0.842	0.866	0.909	0.862	0.982	0.900	0.576	0.917	0.976	1.000	0.951
TRI noNCT	2	13.91	10.46	32.04	7.72	16.19	15.13	74.84	17.15	3.69	5.40	32.16
	1	44.27	95.14	54.67	7.59	67.67	19.15	91.09	51.96	11.98	40.36	74.96
	3	49.25	103.20	57.42	35.23	90.61	64.94	82.07	58.03	30.30	72.49	86.97
	<i>r</i>	0.924	0.903	0.911	0.864	0.976	0.900	0.444	0.927	0.977	1.000	0.951

2.3.6 Rank order of tasks

Due to the complex loading configurations and the presence of multiple degrees of freedom in the activation patterns of multiple muscles for resisting against each loading configuration, the amount of activation in ECU and TRI for each configuration was expected to be variable between subjects. Accordingly, the rank order of tasks was determined based on mean shear modulus in each subject. When NCT was not removed, the mean shear modulus at the lowest and highest ranks were 59.6 ± 19.1 and 122.8 ± 32.0 kPa for ECU and 3.2 ± 1.9 and 47.6 ± 20.6 kPa for TRI, respectively. When NCT was removed, they were 56.8 ± 19.2 and 123.2 ± 29.3 kPa for ECU and 3.1 ± 2.0 and 48.2 ± 21.1 kPa for TRI, respectively. The differences in rank order of the tasks by mean shear modulus due to the inclusion/exclusion of NCT were determined within subjects in each muscle. Out of 13 ranks, the error at each rank ranged from 1 to 6 instances for

ECU and from 0 to 6 instances for TRI, respectively. In total, rank errors occurred in 51 instances for ECU and 33 instances for TRI, respectively, out of 143 possible instances across all tasks and subjects (Figure 11). These rank errors corresponded to the error rate of 36% and 23% in ECU and TRI, respectively.

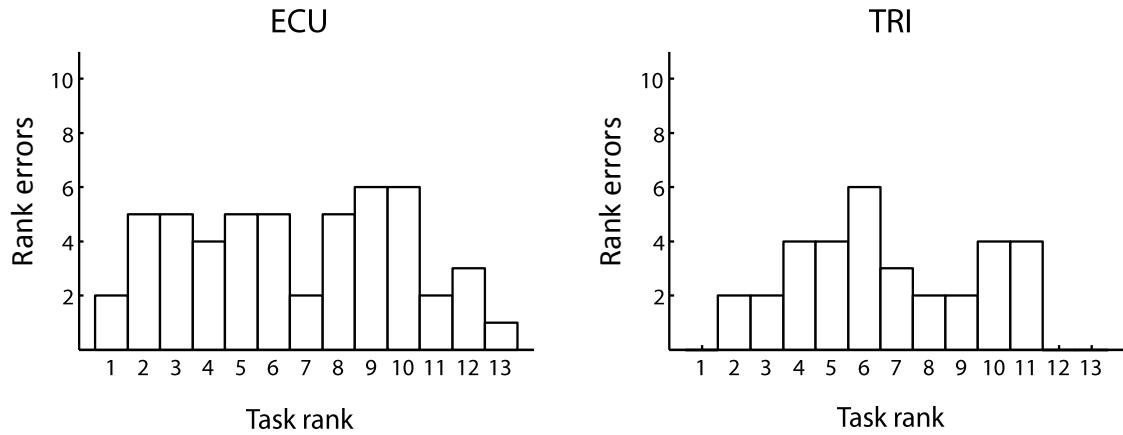


Figure 11: Histogram of errors in determining the rank order of tasks based on mean shear modulus. For each subject, tasks are ranked from lowest to highest mean shear modulus with and without NCT. Rank order without NCT is displayed along the x-axis. The number of subjects for which the rank without NCT differs from the rank with NCT is tallied for each task ranking.

2.4 Discussion

The current study developed image processing algorithm for automatically removing NCT from ultrasound elastography videos of contracting muscles and found substantial effects of removing NCT on the assessment of muscle shear modulus in ECU and TRI, including the changes in the rank order of mean shear modulus across various muscle loadings.

2.4.1 *Image processing algorithm*

For identifying NCT from an ultrasound image, a clustering algorithm based on the intensity values of the B-mode image was employed. In the musculoskeletal system, muscle pennation angle, thickness and volume have been estimated from ultrasound and MRI images both manually and with automatic image processing^{80,81,87}. For image processing, these features are often captured using edge or line detection algorithms such as the Hough transform⁸⁷, intensity gradients⁸⁰, and other standard methods. For identifying NCT from an ultrasound image, a method that identifies areas instead of edges and lines is more appropriate. This sort of image segmentation has been performed primarily based on intensity values⁸³ or, if intensity values do not differ, visual texture of the captured tissues.⁸⁶ As the tissues of interest here were distinguishable by their differing intensities, the clustering algorithm was based on these intensity values. Clustering has been used to capture multiple tissues by minimizing the combined intra-cluster variance (kmeans), with some variations (cmeans, a probabilistic grouping)⁸³. For the developed algorithm, Otsu's method was implemented for just two groups, NCT and contractile muscle tissues. This clustering produced an intensity threshold separating areas of high-intensity pixels (NCT) and low-intensity pixels (contractile muscle tissues). As Otsu's method alone was not expected to provide adequate NCT detection ($\geq 90\%$ correctly identified) across subjects and muscles, optimization was used to modify the intensity threshold and elongate the clusters to reflect the band-like shape of the NCT.

By building upon established clustering methods, the currently algorithm was developed to produce the largest amount of correctly identified NCT and contractile tissue (Results: 90.01% of NCT, 81.46% contractile tissue). Optimization of the involved parameters for multistep culling and lengthening of identified tissues enhances the segmentation. Allowing the optimization to dictate the thresholds and multipliers showed that Otsu's method itself did not produce optimal results as none of the parameter optimization iterations selected the parameter set. Further, 23% less NCT was identified without optimization. Collectively, the addition of optimization beyond basic black-white thresholding provides additional accuracy of tissue segmentation for removal of NCT and is therefore expected to optimize the calculation of muscle shear modulus.

2.4.2 *Elastography data*

The wide range of shear modulus confirms that subjects produced various levels of muscle contractions in ECU and TRI for holding a robotic handle that received different combinations of forces and torques. The range of shear modulus across loading configurations was about 2-fold from 60 to 123 kPa for ECU and about 15 times from 3.2 to 48 kPa for TRI. In the triceps brachii, shear modulus at rest has been reported as 3-10 kpa^{68,72}, suggesting that some of the tasks in this study may have left the triceps at or close to a resting state. Though there is no report on shear modulus of the contracting triceps muscle, shear modulus up to 47 kPa in the current study is within the reported changes in the contracting elbow flexors: 5-60 kPa during contraction from 0-35%MVC¹⁵ and at 25-200 kPa during contractions from 0-70%MVC⁸⁸. While there is no report on

shear modulus for resting or contracting ECU, the lowest value of 60 kPa in the current study is higher than the resting value in other muscles (10 kPa or below). It is likely that ECU was contracting across tasks as subjects were grasping the robotic handle throughout.

The appropriateness of the algorithm for NCT removal was demonstrated as a reduction in spatial variability (i.e. SD) of shear modulus within ROI across muscles. Since shear moduli of NCT are distinct from contractile tissues^{70,72}, the variability of shear modulus within the ROI was expected to be decreased with the “outlier” NCT removal. The amount of reduction in spatial variability of shear modulus is influenced by both the amount of outliers and the deviation of outliers from the shear modulus of the contractile tissue. The significant and greater amount of SD reduction in ECU compared with TRI after NCT removal is in line with the greater amount of outliers in ECU as its total amount of NCT area was greater compared with TRI. The deviation of outliers from the shear modulus of the contractile tissue can be altered depending on the contraction level of the contractile tissues. More variable reduction in SD across subjects in TRI compared with ECU may be related to the greater range of shear modulus across loading configurations that may have allowed for greater variability of contraction level in TRI. It appears that the currently developed algorithm for automatic NCT removal is sensitive enough to significantly influence the variability of shear modulus within ROI across muscles with different levels of contractions.

The impact of NCT removal on the assessment of shear modulus was expected as a reduction of mean shear modulus, assuming most of the NCT within images are connective tissues. Despite large variability of stiffness and NCT content across subjects,

a significant main effect of NCT removal on reductions in mean shear modulus was shown (Figure 9) in support of the hypothesis. With a significant interaction, the reduction in mean shear modulus due to NCT removal was significant in ECU, though not in TRI, indicating the reducing effect of NCT removal was greater and more consistent in ECU. Variations in the change in mean shear modulus with the removal of NCT can be due to 1) the amount of intramuscular connective tissue content and 2) the amount of adipose tissue, both of which are removed as NCT based on their high-intensity pixels. The former has high shear modulus while the latter has low shear modulus. The presence of many subjects who showed an unexpected increase in mean shear modulus after the removal of NCT in TRI implies that many TRI images appear to include large areas with lower shear modulus tissues, likely adipose tissue in the superficial level, and removal of this tissue counteracts the expected reduction of mean shear modulus via removal of higher shear modulus connective tissues. In support of this implication, NCT at the most superficial level made up the majority of overall NCT removal in TRI. Further, removal of superficial NCT was greater in TRI compared with ECU. These results are in favor of the suggestion that superficial adipose tissue with low shear modulus constituted the majority of NCT removal in TRI, which would counteract and prevent the decrease in mean shear modulus. Considering these examples of differences between muscles, it is conceivable that NCT removal may have various effects on mean shear modulus depending on individual cases, including the differences in individuals, muscles, constituents of muscles, location of ROI, and muscle contraction levels.

As elastography is expected to be used as an alternative measure of muscle contraction level ⁷¹, it is of great importance to understand how methods of image processing affect the assessment of relative muscle shear modulus across tasks or conditions within individuals. In particular, the assessment during variable loading tasks in interacting with a robotic system would be sensitively benefited by such understandings. Removal of the NCT is expected to improve the accuracy of assessing differences in contraction level by removing the “noise” introduced by data from the non-contractile elements. The removal of this noise appears to have benefited the linearity of elasticity data with linear loading, analyzed across Tasks 1, 2, and 3. In seven of eleven subjects in both TRI and ECU, the Pearson coefficient was increased. In other tasks, linearity was similar or slightly diminished. In subjects and muscles, the algorithm may have induced non-linearity or revealed the true non-linearity of the loading. Further analyses of these cases will be explored in future work

Regarding variable loading, removal of NCT in ECU altered the rank order of tasks by mean shear modulus in 36% of the tested cases within the 2-fold distribution across tasks. In TRI, it was altered in 23% of the tested cases within the 14-fold distribution across tasks. The lower occurrence of rank alteration in TRI compared with ECU may partially be due to the wider distribution of shear modulus across tasks in TRI. Nonetheless, the findings indicate that one out of 3-4 cases can be inappropriately ranked for mean shear modulus within individuals unless the NCT are removed. This finding is even more notable given that changes in mean shear modulus after NCT removal were small when the average values across subjects were compared. That such a large portion of tasks is ranked differently depending on NCT inclusion suggests a significant impact

of NCT on the comparison of muscle contraction level across tasks or configurations within individuals. In considering the potential clinical application of elastography in the assessment of a treatment in individual patients, for example, such a substantial impact of NCT within individuals would be critical.

Removing connective tissues has implications for the selection of a measurement area within the region of interest, as the measurement area would usually be a continuous region positioned in a region of uninterrupted contractile tissues. The included Q-BOX software in the ultrasound elastography device allows for circle shaped measurement areas of variable size, but uses all the values in the selected areas in its calculation. The vast majority of elastography studies are conducted on larger muscles of the proximal arm or leg, where there is ample muscle volume from which to take shear modulus measurements^{15,17,68,88}. Although the report is on animals (cow forelimb), distal muscles appear to have greater amounts of connective tissues compared with the proximal muscles⁸⁹. In small muscles or where there is higher concentration of NCT in the distal muscles like ECU, available uninterrupted contractile tissues may be limited and potential measurement areas will likely be closer to bands of connective tissues. The developed image processing algorithm would especially be helpful in these situations where a selection of more flexible and appropriate measurement area with NCT removal is required. These considerations are also applicable to configurations where muscles are likely to lose contractile tissues and/or gain NCT (e.g. limb immobilization, muscular dystrophy), especially for the assessment within individuals.

Identification of NCT and removal of corresponding elasticity values from the calculation of mean shear modulus was performed with the current assumption that the

presence of NCT did not significantly affect measurements in the surrounding contractile tissues. The examination of this assumption is beyond the scope of the present study geared toward application and would require a systematic modeling and/or experimental study in a different research design. The focus of this work was to provide an improvement upon the conventional (i.e. manual) method of image analysis and data recording. The developed algorithm has fundamental features that may be applied beyond the scope of the current study. For shear modulus determination, the direct application of the algorithm to resting muscle is possible, in which analysis of a single frame would be sufficient. The application of the NCT identification portion would be generalizable to B-mode images from other ultrasound systems as well and will likely provide an improvement over a simple application of Otsu's intensity based thresholding method. Efforts were made not to use absolute cutoff values for the algorithm, but to instead use multipliers and quantiles that would naturally adjust to the image quality and architecture of the muscle of interest. Only small adjustments, if any, would be needed when applied to other muscles or used on images from other systems.

2.5 Conclusion

The developed algorithm with an optimized clustering and thresholding algorithm successfully removed NCT from muscle elastography videos as supported by reductions in the spatial variability of shear modulus in the ROI in forearm and upper arm muscles. Removal of NCT can alter the spatial mean value of shear modulus and altered the rank order of various static motor tasks based on mean shear modulus when compared with

rankings with NCT included. These results suggest that NCT can be automatically removed in the analysis of elastography, and NCT removal has a substantial impact on the comparison of mean shear modulus across motor tasks with various loading configurations.

CHAPTER 3. EFFECTS OF VIBRATION AND CO-CONTRACTION ON NEUROMOTOR OSCILLATIONS AND STEADY MUSCLE ACTIVATION

3.1 Introduction

When interacting with an unstable environment or a vibrating object (e.g. power tools), we naturally co-contrast antagonistic muscles.⁹⁰⁻⁹² Steadiness of the co-contracted muscles would influence the stability of the unstable or vibrating object being manipulated. While there are numerous studies on steadiness during contractions that do not require substantial co-contraction of antagonistic muscles^{42,63} or after vibration^{52,93,94}, neurophysiological mechanisms underlying steadiness in motor output during contraction or vibration are not well studied or understood. Vibration of a muscle acutely increases the afferent input from muscle spindles⁹⁵⁻⁹⁷ that can influence oscillatory neural activity of the corresponding motor cortex and muscle.^{38,39} Co-activation of antagonistic muscles can alter the discharges of muscle spindles⁹⁸, amplitude of stretch reflex⁹⁹, and recruitment of the corticomotor neurons.³² Muscle vibration is applied as a part of neuromotor rehabilitation for stroke survivors¹⁰⁰⁻¹⁰², and co-contraction is often increased in various clinical populations with neuromotor impairments (e.g. cerebral palsy, stroke).¹⁰³⁻¹⁰⁵ With the involvement of unique neural pathways and clinical applicability, it is imperative to first understand the effect of vibration and co-contraction on neural activity for steady motor output in healthy adults.

During steady control of muscle contraction, neural oscillations in beta-band are prominent in the motor cortex and muscle, and their correlated oscillations have been determined as beta-band corticomuscular coherence (CMC). The role of beta-band CMC is not fully understood, but correlations with steady motor control have been proposed^{44,45}. As a functional consequence during steady contraction, a positive correlation was reported between the amount of beta-band CMC and low-frequency oscillations in mechanical motor output during ankle dorsiflexion⁴⁵. It is unknown how sustained vibration and muscle co-contraction influence these neural oscillations and their associations. Co-contraction about the wrist is of particular interest for its role in precision tasks of the hand and interactions of the hand with unstable environments. For stabilizing the wrist joint in the flexion-extension plane, the flexor carpi radialis (FCR) and the extensor carpi radialis (ECR) have unique neural pathways compared with other limb muscles, lacking recurrent inhibition of I-originated reciprocal inhibition¹⁹. The purpose of this study was to understand the effects of sustained vibration and muscle co-contraction on beta-band neural oscillations, steady motor output, and their relationships in the wrist muscles in healthy young adults.

Accurate control of motor output level is important when attempting to perform a stable task, particularly during joint stabilizing co-contraction where the activation level of opposing muscles must be appropriate. In many limb muscles, Renshaw cells from agonist motor neurons inhibit Ia inhibitory interneurons to the antagonist motor neurons, thus disinhibiting the antagonist^{27,106}. This recurrent inhibition is facilitated during co-contraction²⁴ where antagonist disinhibition would be advantageous, whereas this pathway of recurrent inhibition is uniquely absent between FCR and ECR¹⁹. Instead,

recurrent inhibition can mutually inhibit both FCR and ECR motor neurons ²⁰. This means that during FCR contraction and co-contraction, Ia afferent input to ECR can involve both group I inhibition and recurrent inhibition of FCR. While electrophysiological observation with conditioned H-reflex in a couple of subjects suggested abolishment of Ia-originated inhibition during co-contraction in the wrist muscles ¹¹, their generalizability and functional impact on the control of muscle activation level is unclear. The unique inhibitory mechanisms in the wrist muscles would be incapable of attenuating Ia-originated antagonist inhibition and cause a tendency toward undershooting an intended amplitude of agonist activity during co-contraction. Hence, the first hypothesis was that ECR vibration would reduce FCR activity, and this reduction would not be attenuated by co-contraction.

As related to the application of vibration, beta-band CMC during steady contraction is transiently reduced by a brief stimulation of the peripheral nerves ^{38,39} probably because the briefly increased afferent input supersedes the descending drive. This suggests that sustained afferent input would lead to a net reduction in beta-band CMC across the stimulation period. However, accommodation within the afferent network may allow recovery of beta-band CMC given enough time. As related to co-contraction, involvement of Renshaw cells mediating mutual recurrent inhibition between antagonistic muscles ²⁰ may reduce beta-band CMC during co-contraction because greater recurrent inhibition is associated with attenuated beta-band CMC at least during agonist contraction ⁴⁹. The potential alteration in the recruitment of corticomotor neurons during co-contraction ^{30,32} may also lead to reduced CMC. Taken together, the second hypothesis was that beta-band CMC is reduced by vibration and by co-contraction.

Lastly, steady motor performance results from a combination of controlling the mean level and minimizing fluctuations in muscle activity. Given that beta-band CMC is associated with stable tasks while beta-band CMC is variable between muscles³¹, it is important to understand the relationship between beta-band CMC and fluctuations in motor output in specific muscles of interest. In the agonist contraction with the ankle dorsiflexors, the amount of beta-band CMC in the tibialis anterior is correlated with the amount of low-frequency (delta-band: 1-3 Hz) oscillations in the dorsiflexion force⁴⁹. It is unknown whether the association between beta-band CMC and low-frequency oscillations in motor output also exists during co-contraction and in the wrist muscle. Low-frequency fluctuations of mechanical motor output (i.e. force) reflect those of neural motor output including the motor unit discharge rate and rectified EMG^{107,108}. Hence, the third hypothesis was that the amount of beta-band CMC is correlated with low-frequency power in rectified EMG (i.e. unsteadiness) during co-contraction of the wrist muscles.

To test the above-mentioned three hypotheses, the effects of co-contraction and vibration on neural activity in terms of its oscillations and magnitude were examined for the wrist joint muscles (FCR and ECR) in healthy young adults.

3.2 Methods

3.2.1 Subjects

Forty healthy young adults (20.8 ± 3.4 year old, 19 men, 11 women) participated in the study. All subjects were right-handed, as confirmed by the Edinburgh handedness inventory¹⁰⁹. Participants did not have a history of injury or disorders that may affect the nervous and/or musculoskeletal systems such as brain or nerve disorder, arthritis, fractures in arm (within the past two years), sensory deficits in arm, diabetes, or use of medication that affects muscle control and/or brain and nerve function. Participants with skin allergies that might be affected by the adhesives and other materials used for the study were also excluded. All subjects gave written consent in accordance with the Institutional Review Board of the Georgia Institute of Technology.

3.2.2 *Motor task*

For the assessment of neuromotor oscillations and amplitudes during wrist stabilization, FCR and ECR were selected because 1) their spinal mechanisms have been investigated and characterized in several studies^{18-20,110}; 2) distal limb muscles have a greater number of corticomotor neurons and are expected to have significant corticomuscular coherence^{29,30}; and 3) their muscle bellies are superficial and thus accessible for vibration. The wrist stabilization task involved intentional flexion-extension co-contraction to simulate the activation of true antagonists at a hinge joint and emphasize the antagonist activity of FCR and ECR.

Subjects were seated in an electrically shielded, dimly lit room. The right arm was tested in the motor task. The right forearm and hand were stabilized in a brace affixed to a small table such that the wrist was constrained in the neutral position between

supination and pronation in a lightly padded arm brace. In this orientation, contraction of wrist flexor and extensor muscles corresponded to the force production toward left and right, respectively. The right shoulder was abducted 15° and flexed 35° . The left arm was rested on the armrest of the chair. The legs were not crossed and the knees were flexed to 90° .

Subjects performed maximal voluntary contractions (MVC) with wrist flexors and extensors independently to determine the maximal amplitude of EMG in FCR and ECR. The MVC task involved a gradual increase in muscle activation from zero to maximum effort over 3 s with maximal effort held for 2 to 3 s. Subjects were asked to perform the task in either wrist flexion or extension three times in alternating order. Root mean square amplitude of EMG was computed during the recording. Verbal encouragement was given to achieve maximal effort while visual feedback of the EMG amplitude was displayed for the appropriate muscle. Three to four trials were performed for each muscle group, and the maximal EMG amplitude across trials was determined in FCR and ECR.

After the MVC task, subjects performed two contraction types of steady motor tasks: 1) isometric contraction of elbow flexors and 2) co-contraction of elbow flexors and extensors. For both tasks, the target amplitude of EMG was 15% of maximal EMG during MVC for each muscle. For each contraction type, there were three conditions in muscle vibration: 1) no vibration, 2) FCR vibration or 3) ECR vibration. Thus, subjects performed six (2×3) contraction-vibration combinations. Subjects were instructed to minimize movement of the head and body, including eye movement or blinks, during the

trials. Trials during which excessive movement occurred were discarded and subjects were asked to repeat the trial.

Prior to each trial, the experimenter informed subjects of which contraction type to perform, but not the vibration condition. The experimenter then adjusted the visual feedback such that only instructed muscles were presented to the subject (i.e. ECR was not displayed to the subject during elbow flexion), and instructed the subject to proceed with target matching. Once the EMG amplitudes matched the targets steadily for 2 s, the vibration condition began and lasted for 17 s, and was then turned off. Subjects continued matching the targets after vibration ended until they were instructed to relax. At least 1 min of rest was given between trials, with extra time provided as needed to avoid neuromuscular fatigue or to alleviate any discomfort by removing the arm from the brace temporarily. Each subject completed six trials of each contraction-vibration combination in random order.

Visual feedback of EMG amplitudes was provided as two vertical bar graphs: FCR feedback to the left and ECR to the right to reflect the direction of flexion or extension, respectively. For both bar graphs, a red line marked the 15% MVC target and was positioned at the vertical midpoint. Each bar showed EMG amplitude between 0% MVC and 30% MVC. The height of the bar from 0% MVC and 30% MVC was 20 cm on the monitor that was placed 1.8 m in front of the subjects. As a result, the gaze angle between the baseline (0% MVC) and target (15% MVC) was approximately 3.2°. Each bar indicated the current amplitude of EMG and was refreshed at a rate of ~20 times/s. The target line was always visible even when the bar went above the target. The width of

the bars and target line was 5 cm. Knowledge of results on their motor performance was not provided to the subjects.

3.2.3 Vibration

Vibration was applied to the forearm muscles to increase afferent input. Distal to the EMG electrodes, small vibration units (Diameter: 12 mm, Model 312-101, Precision Microdrives, United Kingdom) were placed on the skin over the muscle bellies of FCR and ECR to apply ~100 Hz vibration with a peak-to-peak amplitude of ~0.3 mm. A custom-made battery box and switch system was built to manually control the vibration units and send a trigger signal to the EMG recording system. Each vibration unit was attached to a 20 × 20 × 5 mm plastic piece. Each unit was affixed over the muscle with vibration unit facing the skin, using stiff foam padding and tape. This configuration provided a comfortable but durable and firm attachment of the vibration unit to the skin surface. Prior to the trials, subjects confirmed their ability to detect which muscle was vibrated and reported any motor illusions caused by the vibrations with eyes closed or open, and with muscles contracted or relaxed. Pilot experiments confirmed that neither electrical nor mechanical artifacts were evident in the neural signal recordings.

3.2.4 Recordings

Surface EMG of the right FCR and ECR and EEG of the left motor cortex at C3 were recorded with the ActiveTwo Biosemi electrode system (Biosemi, Amsterdam, The

Netherlands). Examples of these raw signals during and after vibration are shown in Figure 12. This system is equipped with a miniature preamp adjacent to each electrode to reduce the contamination of electrical noise. To further reduce the noise, this system includes a battery-powered A/D box that digitizes the signals and transfers them to a computer through a fiber optic connection. Two active Ag-AgCl EMG electrodes (diameter: 4 mm) were placed over the belly of each muscle 2 cm apart. Electro-oculogram (EOG) signals were also collected to capture eye or facial movement. The ground electrodes for the system were attached to the scalp near the apex of the head. The ActiveTwo system used a gain of least significant bit equal to 31.25 nV, with a 1% gain accuracy. All signals were sampled at 2048 Hz and digitized on a computer using ActiView software (Biosemi, Amsterdam, The Netherlands). The signals were monitored in real-time via a user interface constructed in LabView (National Instruments, TX, USA). The LabView interface was further modified to include visual feedback of EMG amplitudes to the subjects. In the visual feedback with bar graphs, each bar indicated the current amplitude of EMG in a bipolar configuration.

3.2.5 Data analysis

Data during the steady state of task performance (the last 15 s of the task vibration ON) were used for statistical analysis. For each contraction-vibration combination, data from all 6 trials in each subject were concatenated into one record of 90 s for further processing. Data were analyzed using custom-written script in MATLAB (Mathworks, Natick, MA, USA).

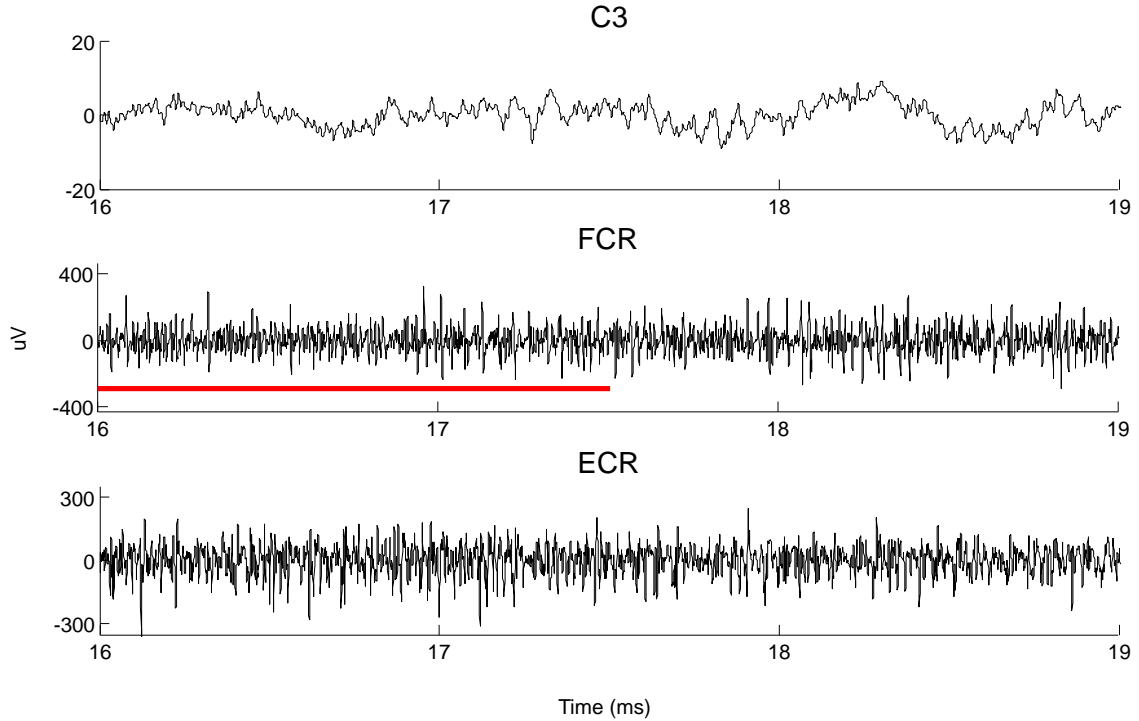


Figure 12: Representative recording of EEG at C3, EMG of FCR, EMG of ECR during co-contraction. In this example, vibration was applied to FCR (horizontal red line denotes vibration). Time was relative to the start of vibration.

EMG of FCR and ECR was calculated in a bipolar configuration and then bandpass filtered (10-500 Hz). Root mean square amplitude of EMG was calculated to determine the amplitude of EMG. EEG from C3 was bandpass filtered (5–200 Hz) and detrended. EOG collected superior, inferior and lateral to each eye were monitored in real-time for eye blinks and other artifacts of facial movement that could corrupt the EEG signal. Tasks during which EOG signals showed the mentioned artifacts were repeated and the original data was excluded from analysis. To obtain CMC in the beta-band (14-35 Hz), EEG in the left motor cortex at C3 and unrectified EMG in the right FCR were used in the following calculation. CMC is the linear relationship between cortical and

muscular signals in the frequency domain. Unrectified EMG was used as rectification may introduce noise, has inconsistent effects, and is unnecessary to detect coherence^{39,111}. CMC was calculated from the auto- and cross-spectra of the involved signals as described in Halliday et al¹¹²:

$$C_{xy} = P_{xy}^2 / (P_{xx} \cdot P_{yy}) \quad (1)$$

where P_{xy} is the cross-spectrum of the EEG and EMG signals and P_{xx} and P_{yy} are the auto-spectra. The CMC values were calculated at 1 Hz resolution using a 0.5 second (1048 point) Hann window without overlaps in order to avoid including concatenated ends within a given window. The total area under the C_{xy} graph and peak within the beta-band were calculated for each contraction-vibration combination. The confidence interval of CMC was calculated as described in Rosenberg et al¹¹³:

$$CI = 1 - (\alpha)^{(1/(L-1))} \quad (2)$$

where L was the number of segments included from the signal, or the signal length divided by the window length used, and α was the level of significance set to 0.05. CI was used to determine whether peak CMC was significant. The arc hyperbolic tangent transform of the CMC values was used to stabilize the variance in the distribution of coherence¹¹² in preparation for statistical analyses. In the course of this CMC calculation, spectral power of EEG at C3 and EMG of FCR was obtained for the absolute beta-band power and as a percentage of total power.

There are reports that used rectified EMG rather than unrectified EMG in the calculation of CMC^{38,44,45,49}. To supplement the examination of CMC, beta-band CMC

between EEG and *rectified* EMG were also determined in the same manner as described above. Auto-spectra of EEG, unrectified EMG, and rectified EMG were used to calculate the beta-band power normalized to all signal power from 1-75 Hz (delta thru gamma-bands) in each signal. Low-frequency oscillations in muscle activation can be extracted from low-frequency power in rectified surface EMG ¹⁰⁷. To examine the amount of low-frequency fluctuations in muscle activation, spectral power for rectified EMG within the delta-band (1-3 Hz) was obtained and normalized to all signal power (1-75 Hz) in the course of this supplementary CMC calculation.

3.2.6 *Statistical analysis*

Dependent variables were beta-band CMC using unrectified EMG and rectified EMG from FCR, beta-band power in EEG at C3 and unrectified EMG in FCR, mean EMG amplitudes of FCR and ECR, and delta-band power in rectified FCR EMG. Effects of contraction type and vibration on these variables were tested with a two-way analysis of variance (ANOVA) with repeated measures.

Given the hypothesis that beta-band CMC would be reduced by co-contraction and vibration, data from subjects whose peak CMC reached significance in flexion without vibration were used for ANOVA on CMC: twenty-six and twenty-four subjects for CMC using unrectified and rectified EMG, respectively. Bonferroni post-hoc analysis was performed for pair-wise comparisons when appropriate. To find the potential association between beta-band neuromotor oscillations and low-frequency oscillations in muscle activation, linear regression analysis was performed for beta-band

CMC and relative power for beta-band EEG and beta-band unrectified EMG in relation to relative delta-band power in rectified EMG across all subjects. An alpha level of 0.05 was chosen for determining statistical significance. $P < 0.05$ and $P < 0.01$ are noted when significant.

3.3 Results

3.3.1 EMG amplitudes during vibration

Representative FCR amplitude data, expressed as %MVC, is shown in Figure 13. Amplitudes are shown from 1 second prior to vibration onset until 8 seconds after onset. While there is no obvious transient response to the onset of vibration, there are some trends of facilitation and inhibition developing over time, despite the supplied visual feedback. Note the unsteadiness of the signal, particularly the low frequency oscillations. This activity was expected to be captured in the analysis of delta-band oscillations in the rectified EMG.

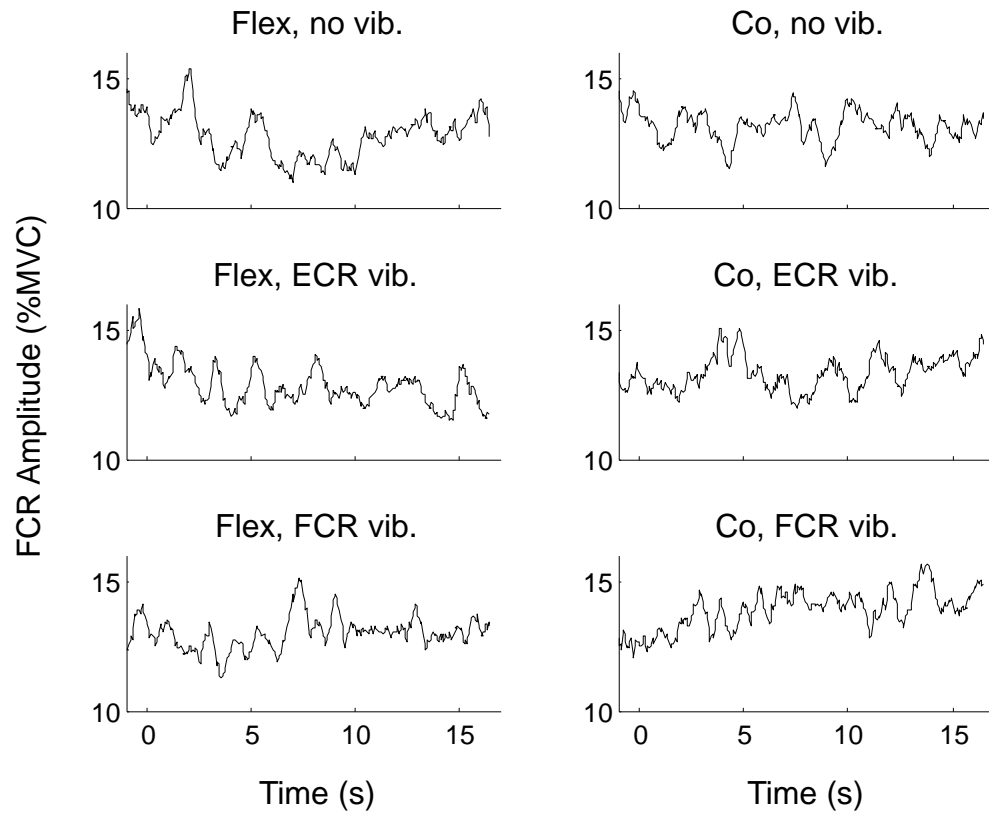


Figure 13: Representative FCR amplitude (%MVC) from 1 second prior to vibration onset to 17 seconds after.

Despite the presence of real-time visual feedback, the mean EMG amplitude in FCR was less than the target level (15% MVC) across conditions, on average (Figure 14). With a main effect of vibration condition ($P < 0.01$), the mean EMG amplitude was reduced during ECR vibration by 2.3% compared with no vibration ($P < 0.05$) and 3.6% compared with FCR vibration ($P < 0.01$). There was no significant effect of contraction type on the mean EMG amplitude.

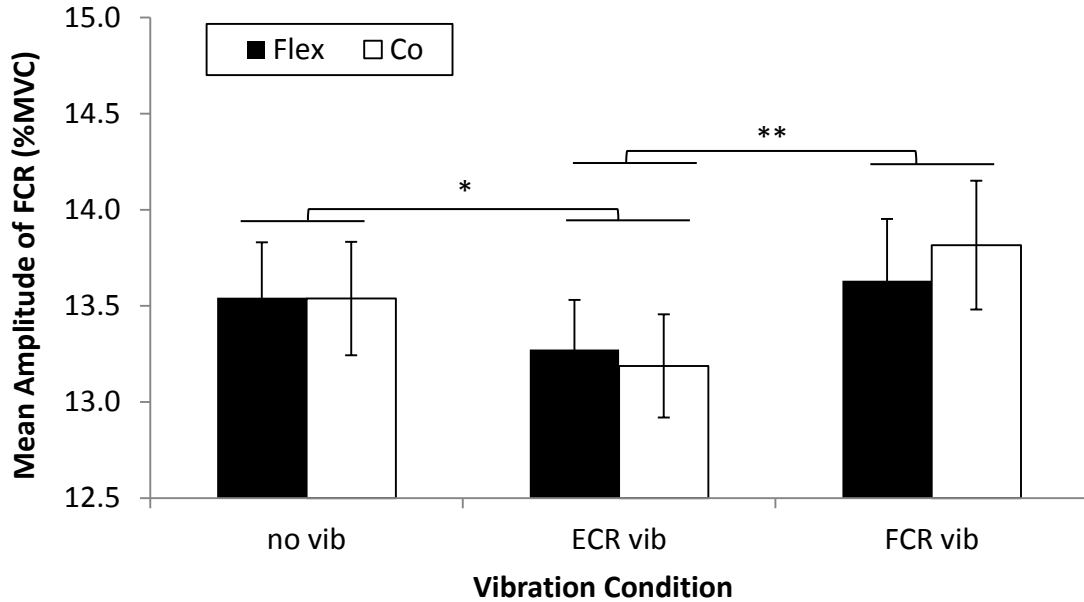


Figure 14: Effects of vibration and contraction type on mean EMG amplitude of FCR. * $p < 0.05$, ** $p < 0.01$, * $p < 0.001$**

The two-way ANOVA of ECR amplitudes revealed significant effects for task and vibration (Figure 15). ECR vibration increased ECR amplitudes by 8.3% relative to the no vibration condition ($p < 0.001$) and by 7.9% relative to the FCR vibration condition ($p < 0.01$). Also, ECR amplitudes were greater during co-contraction than during flexion ($p < 0.001$) as expected.

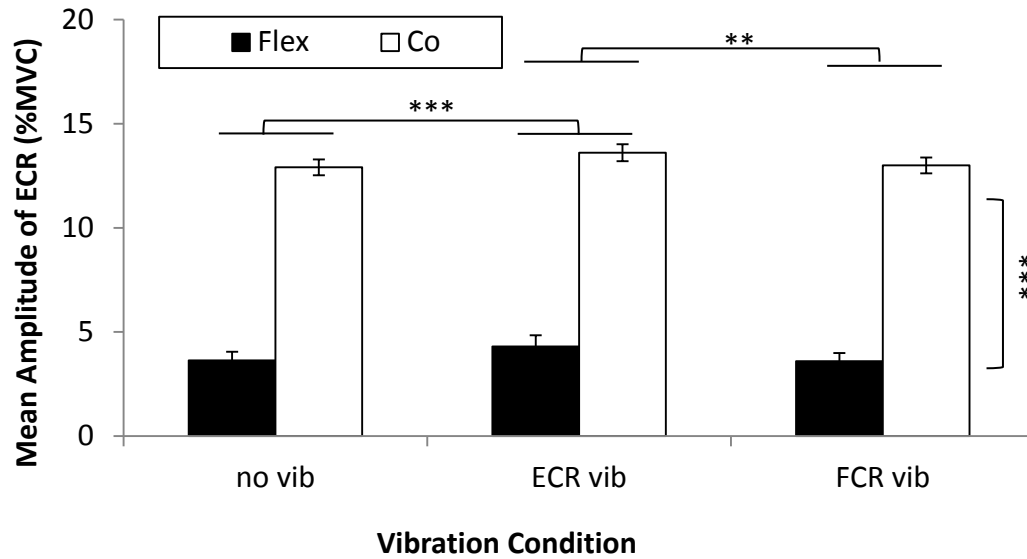


Figure 15: Effects of vibration and contraction type on mean EMG amplitude of ECR. * $p < 0.05$, ** $p < 0.01$, * $p < 0.001$**

3.3.2 Beta-band oscillations and coherence

The following figures are representative examples of the beta-band neural oscillations of focus in this chapter. In Figure 16, power in unrectified EMG of FCR, EEG from C3 over the left motor cortex, and coherence between these signals is shown for flexion and co-contraction without vibration. These graphs were generated from the concatenated 90 seconds of data across six trials of each condition. In the EMG power, there is a notable peak in the beta-band around 17Hz. The EEG power also has a peak in beta-band at around 19Hz. Coherence of these signals peaks at 17Hz.

CMC is presented over time from 1 second prior to application of vibration to 8 seconds after in application of vibration. Time windows of 500ms were advanced in 50ms increments. Note that coherence is non-stationary and fluctuates through time.

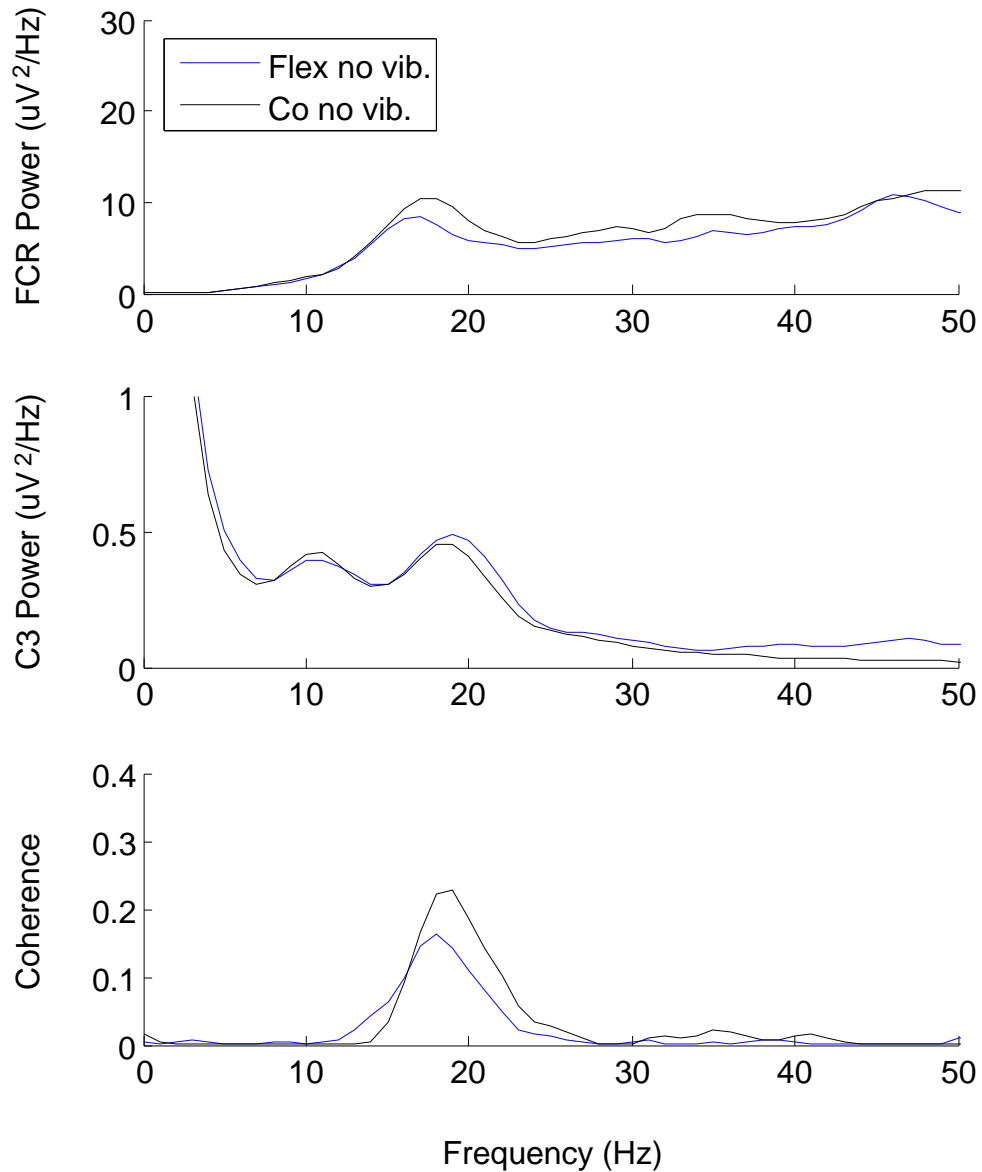


Figure 16: Unrectified FCR power, C3 power and FCR-C3 corticomuscular coherence in one subject

In Figure 17, power in unrectified EMG of FCR at 17Hz is presented over time from 1 second prior to application of vibration to 8 seconds after application of vibration. Time windows of 500ms were advanced in 50ms increments across each trial and averaged. A similar analysis for EEG power at 17Hz is shown in Figure 18. Note that 17Hz power shows low frequency oscillates throughout the time window, and that these signals appear to oscillate with similar timing.

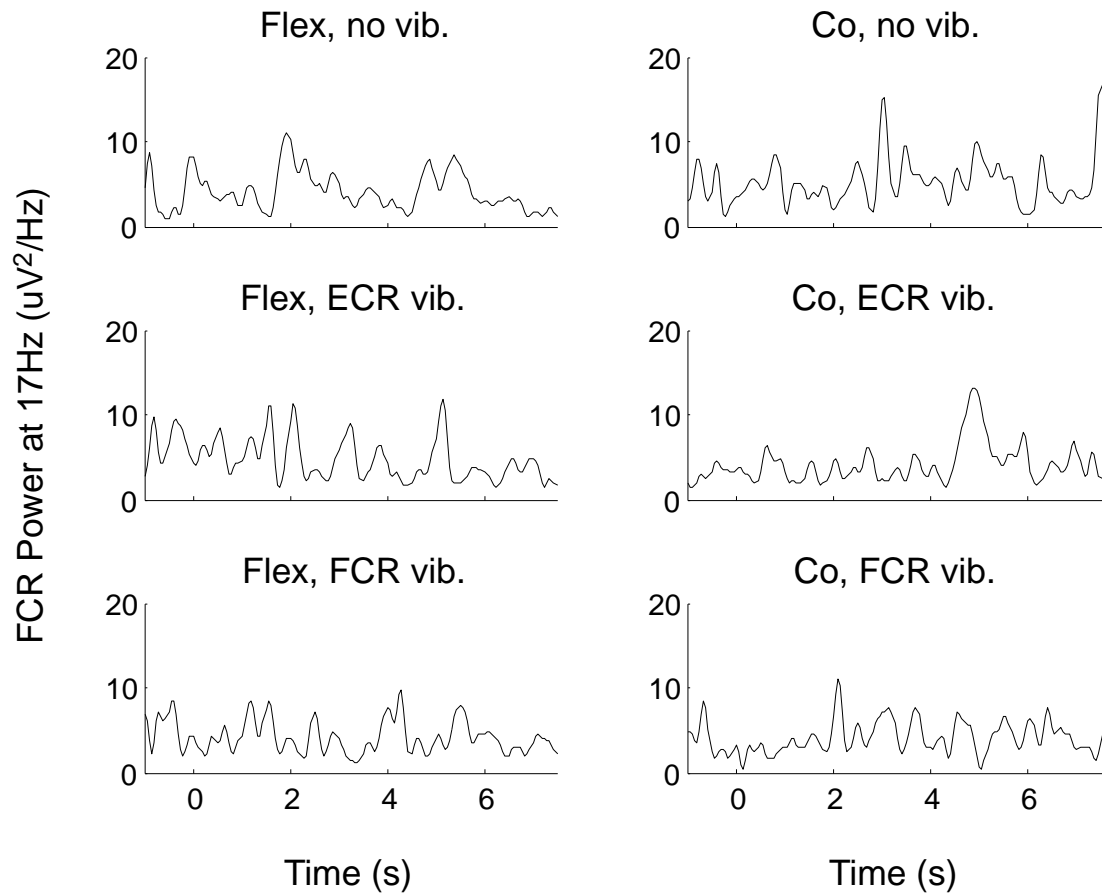


Figure 17: FCR power at the 17Hz, the peak frequency of CMC, during initiation of vibration in one subject. Vibration is applied at Time = 0.

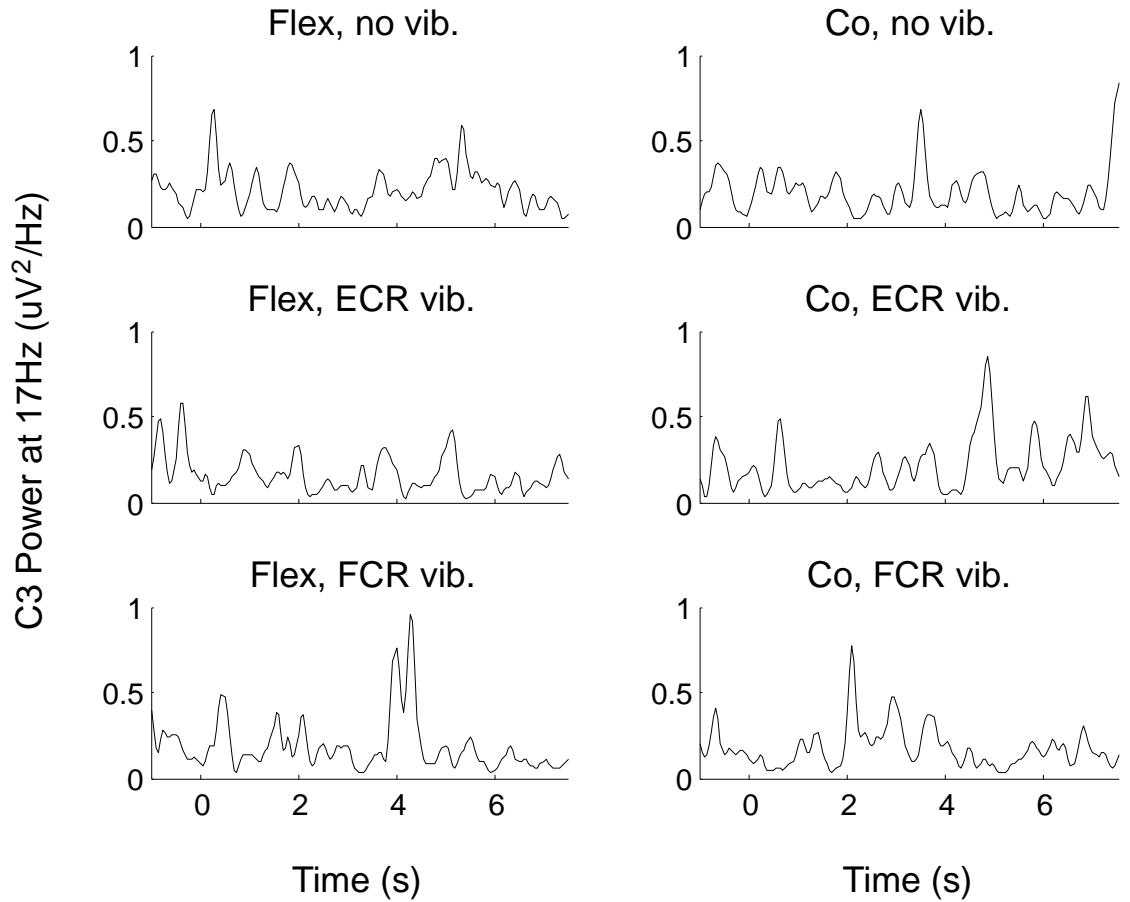


Figure 18: EEG power from C3 at 17Hz, peak frequency of CMC, during initiation of vibration in one subject. Vibration is applied at Time = 0.

In Figure 19, coherence from 0-40Hz is displayed over -1 to 8 seconds relative to vibration being applied. The dark blue represents non-significant coherence while the brighter colors represent significance coherence. Peaks in coherence can be seen at 17Hz with the characteristic fluctuations shown in the constituent signals. The same

analyses were done on EMG of FCR (Figure 20), EEG from C3 (Figure 21), and coherence (Figure 22) for the removal of vibration. Lastly, total beta-band coherence using the concatenated 90s of data across trials for each task and vibration condition is displayed in Table 3 for each subject. Amounts of coherence varied greatly across subjects.

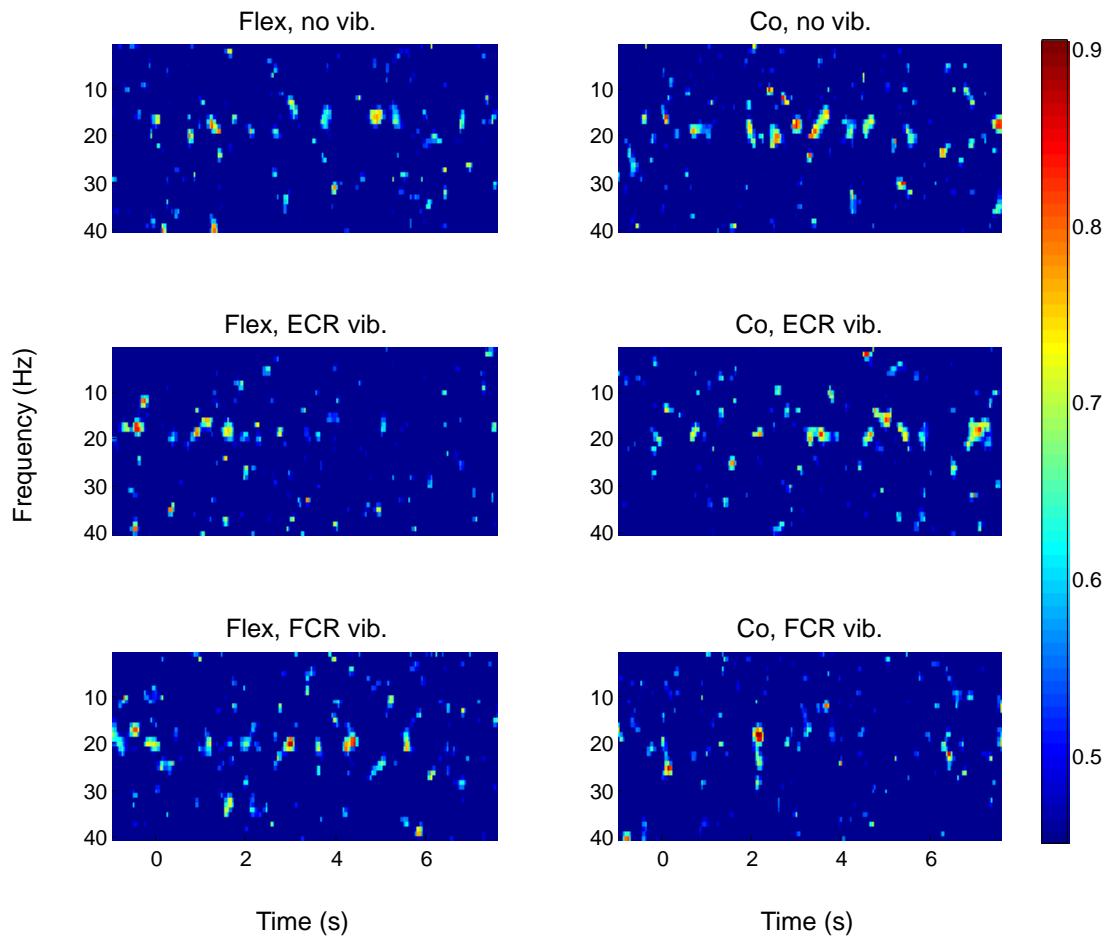


Figure 19: Coherence during initiation of vibration in one subject. Vibration is applied at Time = 0. The color scale for coherence is displayed to the right.

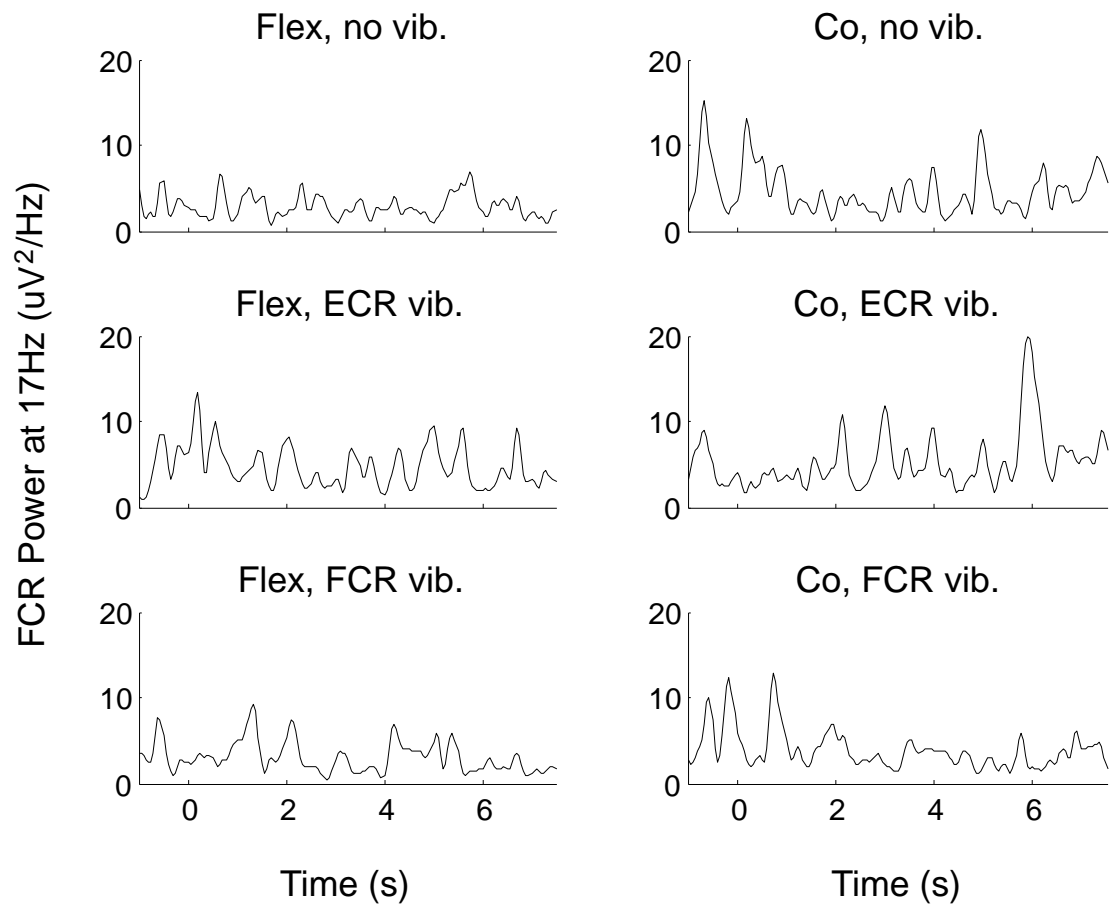


Figure 20: FCR power at the peak frequency of CMC during removal of vibration in one subject. Vibration is removed at Time = 0.

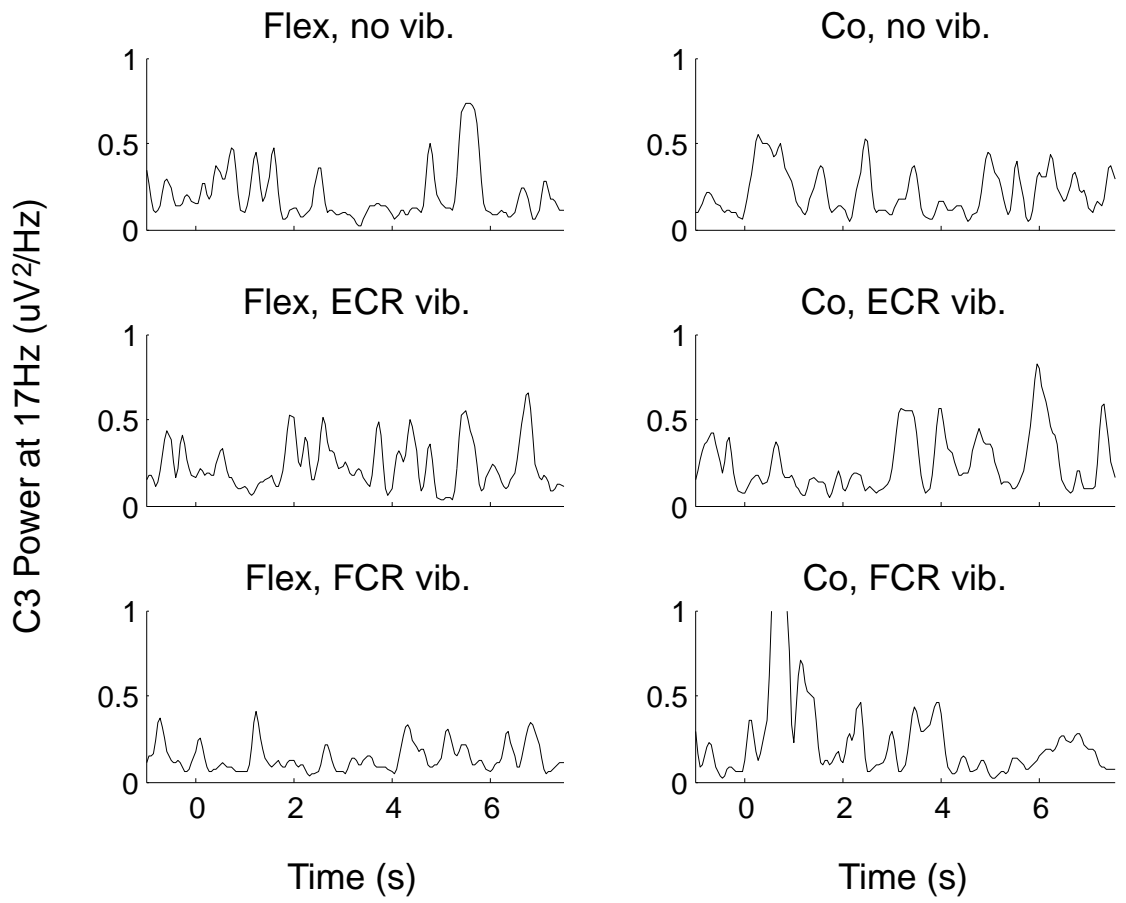


Figure 21: C3 power at the peak frequency of CMC during removal of vibration in one subject. Vibration is removed at Time = 0.

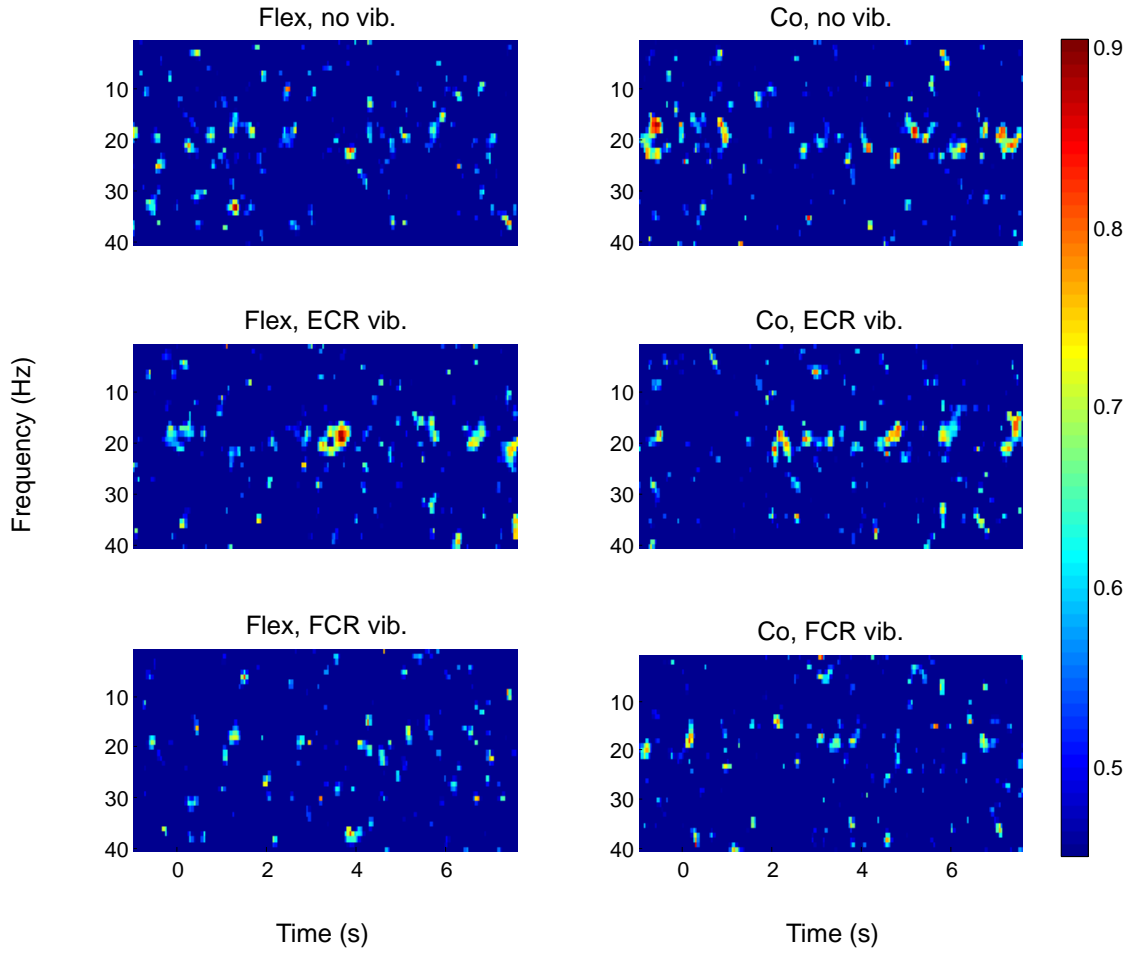


Figure 22: Coherence during removal of vibration in one subject. Vibration is removed at Time = 0.

Table 3: Total z-transformed total beta-band coherence for each subject

Subj.	Flexion			Co-contraction		
	no vib	ECR vib	FCR vib	no vib	ECR vib	FCR vib
1	1.91	1.54	1.38	1.49	1.63	1.59
2	1.18	1.34	1.78	1.53	1.11	1.43
3	1.48	1.94	1.87	1.05	1.79	1.29
4	1.75	1.35	0.84	1.61	1.46	1.65
5	1.80	1.29	1.07	1.47	1.39	1.61
6	1.67	1.36	1.37	1.55	1.58	1.21

7	1.44	1.09	1.45	1.87	0.91	1.11
8	1.48	1.55	1.90	1.43	1.11	1.34
9	1.68	1.11	1.88	0.91	1.20	1.41
10	1.53	1.73	1.25	1.47	0.95	1.26
11	1.46	1.27	1.87	1.35	1.54	1.11
12	1.47	1.59	1.46	1.30	1.73	1.40
13	1.44	1.30	1.68	1.47	1.51	1.30
14	2.13	2.01	1.45	1.82	1.67	1.82
15	1.68	1.18	1.87	2.15	1.01	1.44
16	1.95	1.56	1.29	1.36	1.17	1.23
17	0.98	2.43	1.65	1.23	1.34	1.13
18	1.80	1.77	2.00	1.31	1.55	1.76
19	2.49	2.18	2.20	1.35	1.63	1.20
20	1.45	1.27	1.23	1.24	1.40	1.81
21	1.26	1.51	1.03	1.86	1.60	1.77
22	1.91	1.69	1.20	2.72	2.46	2.42
23	2.06	2.20	1.26	1.54	1.84	1.59
24	1.49	1.40	1.58	1.35	1.53	1.30
25	1.97	1.92	1.95	1.67	1.26	1.76
26	2.06	1.26	1.03	1.63	1.56	1.35
27	1.76	1.30	1.32	1.31	1.45	0.88
28	1.32	1.18	1.55	1.41	1.34	1.16
29	1.18	1.22	1.28	1.52	1.31	1.20
30	2.67	2.53	2.05	1.48	2.23	2.07
31	1.49	1.37	1.45	1.31	1.36	1.56
32	1.65	1.67	1.62	1.94	2.23	1.29
33	1.86	0.95	1.52	1.15	1.21	1.61
34	1.52	1.44	1.24	1.82	1.37	1.96
35	1.62	1.24	1.35	1.57	1.27	1.53
36	2.05	1.51	1.46	0.90	0.83	0.98
37	4.26	4.42	3.85	5.45	3.82	4.57
38	1.49	1.49	1.29	1.38	1.37	1.05
39	1.52	1.49	1.28	1.38	0.93	1.50
40	1.28	1.51	1.59	1.50	1.31	1.64

3.3.3 Effects of vibration and co-contraction on beta-band CMC

Using unrectified EMG in the calculation of CMC, there was an interaction of contraction type and vibration ($P < 0.05$) on beta-band CMC. In the no-vibration

condition, beta-band CMC was reduced during co-contraction by 13.1% compared with flexion, on average ($P < 0.05$) (Figure 23). Compared with the no vibration condition, beta-band CMC was reduced with vibration of FCR and ECR by 16.9% ($P < 0.01$) and 11.9% ($P < 0.01$), respectively, during flexion. The number of subjects who maintained significant beta-band CMC in each task-vibration condition (i.e. vibration, co-contraction, or vibration during co-contraction) was also reduced to 11-14 (42%-54%) out of the 26 subjects who had significant CMC during flexion without vibration. For the 13 subjects that maintained significant CMC during co-contraction, there was no significant effect of vibration. There was no significant effect of contraction type or vibration on beta-band power of EEG. With a main effect of contraction type ($P < 0.01$), beta-band power of EMG was increased by 11.8% in co-contraction. When rectified EMG was used in the calculation of CMC, a similar trend was observed in the effect of contraction type and vibration on the mean values although no statistical significance was found.

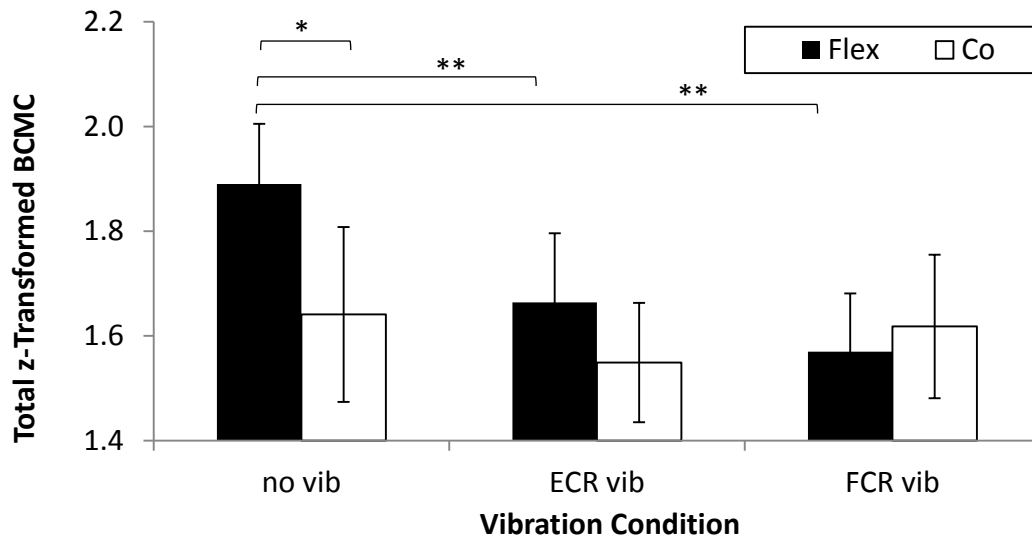


Figure 23: Effects of vibration and contraction type on beta-band CMC.

3.3.4 Beta-band oscillations and low-frequency oscillations in motor output

There was no significant correlation between beta-band CMC, whether rectified or unrectified EMG was used, and relative delta-band power in rectified EMG (

Table 4). In contrast, relative beta-band power in EEG was significantly correlated with relative delta-band power of rectified EMG across contraction types and vibration conditions ($P < 0.05$ or $P < 0.01$) except when vibration was applied to FCR during flexion. Relative beta-band power in unrectified EMG was significantly correlated with relative delta-band power of rectified EMG across contraction types and vibration conditions ($P < 0.05$ or $P < 0.01$).

Table 4: Correlation coefficient between beta-band neuromotor oscillations and delta-band power in rectified EMG.

Contraction Vibration	Flexion			Co-contraction		
	w/o	ECR	FCR	w/o	ECR	FCR
EEG Power (%)	0.364*	0.319*	0.192	0.341*	0.427*	0.479**
EMG Power (%)	0.343*	0.349*	0.317*	0.506**	0.562**	0.530**
CMC	0.011	0.085	-0.027	0.132	0.09	0.108
rCMC	0.02	-0.104	-0.106	0.182	-0.129	0.177

ECR, extensor carpi radialis; FCR, flexor carpi radialis; EEG Power, relative beta-band power in C3 EEG; EMG Power, relative beta-band power in unrectified EMG in FCR; CMC, corticomuscular coherence in beta-band; rCMC, beta-band corticomuscular coherence using rectified EMG in FCR. *, $P < 0.05$; **, $P < 0.01$

3.4 Discussion

There are three major findings in this study: 1) vibration of ECR reduced the mean EMG amplitude of FCR even during co-contraction; 2) beta-band CMC was reduced with co-contraction under no vibration condition and also with vibration of either muscle during flexion; and 3) low-frequency (delta-band) power of rectified EMG was not significantly correlated with beta-band CMC, but with beta-band power in EEG and unrectified EMG; and.

3.4.1 Muscle activation level

On average, the mean EMG amplitude being lower than the target level across tasks indicates that subjects tended to undershoot the visible target, possibly to avoid surpassing the target line. Since such avoidance was not instructed, the employed task details, including the fluctuating bar about a target line, might have produced unconscious constraints to the subjects. The significant reduction in the mean EMG amplitude of FCR due to ECR vibration during flexion is in line with the reduced EMG amplitude of the extensor carpi ulnaris due to antagonist extensor vibration during wrist extensor contraction with closed eyes ¹¹⁰, but in a smaller amount (2.3% vs. 12%). The smaller reduction is probably because the spatial resolution of the current visual feedback was high enough for subjects to prevent larger deviations in target matching, but too low to notice subtle changes in the mean amplitude of fluctuating EMG. Still, subjects were able to compensate for the excitatory effect of FCR vibration, but not for the inhibitory effect of ECR vibration. Antagonist ECR vibration can stimulate muscle spindles and lead to group I disynaptic inhibition to FCR in the spinal cord ¹¹⁰. Although the apparent

EMG reduction in response to antagonist vibration was rather small, the significant reduction of voluntary activation in the presence of visual feedback implies that the underlying group I disynaptic inhibition would be substantial.

Based on electrophysiological observations (i.e. conditioned H-reflex), the spinal disynaptic inhibition is reported to be totally abolished during muscle co-contraction about the ankle as well as wrist, possibly due to disinhibition via recurrent inhibition to the inhibitory interneurons ¹¹. This disinhibition mechanism would help avoid mutual inhibition between antagonist muscles during co-contraction. In contrast to these electrophysiological observations, the indifferent reductions in mean EMG amplitude of FCR by ECR vibration between co-contraction and flexion in the current study suggest that the inhibition due to antagonist vibration was not functionally attenuated (i.e. not disinhibited) by the co-contraction of the antagonist muscle about the wrist joint. Hence, the current results support the hypothesis that co-contraction does not abolish the reduction of agonist muscle activation due to antagonist vibration in the wrist muscles. The discrepancy may be attributed to the facts that the previous examination of conditioned H-reflex ¹¹ does not include muscle spindles and was only on observations in a limited number of subjects (two) for FCR. Considering that the spindle sensitivity can be variable depending on agonist and antagonist activities ⁹⁸, the current statistical examination of mean EMG amplitude under sustained vibration may better allow for understanding of the functional net effect of spindle-originated antagonist inhibition during co-contraction. . It is likely that the absence of mutual recurrent inhibition to the inhibitory interneurons in FCR and ECR ¹⁹ has a profound effect in limiting the disinhibition of the spinal disynaptic inhibition.

3.4.2 Effects of vibration and co-contraction on beta-band CMC

The reduction of beta-band CMC in FCR due to co-contraction with ECR indicates that beta-band CMC is reduced with the concurrent activity of antagonistic muscles for stabilizing in flexion/extension plain about the wrist joint. This finding presents new information regarding the task dependence of beta-band CMC. Beta-band CMC is less prominent during tasks with dynamic rather than static contractions^{35,36,114}, with lower-resolution in visual feedback¹¹⁵, against less compliant loads^{35,36}, for higher-intensity contractions³³, and for posture rather than force maintenance^{116,117}. While the neurophysiological mechanisms for the altered beta-band CMC under various task requirements have not been clearly delineated, the current findings provide a new insight that the reduction associated with concurrent activation of antagonist muscles may underlie some of the task dependencies. In particular, activation of antagonist muscles often accompanies higher-intensity contractions¹¹⁸ and postural tasks in which a joint or body segment is stabilized in a given position^{7,119}. The observed task-dependent changes in beta-band CMC may be regarded as the net changes due to multiple causes, in which the consideration of potential contribution of antagonist activation may help better understand the neurophysiological mechanisms underlying task-dependency of beta-band CMC in future studies.

The task-dependent beta-band CMC would be influenced by the task-dependent availability and activation of cortical neurons that directly synapse onto motor neurons, or corticomotor neurons, for the involved muscles. The influence of the available

corticomotor neurons is inferred by the observations that beta-band CMC was most prominent in the distal limb segments³¹ where the involved muscles have a greater number of corticomotor neurons^{29,30}. Task-dependent selectivity in their activation has been demonstrated in primate studies, in which specific populations of corticomotor neurons are active during agonist tasks but inactive during concurrent contraction of antagonist muscles^{30,32}. Assuming the findings in primates are applicable to humans, partial inactivation of corticomotor connections would contribute, at least in part, to a reduction in beta-band CMC during co-contraction compared with agonist contraction in the distal limb segments.

The reduction of beta-band CMC in FCR due to the vibration of ECR or FCR during flexion indicates that beta-band CMC is reduced with externally-induced sustained mechanical afferent inputs from agonist or antagonist muscles about the wrist. Collectively, the current findings support the second hypothesis that beta-band CMC is reduced with vibration and co-contraction. Beta-band CMC is known to be influenced by the state of afferent input^{35,37-41} and the observed effect of afferent input has been variable between upregulation and downregulation. Reductions of beta-band CMC with an acute removal of afferent input due to anesthesia³⁷, cooling⁴¹, and deafferentation⁴⁰ would suggest the upregulating role of afferent input for beta-band CMC. In the intact state, however, brief electrical or mechanical stimulation of peripheral motor or sensory nerves transiently reduced beta-band CMC for ~400 ms, followed by a rebound beyond pre-stimulus values after the stimulation of either agonist or antagonist muscle^{38,39}. Since the stimulation was very brief (e.g. 1 ms for electrical stimulation) in these studies^{38,39}, the persisting role of sustained afferent input for beta-band CMC was unclear.

Considering the real-life situations of controlling muscle contractions under exposure to vibration (e.g., maneuvering a vehicle, using power tools), it is important to understand the role of sustained afferent input for beta-band CMC. With the use of sustained mechanical stimulation, the results indicate that the net effect of sustained afferent input is a reduction of beta-band CMC at least in response to mechanical stimulation. This apparent discrepancy from the suggested upregulating role may originate from the differences in the details of experimental design, including the duration of stimulation, involved afferents, motor task, and intact/non-intact state. The comparable responses in beta-band CMC between the sustained vibration of agonist FCR and antagonist ECR agree with the observations in brief stimulations³⁸, suggesting that the stimulated muscle does not matter (i.e. agonist or antagonist) in altering beta-band CMC in response to afferent stimulations whether the stimulation is brief or sustained.

3.4.3 Beta-band oscillations and low-frequency oscillations in motor output

Motor output during steady muscle contraction involves non-steady components that are observed in both neural and mechanical motor outputs¹⁰⁷. Since the majority of non-steady mechanical components in isometric contraction reside in lower-frequencies, the current study focused on the low-frequency oscillations in neural motor output from the spinal cord by analyzing delta-band power in rectified EMG. In supporting that low-frequency oscillations in neural motor output from the spinal cord are reflected in those in mechanical motor output, the temporal profile of force fluctuations is correlated with the low-frequency (< 5 Hz) profile of rectified EMG signal and motor unit discharges^{108,107}.

For the first dorsal interosseous muscle ¹²⁰ and the tibialis anterior ⁴⁵, the magnitude of low-frequency power in force was correlated with that of beta-band CMC across individuals when rectified EMG was used in the CMC calculation. In the current study on FCR, in contrast, the low-frequency (delta-band) power in rectified EMG did not correlate with beta-band CMC (whether unrectified or rectified EMG was used), but with beta-band EEG power and beta-band EMG power in most conditions. This finding does not support the third hypothesis of a correlation between beta-band CMC and low-frequency power in rectified EMG, but revealed new relationships. The reasons for the discrepancy from the previous studies ^{107,120} are yet to be determined, including the details of the research design such as the tested joint/muscle and variables (e.g. neural rather than mechanical motor output). It is important to note that the amount of cortical gross beta-band activity is not necessarily associated with that of beta-band CMC ^{49,121}, leaving room for cortical and motor output signals to have associations that are independent of those with beta-band CMC. The presence of correlation with gross beta-band oscillations in the current study thus indicate that individuals with greater low-frequency oscillations in neural motor output for the wrist muscle tend to have greater beta-band oscillations in the cortex and muscle (i.e. spinal cord), but not necessarily greater beta-band CMC.

As potential neural mechanisms that may enhance beta-band oscillations in the cortex and spinal cord, GABAergic intracortical inhibition and Renshaw cell recurrent inhibition can be listed, respectively, according to the literature ^{49,50,121}. In the cortex, pharmacological enhancement of GABAergic intracortical inhibition increased beta-band cortical activity but not beta-band CMC in the intrinsic hand muscles within

individuals¹²¹. Across individuals, people with greater GABAergic intracortical inhibition showed greater beta-band cortical activity, but not greater beta-band CMC in the first dorsal interosseous⁴⁹. In the spinal cord, the presence of Renshaw cell recurrent inhibition increased ~30 Hz (i.e. within beta-band) power in the population discharge of the motor neuron pool in a model study⁵⁰. The presence of homonymous and heteronymous recurrent inhibition was experimentally confirmed in human wrist muscles, including FCR^{122 19,20}. Hence, the variability in the involvement of these neural mechanisms may underlie the variability in beta-band oscillations in the cortex and spinal cord across individuals. Based on the current findings, a future study would be warranted that examines the potential relationships between these beta-band modulating mechanisms and low-frequency oscillations in motor output to better understand the neurophysiology underlying steady motor output about the wrist.

3.5 Conclusion

In conclusion, the current study on FCR and ECR has clarified that 1) muscle co-contraction does not attenuate the vibration-induced reduction of agonist muscle activation about the wrist joint; 2) muscle co-contraction or sustained vibration of a muscle reduces beta-band CMC; and 3) individuals with greater beta-band power in neural activity in motor cortex or spinal cord, but not in beta-band CMC, tend to have greater low-frequency power in motor output; and

In the absence of recurrent inhibition to the inhibitory interneurons between FCR and ECR, there is instead mutual recurrent inhibition. The functional consequences of

the former during wrist co-contraction were examined here in Chapter 3. A feasibility study for assessing mutual recurrent inhibition during co-activation of FCR and ECR is presented in Chapter 4, with additional attention on the multiaxial nature of the wrist joint and wrist stability. Studying mutual recurrent inhibition at the wrist may shed light on why it is useful, what the underlying motor control objectives are, and how they are enacted via task-dependent modulation of the strength of recurrent inhibition.

CHAPTER 4. RECURRENT INHIBITION IN MULTI-AXIAL WRIST ACTIVITY

4.1 Introduction

Though the Ia pathways between FCR and ECR are similar to those of true antagonists, recurrent inhibition pathways more closely resemble synergistic activity. For true antagonists, Renshaw cell activity supports antagonistic function by inhibiting the agonist while disinhibiting the antagonist. In contrast, FCR and ECR share synergist-like spinal connections, as FCR-coupled Renshaw cells inhibit ECR motor neurons and vice versa in what is called mutual recurrent inhibition. Mutual recurrent inhibition is thought to allow for parallel control of gain across synergists ²¹. For FCR and ECR, mutual recurrent inhibition is expected to contribute to control of radial deviation ^{19,20}, but may also contribute to the control of co-contraction.

Modulation of the strength of recurrent inhibition between muscles changes with the functional roles of the involved muscles in performing a given task. For example, modulation of mutual recurrent inhibition may depend on whether the active muscles are acting synergistically in a given task. In the leg, mutual recurrent inhibition between the quadriceps and soleus is decreased when both are active in preparation for jumping compared to when both are activated during sitting. It is unknown whether these principles of recurrent inhibition for posture control apply to the upper limb and, further, to a pair of muscles working at the same joint. These principles may provide a new perspective on how recurrent inhibition contributes to the posture/stabilization control of

the wrist. If the synergistic activity of the quadriceps and soleus is analogous to the synergistic activity of FCR and ECR in radial deviation, and the non-synergistic activation of the quadriceps and soleus during sitting is analogous to the non-synergistic (antagonistic, in this case) activation of FCR and ECR during flexion/extension co-contraction, then recurrent inhibition between the concurrently active FCR and ECR can be modulated in a task-dependent manner. It was hypothesized that recurrent inhibition during synergistic activity of FCR and ECR (radial deviation, radial/ulnar co-contraction) would be reduced relative to the non-synergistic activation of FCR and ECR (flexion/extension co-contraction).

The strength of recurrent inhibition may also depend on the intensity of muscle contraction. Homonymous recurrent inhibition of muscle at a hinge joint (and in turn, mutual inhibition among synergists) decreases with contraction intensity²⁴, likely to enhance motor pool excitability. However, homonymous recurrent inhibition is not decreased with contraction intensity when the antagonist is also contracting²⁴. It is not yet known how recurrent inhibition between synergistic wrist muscles will be controlled in comparison to known patterns of control in true antagonists at a hinge joint. It was hypothesized that recurrent inhibition will be reduced between FCR and ECR with increased contraction intensity for a given task. To explore task-dependency and influences of contraction intensity, an experiment was designed to compare recurrent inhibition between flexion/extension co-contraction and radial deviation as well as between different co-contraction intensities in on-going EMG.

In addition to recurrent inhibition, results from Aim 2 suggest that group I inhibition exists between FCR and ECR in both agonist contraction and co-contraction

tasks. As such, a special effort was made to distinguish the heteronymous recurrent inhibition of interest in this study from Ia inhibition. Recurrent inhibition can be induced by high-intensity electrical nerve stimulation that generates an M-wave^{20,123}, as well as motor output caused by Ia-mediated pathways (e.g. H-reflexes¹²⁴ and tendon taps¹²⁵). In each of these stimulation protocols, group I inhibition is expected to occur in the antagonist at a fixed latency relative to stimulation. However, the latency of recurrent inhibition is expected to shift with the latency of motor output, determined by stimulation intensity. It is hypothesized that the latency of recurrent inhibition will be shorter during high-intensity stimulations inducing an M-wave than during low-intensity stimulations that induce an H-reflex without an M-wave, and that this latency shift will be comparable to the difference in latency between the H-reflex and an M-wave. If the latency remains constant, then the inhibition is likely not attributable to recurrent inhibition and may instead be group I inhibition. To explore the stimulation-dependency, another experiment was designed to compare recurrent inhibition between high and low stimulation intensities during wrist extensor contraction.

The purpose of this study was to obtain preliminary data in newly designed experiments to shed light on the role of mutual recurrent inhibition between the active FCR and active ECR during wrist stabilization tasks where FCR and ECR are expected to function as agonists or antagonists. The results would enhance the understanding of the role of Renshaw cell activity in the multi-axial control and stabilization of the wrist.

4.2 Methods

4.2.1 Subjects

To quantify recurrent inhibition in ongoing EMG, two subjects with no history of neurological impairment or injury of the right arm participated in this study. Both subjects gave written consent in accordance with the Institutional Review Board of the Georgia Institute of Technology. Each subject participated in separate experiments. The first subject, a 20 year old female, participated in an experiment to test recurrent inhibition across tasks involving activation of both FCR and ECR (Task-dependency experiment). A second subject, also a 20 year old female, participated in an experiment to clarify the impact of stimulation intensity on recurrent inhibition (Intensity-dependency experiment).

4.2.2 Motor tasks

For these experiments, subjects were seated with the right forearm and hand stabilized in a brace affixed to a small table. The wrist was constrained in the neutral position between supination and pronation in a lightly padded arm brace. In this orientation, contraction of wrist flexor and extensor muscles corresponded to the force production toward left and right, respectively. The right shoulder was abducted 15° and flexed 35° . The left arm was rested on the armrest of the chair. The legs were not crossed and the knees were flexed to 90° .

Subjects performed maximal voluntary contractions (MVC) in radial deviation to determine the maximal amplitude of EMG in FCR and ECR in this task. Radial deviation was used because MVCs in flexion and extension were expected to differ from those of

co-contraction tasks and the matching of these targets during flexion/extension co-contraction would only require movement in the flexion-extension axis. The MVC task involved a gradual increase in muscle activation from zero to maximum effort over 3 s with maximal effort held for 2 to 3 s. Subjects were asked to perform the task three times with a minute of rest between trials. The amplitudes of detrended, rectified and smoothed (0.1s window) EMGs from FCR and ECR were computed and displayed in real time to provide visual feedback to subjects. Verbal encouragement was given to achieve maximal effort. The maximal EMG amplitude across trials was determined in FCR and ECR.

After the MVC task, subjects performed the steady motor tasks. In the Task-dependency experiment, the subject performed three tasks: 1) radial deviation at 10% MVC for FCR and ECR; 2) flexion/extension co-contraction at 10%; and 3) flexion/extension co-contraction at 50%MVC. In the stimulation-dependency experiment, the subject performed isometric wrist extension at 30%MVC for ECR. In each experiment, five trials of task were performed for 30-35 seconds each with at least one minute of rest between trials. For both experiments and all motor tasks, stimulation of the median nerve to activate the alpha motor neurons of FCR was used to induce recurrent inhibition in the ongoing EMG of ECR.

4.2.3 Electrical Stimulation

Based on previous studies,^{20,123} high intensity electrical stimulations of the median nerve were applied at the cubital fossa at 50% M_{\max} for FCR to induce FCR

induced recurrent inhibition of ECR. Electrical stimulation was applied using transcutaneous bipolar stimulating electrodes, separated by 2 cm, connected to a constant current stimulator (S88-SIU5-CCU1, Grass Products, Natus Neurology Inc., Warwick, RI, USA). M_{\max} of the FCR muscle was assessed with a 1 ms square-wave electrical stimulation delivered to the median nerve at a supramaximal intensity of approximately 125% of intensity that elicited maximum compound muscle action potential. The M_{\max} motor responses were induced in the resting FCR, with stimulations occurring every 4-6 seconds. This same timing was used during the experimental tasks to allow eight stimulations per trial. For both experiments, forty stimulations were applied for each combination of motor task, contraction intensity, and stimulation intensity.

During the Stimulation-dependency experiment, lower intensity stimulations inducing an H-reflex without an M-wave were applied in addition to the high intensity stimulations at 50% M_{\max} . The intensity of H-reflex stimulations, also determined in the resting FCR prior to the experimental tasks, was set at the motor threshold. H-reflexes were identified by visual inspection of EMG records in real-time and palpable twitch of the FCR muscle. The amplitudes of H-reflexes and 50% M_{\max} motor responses were monitored across tasks and throughout each experiment for consistency.

4.2.4 Recordings

Bipolar surface EMG signals from FCR and ECR were recorded with a sampling rate of 1kHz. Pairs of Ag-AgCl electrodes (E224A, IVM, Healdsburg, CA, USA) were placed over each muscle belly separated by 2cm. A disposable electrode

(Telectrode/T716, Bio Protech, Wonju si, Gangwon-do, Korea) was placed on the medial epicondyle of the right arm as a reference. The EMG signals were pre-amplified (300x) and bandpass filtered from 15- 2,000Hz (Y03-000, MotionLabs, NY, USA). The EMG signals were then passed to an analog-to-digital converter (Power 1401, Cambridge Electronic Design Ltd, Cambridge, UK) for display and recording in data acquisition software (Spike 2 v.7, Cambridge Electronic Design Ltd, Cambridge, UK).

4.2.5 Data Analysis

Raw EMG of ECR were processed and analyzed off-line in Matlab using custom code. The EMG signals were bandpass filtered (100Hz-1kHz) and full-wave rectified for quantification of the recurrent inhibition. All EMG traces for a given task intensity were averaged relative to the time of stimulation. The amount of recurrent inhibition was calculated as the percent reduction of EMG amplitude in the post stimulation period of inhibition compared to the mean EMG amplitude immediately pre-stimulation (averaged from 5-150 ms before stimulation), or %RI. The reduction of EMG amplitude was determined by the minimum EMG amplitude during the post-stimulation period for recurrent inhibition (approximately 22-43 ms after stimulation for this subject). The latency of recurrent inhibition was determined as the time point after median nerve stimulation when the EMG amplitude started to become lower than the pre-stimulation value consistently for more than 5 ms.

4.3 Results and discussion

4.3.1 *Experiment 1: Recurrent Inhibition during FCR-ECR Co-contraction*

To support the hypotheses, there should be a greater difference in %RI when FCR and ECR act as synergists during radial deviation than when FCR and ECR are antagonists during flexion/extension co-contraction. There should also be no difference of %RI between co-contraction intensities. To find the latencies of the M-wave and H-reflex and the amplitude of M_{\max} in FCR, a series of stimulations of the median nerve were performed. Figure 24 shows average EMG in FCR across 15 stimulations during radial deviation at 50% M_{\max} . In Figure 25, average EMG in ECR is presented for radial deviation at 10% MVC and flexion/extension co-contraction at 10% and 50% MVC in the Task-dependency experiment. Pre-stimulus ECR amplitudes (control) are shown as a dashed black line and the duration of inhibition is highlighted in red. As expected, motor output from FCR created a long-lasting (~15-18ms) inhibition in the ongoing EMG of ECR.

In this subject, heteronymous recurrent inhibition reduced ECR amplitudes by 61%, 74%, and 59% across the three tasks, respectively. These %RI pilot data values appear to show that small differences in recurrent inhibition are evident at low %MVC values. The greater %RI in flexion/extension co-contraction at 10% MVC when compared with radial deviation at 10% MVC suggests that recurrent inhibition is reduced for synergistic activity of FCR and ECR. This finding supports the hypothesis of reduced recurrent inhibition during synergistic activity. Additionally, recurrent inhibition during flexion/extension co-contraction was reduced during 50% MVC compared with the 10% MVC task. Despite the antagonist activity of FCR and ECR, disinhibition may still have

occurred to facilitate activity of both muscles. This second finding supports the hypothesis of reduced recurrent inhibition with increased contraction intensity.

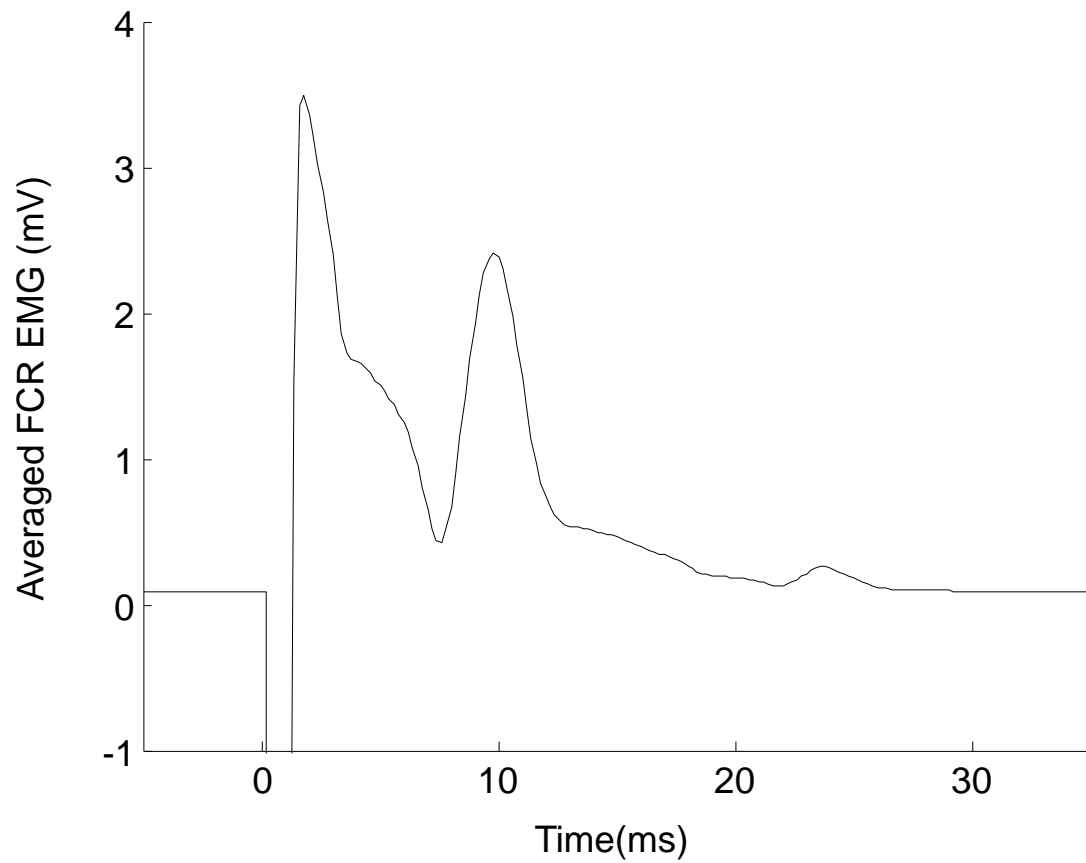


Figure 24: Averaged stimulations of the median nerve 50% M_{\max} stimulation during radial deviation at 10% MVC for FCR and ECR.

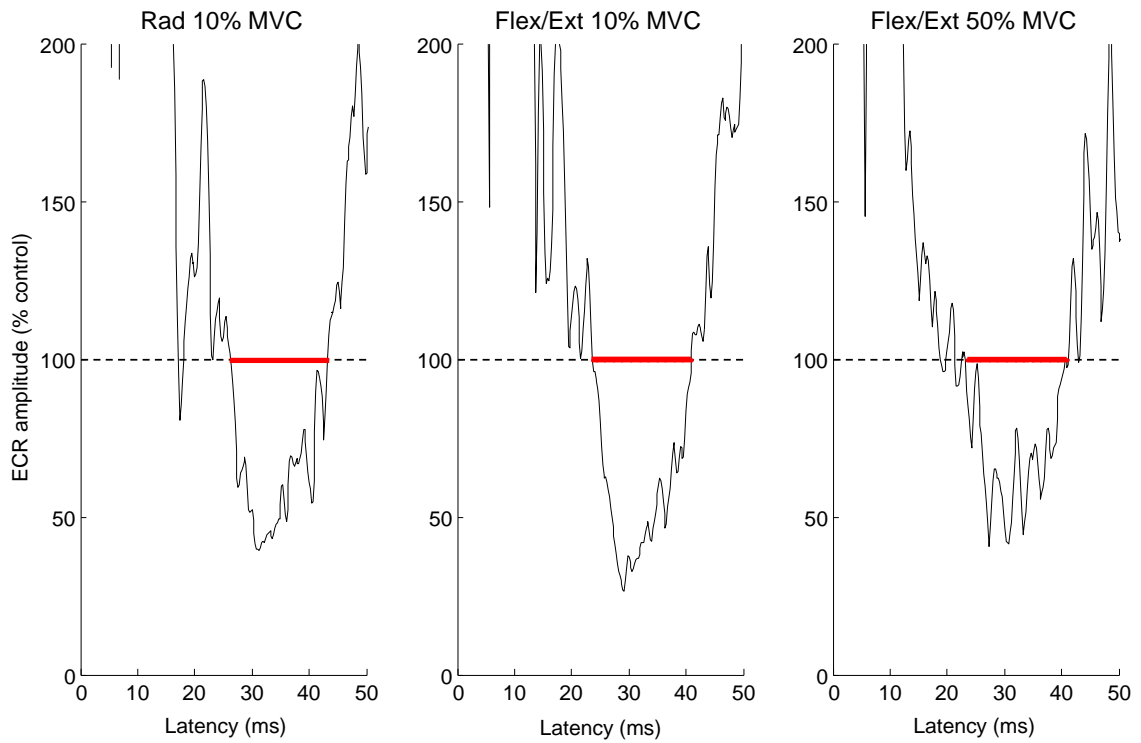


Figure 25: Task dependent recurrent inhibition of ECR during co-contraction of FCR and ECR. Latency is relative to median nerve stimulation. EMG amplitude of ECR is expressed as a percent relative to the pre-stimulus amplitude (control). The horizontal dashed line marks the control value. The horizontal red line represents the duration of inhibition.

4.3.2 Experiment 2: Exclusion of H-reflex Influence

With the presence of both the M-wave and H-reflex in FCR due to the high intensity median nerve stimulation, and the latency of the inhibition in ECR, it is difficult to separate the contributions of their respective motor responses to the inhibition of ECR. As a step toward showing their differing effects, a second experiment was performed. In the Stimulation-dependency experiment, the subject performed simple wrist extension at

30% MVC of ECR. Stimulations were applied at $\sim 50\%$ M_{\max} and at a lower stimulation intensity that only produced an H-reflex. Forty stimulations of each intensity were applied and the data were processed as stated above. In Figure 26, recurrent inhibition in ECR during high and low intensity stimulations are shown. The vertical red and blue lines mark the latencies of the M-wave ($\sim 3\text{ms}$) and H-reflex ($\sim 16\text{ms}$) in FCR, respectively. Note that the latency of the initiation of ECR inhibition shifted from $\sim 22\text{ms}$ during high intensity stimulation to $\sim 33\text{ms}$ during low intensity stimulations in accordance with the earlier motor response. This shift is in line with the hypothesized shift in the latency of recurrent inhibition.

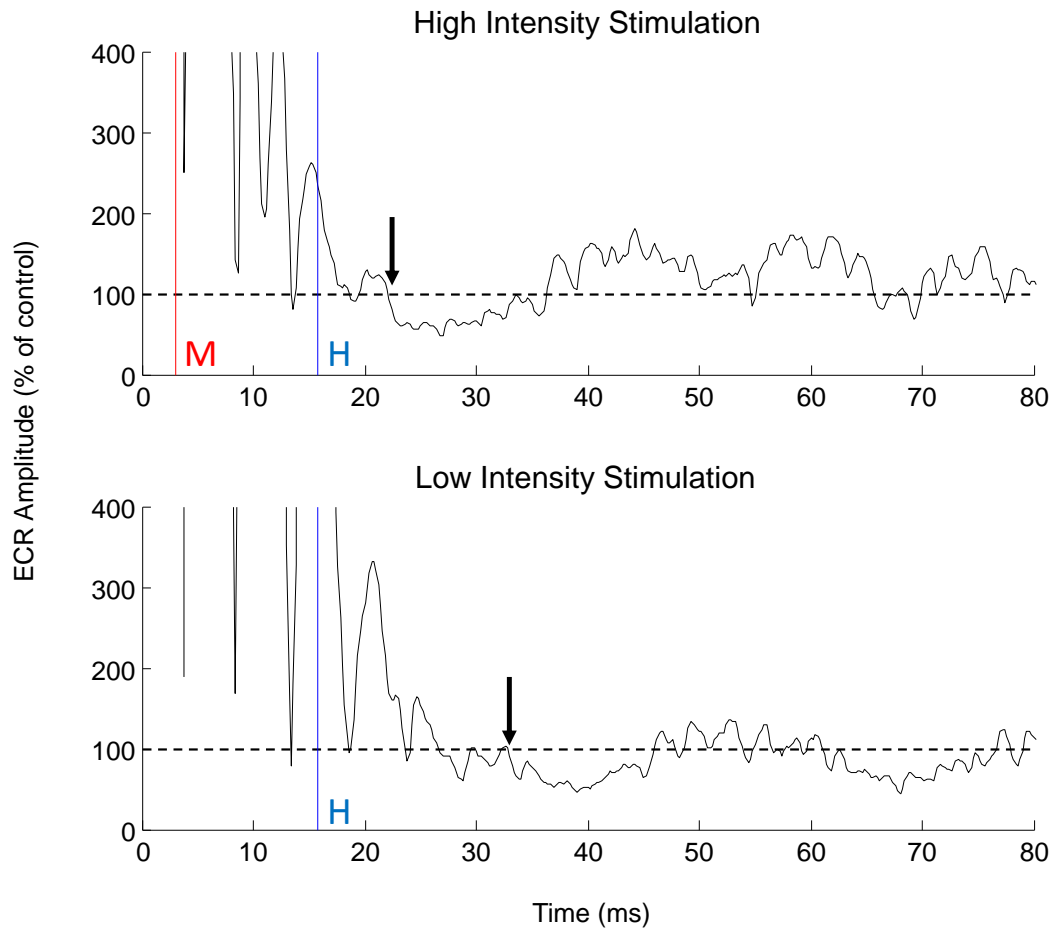


Figure 26: Recurrent inhibition of ECR during wrist extension. Latency is relative to median nerve stimulation. ECR amplitude is expressed as a percent relative to the pre-stimulus amplitude (control). The horizontal dashed line marks the control value. The vertical red and blue lines represent the M-wave and H-reflex latencies, respectively. Arrows indicate the onset of prolonged inhibition.

4.4 Conclusion

A methodology and preliminary data from two subjects was presented towards studying the modulation of mutual recurrent inhibition at the wrist joint during isometric force and stability tasks in the flexion/extension plane and radial/ulnar deviation plane. The preliminary data using different tasks and contraction intensity are in line with the hypothesized reductions in recurrent inhibition during synergistic activity and during stronger muscle contractions. The preliminary data using high and low intensity stimulations provide supporting evidence that the inhibition shown is indeed recurrent inhibition.

CHAPTER 5. DISCUSSION

5.1 Integration

5.1.1 *Implications for wrist stability*

The insufficient suppression of group I inhibition during flex/extension co-contraction at the wrist (Specific Aim 2) suggests that neural control during wrist co-contraction may be fundamentally different from that of co-contraction between true antagonists (e.g. tibialis anterior and soleus) where presynaptic inhibition of simple H-reflexes in the agonist is increased¹¹ and reciprocal inhibition from the antagonist is decreased or abolished relative to agonist contraction.¹² Perturbations during elbow joint co-contraction present yet another pattern of control, where the shortened antagonist muscle is not only disinhibited, but can be facilitated depending upon the strength of agonist contraction^{126,127}. This facilitation is thought to be a combination of suppressed reciprocal inhibition allowing Ib antagonist facilitation to emerge. Whether Ia pathways are preserved or diminished has unique implications for joint stability. One aspect of joint stability is control of antagonist muscles toward matching opposing torques at the joint. The preservation of reciprocal inhibition shown in this dissertation could lead to difficulties in maintaining appropriate amplitudes of antagonist muscle activity to oppose agonist activity. Preservation of monosynaptic facilitation would have a similar effect.

Preservation of Ia pathways also has implications for susceptibility to oscillatory instability. Monosynaptic Ia excitation causes a corrective reflex against muscle lengthening and increases muscle stiffness beyond what would be predicted based purely

on mechanical properties ⁹⁹. The accompanying reciprocal inhibition of the antagonist complements this activity. Both would be beneficial for maintaining joint stability as the overall corrective reflex would help preserve the initial joint position. However, strong Ia feedback may result in undesirable overcorrection or oscillatory instability ¹²⁸. If so, the preservation of reciprocal inhibition (Specific Aim 2) suggests that the wrist is more susceptible to oscillatory instability due to Ia reflex involvement. On the other hand, the preservation or enhancement of Ia feedback may be useful in precision tasks as shown by reduction of presynaptic inhibition of Ia afferents during position control is relative to a force control task ¹²⁹. These findings suggest a trade-off between stability and utilization of sensory input for precise control.

While the group I inhibition during co-contraction is analogous to reciprocal inhibition, the intervention may have utilized both group I and recurrent inhibition pathways to create this effect. And while this apparent preservation of group I inhibition may be a result absent Renshaw Cell control over the involved group I interneurons, recurrent inhibition is still present. As such, the oscillatory instability that may be introduced by preserving Ia pathways may be reduced by through the gain regulation ²¹ and tremor suppression ⁵⁰ of recurrent inhibition. An expansion of the feasibility protocol toward comparison of mutual recurrent inhibition during agonist contraction and co-contraction would be beneficial in parsing out these effects.

Joint stiffness and stability are also determined by the mechanical properties of the tissues within and across the joint. In Specific Aim 1, the coupling of muscle stiffness with contraction intensity and the differences in stiffness between proximal and distal joints were displayed. Increasing activation of the muscles increases both muscle

stiffness and overall stiffness at the joints the muscle crosses^{15,16}. High stiffness non-contractile tissue also contributes to stiffness, but possibly in a non-linear relationship with force, as shown by increases in linearity with NCT removal (Specific Aim 1). It can also be seen in Figure 9 that TRI shear modulus values were only about 1/6th of those at the wrist during the same loading conditions. ECU's high contractile tissue stiffness values and greater concentration of NCT emphasize the need for mechanical stability at the wrist.

5.1.2 Beta-band CMC and Spinal Mechanisms

At comparable FCR activation, beta-band CMC was reduced during wrist co-contraction compared with flexion (Specific Aim 2). This is a novel finding for the task-dependence of beta-band CMC, revealing the impact of antagonist contraction on agonist CMC. Potential underlying mechanisms for this reduction of CMC during wrist co-contraction include reduced or altered activation of corticomotor neurons^{30,32} and activation of additional spinal mechanisms via antagonist activation. The contribution of reduced or altered corticomotor neuron activity cannot be ruled out because this was not tested directly. However, there is evidence for the influence of spinal mechanisms, particularly Ia afferent pathways. First, the application of additional afferent input was effective, shown by statistically significant differences in FCR EMG amplitudes during both co-contraction and flexion (Specific Aim 2). Second, no further reductions in CMC occurred during co-contraction in the presence of additional afferent input (Specific Aim 1), suggesting these pathways had already been utilized in the absence of additional

afferent input. Further, the lack of significant effect of vibration is unlikely due to “floor effect” as nearly half of analyzed subjects retained significant CMC during co-contraction with similar numbers across the vibration conditions and analysis of this cohort still revealed no significant reduction of CMC during vibration.

If increased activation of spinal mechanisms during co-contraction contributed strongly to agonist CMC reduction, this finding presents new information on the effects of spinal mechanisms activated by voluntary contraction of a muscle other than the agonist. Also, the spinal mechanisms involved are probably not limited to the afferent pathways targeted in previous studies³⁷⁻⁴⁰. The intermuscular spinal mechanisms at the wrist include both mutual recurrent inhibition and afferent pathways. Both mechanisms can be activated in parallel via alpha-gamma co-activation⁹⁷ during muscle contraction. With the addition of ECR contraction, collaterals of ECR alpha motor neurons would activate Renshaw cells to both FCR and ECR while activated gamma motor neurons would increase sensitivity of ECR muscle spindles⁹⁷. Since both afferent pathways and recurrent inhibition have been linked to CMC reduction^{38,39,49}, each may have contributed to the reduced CMC during wrist co-contraction. While it would be difficult to separate the contributions of each spinal mechanism, any task-dependent differences found in the feasibility study (Specific Aim 3) would provide important information.

5.1.3 Beta-band neural oscillations and motor output

The lack of correlation between beta-band CMC and motor output oscillations is in disagreement with previous studies^{49,120}. However, these previous studies have not

directly correlated cortical or muscular beta-band oscillations to motor output. CMC has been shown to be correlated to amplitudes of its constituent signals¹³⁰, which may have caused indirect correlations of CMC with motor output. The association of cortical and EMG beta-band activity to motor output, and disassociation of CMC from motor output, highlights the separate functions of CMC and beta-band neural oscillations. These findings also suggest there may be peripheral sources of beta-band oscillations, not just the transmission of cortical beta-band oscillations into spinal pathways. A possible source of peripheral beta-band oscillations is recurrent inhibition. Recurrent inhibition has been linked to both reduced CMC⁴⁹ and higher beta-band EMG oscillations in a modeling study^{7 50}. Task-dependent differences in recurrent inhibition may also explain the apparent increased strength of correlations during co-contraction. The continuation of the recurrent inhibition feasibility study (Specific Aim 3) would be beneficial in clarifying the potential impact of recurrent inhibition on beta-band neural oscillations and their correlations with each other and with motor steadiness.

5.1.4 Contributions

Taken together, the original contributions of this dissertation are:

- 1) Development of an automatic image processing algorithm for ultrasound shearwave elastography to analyze wrist muscle activity.
- 2) Demonstration of the impact of inclusion of connective tissue on comparisons of muscle activity across loading conditions.

- 3) Exploration of the task-dependence of beta-band cortical and muscular neural oscillations and corticomuscular coherence during a wrist stability task (co-contraction) compared to a force task (wrist flexion)
- 4) Clarification of the task-dependent control of reciprocal and mutual spinal mechanisms that impact the motor output of wrist muscles, with emphasis on wrist stabilization and consideration of multiaxial control.

5.2 Significance

For Specific Aim 1, the activity of upper limb muscles was assessed during interaction with a robotic manipulator. As the use of human-robot interaction gains popularity for neuromotor assessment, rehabilitation, and training, advanced methods of assessing muscle activity are needed. The limitations of EMG necessitate the use of alternative methods for accurate recording of muscle activity during complex loading, such as ultrasound shear wave elastography. The ability to monitor wrist activity during complex loading is also applicable to various activities of daily living where grasp and manipulation are utilized.

In agreement with the findings in Specific Aim 1 and previous anatomy studies, distal muscles appear to have greater amounts of connective tissues compared with the proximal muscles⁸⁹. In small muscles or where there is a higher concentration of NCT, such as in the forearm muscles, available uninterrupted contractile tissues may be limited and potential measurement areas will likely be closer to bands of connective tissues. The developed image processing algorithm would especially be helpful in these situations

where selection of a more flexible and appropriate measurement area with NCT removal is required. These considerations are also applicable to configurations where muscles are likely to lose contractile tissues and/or gain NCT (e.g. limb immobilization, muscular dystrophy), especially for the assessment within individuals.

Specific Aim 2 provided scientific insights into the fundamental effects of sustained mechanical input and co-contraction about the wrist joint in healthy young adults, but its potential application to other populations could also be considered. For example, the natural reduction of beta-band CMC in response to muscle vibration could be used for assessing the integrity of the sensorimotor system in peripheral neuropathies and diabetes. While the examination of beta-band CMC has been explored in clinical populations as well as healthy older adults ^{7,131-133}, the natural reduction of beta-band CMC due to co-contraction will need to be taken into account when interpreting beta-band CMC in populations who tend to have antagonist co-contraction (e.g., stroke, spinal cord injury). Also, in trying to understand the neurophysiological mechanisms associated with degraded steadiness in older adults ^{7,120}, for example, examination of gross beta-band activity in the motor cortex and muscle (i.e. spinal cord) would be relevant in addition to CMC. While the tested wrist muscles would be convenient in clinical applications, the applicability of the current findings to other joints will need to be confirmed.

Specific Aim 3 was motivated by the unique spinal mechanisms at the wrist, which appear to be a hybrid between those of true antagonists and synergists. This spinal configuration supports the multiaxial nature of the wrist joint as muscles toggle between antagonistic and synergistic activity. The continuation of Specific Aim 3 would be

beneficial for understanding the impact of inadequate control of recurrent inhibition on multiaxial joint control and synergistic muscle activity at the joint and limb level.

5.3 Future Directions

For Specific Aim 1, one wrist muscle was examined during a stabilization task. Revisiting this protocol while monitoring more wrist muscle simultaneously would more fully capitalize on this newly developed method of assessing muscle activity with spatial resolution. Another approach is to take step back toward a simple loading condition and examine the linear relationship of muscle contractile tissue, NCT, and joint torque. Additionally, one could perform a more systematic study of NCT in the human arm, comparing distal and proximal muscles as has been done in cattle ⁸⁹. Lastly, USSWE could be used to verify the amplitude results in Specific Aim 2, with the co-contraction described or with grasp. Amplitude studies can be prone to EMG crosstalk during a complex task like grasp, and USSWE would provide a good alternative for capturing muscle activity where low sampling rates would suffice. Future improvement of the image sampling rate would enhance the usefulness of automated image processing for capturing time series data and analyzing muscle activity oscillations during static and dynamic loading tasks.

A major finding of Specific Aim 2 was that beta-band CMC in the FCR was reduced by co-contraction relative to flexion. This may be attributable in part to recurrent inhibition. While previous studies have focused on modulation of beta-band CMC by applying electrical and mechanic peripheral stimulation, a similar study has not

been done with recurrent inhibition. Deafferentation of the antagonist muscle (e.g. anesthesia of the radial nerve to ECR) would allow for targeted study of antagonist-mediated heteronymous recurrent inhibition of the agonist (e.g. FCR). In this way, the modulation of agonist beta-band CMC can be examined after electrical stimulation of the radial nerve or voluntary activation of the antagonist. This allows for the separation of spinal mechanism influences, which was not possible in the current study.

Specific Aim 3 presents a protocol and feasibility study for testing task-dependent control of recurrent inhibition at the wrist. A complete study with ample subjects would be necessary to better address this aspect of multiaxial control. In addition to studying recurrent inhibition across synergistic and antagonist activation of FCR and ECR, a study of group I antagonist inhibition may be interesting to highlight any contrasts in the task-dependent modulation of these spinal mechanisms. The results of Specific Aim 2 show no differences in group I antagonist inhibition, but that may be due to the fact that flexion and the co-contraction performed in that study both cause FCR and ECR to operate at antagonists. Group I inhibition may be controlled differently when the FCR and ECR work as synergists, in the same way that mutual recurrent inhibition appears to display task-dependent control.

CHAPTER 6. CONCLUSION

In conclusion, an image processing algorithm for automatic analysis of ultrasound shear-wave elastography data was developed to enhance the capability of capturing forearm muscle activity during a complex loading condition in which EMG recording might be unreliable. In addition, a study of the neural mechanisms of wrist stability showed that 1) spinal mechanisms involved in wrist co-contraction do not reduce or abolish group I antagonist inhibition; 2) performing a wrist stabilization task (co-contraction) or applying additional afferent input to the agonist or antagonist muscle reduces agonist muscle beta-band CMC relative to agonist contraction alone; and 3) individuals with greater power in the beta-band of cortical and spinal neural activity, but not greater CMC, have greater lower frequency oscillations in motor output for both wrist co-contraction and agonist contraction. Lastly, an additional feasibility study focusing on the control of recurrent inhibition during wrist stabilization revealed that synergistic activity and increased contraction intensity may reduce recurrent inhibition at the wrist.

REFERENCES

1. Houtz S. Influence of gravitational forces on function of lower extremity muscles. *J Appl Physiol.* 1964;19(5):999-1004.
2. Milner TE. Adaptation to destabilizing dynamics by means of muscle cocontraction. *Exp Brain Res.* 2002;143(4):406-416.
3. Basmajian J. Motor learning and control: a working hypothesis. *Arch Phys Med Rehabil.* 1977;58(1):38-41.
4. Gribble PL, Mullin LI, Cothros N, Mattar A. Role of cocontraction in arm movement accuracy. *J Neurophysiol.* 2003;89(5):2396-2405.
5. Osu R, Franklin DW, Kato H, et al. Short-and long-term changes in joint co-contraction associated with motor learning as revealed from surface EMG. *J Neurophysiol.* 2002;88(2):991-1004.
6. Lacquaniti F, Maioli C. Anticipatory and reflex coactivation of antagonist muscles in catching. *Brain Res.* 1987;406(1):373-378.
7. Benjuya N, Melzer I, Kaplanski J. Aging-induced shifts from a reliance on sensory input to muscle cocontraction during balanced standing. *The Journals of Gerontology Series A: Biological Sciences and Medical Sciences.* 2004;59(2):M166-M171.
8. Baudry S, Maerz AH, Enoka RM. Presynaptic modulation of Ia afferents in young and old adults when performing force and position control. *J Neurophysiol.* 2010;103(2):623-631.
9. Mizuno Y, Tanaka R, Yanagisawa N. Reciprocal group I inhibition on triceps surae motoneurons in man. *J Neurophysiol.* 1971.
10. Tanaka R. Reciprocal Ia inhibition during voluntary movements in man. *Exp Brain Res.* 1974;21(5):529-540.

11. Nielsen J, Kagamihara Y. The regulation of disynaptic reciprocal Ia inhibition during co-contraction of antagonistic muscles in man. *J Physiol.* 1992;456:373-391.
12. Nielsen J, Kagamihara Y. The regulation of presynaptic inhibition during co-contraction of antagonistic muscles in man. *J Physiol.* 1993;464:575-593.
13. Kong Y-K, Hallbeck MS, Jung M-C. Crosstalk effect on surface electromyogram of the forearm flexors during a static grip task. *J Electromyogr Kinesiol.* 2010;20(6):1223-1229.
14. Mogk JP, Keir PJ. Crosstalk in surface electromyography of the proximal forearm during gripping tasks. *J Electromyogr Kinesiol.* 2003;13(1):63-71.
15. Bouillard K, Hug F, Guével A, Nordez A. Shear elastic modulus can be used to estimate an index of individual muscle force during a submaximal isometric fatiguing contraction. *J Appl Physiol.* 2012;113(9):1353-1361.
16. Koo TK, Guo J-Y, Cohen JH, Parker KJ. Relationship between shear elastic modulus and passive muscle force: an ex-vivo study. *J Biomech.* 2013;46(12):2053-2059.
17. Yoshitake Y, Takai Y, Kanehisa H, Shinohara M. Muscle shear modulus measured with ultrasound shear-wave elastography across a wide range of contraction intensity. *Muscle Nerve.* 2014;50(1):103-113.
18. Aymard C, Baret M, Katz R, Lafitte C, Penicaud A, Raoul S. Modulation of presynaptic inhibition of Ia afferents during voluntary wrist flexion and extension in man. *Exp Brain Res.* 2001;137(1).
19. Aymard C, Chia L, Katz R, Lafitte C, Penicaud A. Reciprocal inhibition between wrist flexors and extensors in man: a new set of interneurons? *The Journal of physiology.* 1995;487(1):221-235.
20. Aymard C, Decchi B, Katz R, et al. Recurrent inhibition between motor nuclei innervating opposing wrist muscles in the human upper limb. *The Journal of physiology.* 1997;499(1):267-282.

21. Renshaw B. Influence of discharge of motoneurons upon excitation of neighboring motoneurons. *J Neurophysiol.* 1941;4(2):167-183.
22. Hultborn H, Lindström S, Wigström H. On the function of recurrent inhibition in the spinal cord. *Exp Brain Res.* 1979;37(2):399-403.
23. Barbeau H, Marchand-Pauvert V, Meunier S, Nicolas G, Pierrot-Deseilligny E. Posture-related changes in heteronymous recurrent inhibition from quadriceps to ankle muscles in humans. *Exp Brain Res.* 2000;130(3):345-361.
24. Nielsen J, Pierrot-Deseilligny E. Evidence of facilitation of soleus-coupled Renshaw cells during voluntary co-contraction of antagonistic ankle muscles in man. *The Journal of physiology.* 1996;493(2):603-611.
25. Berardelli A, Day B, Marsden C, Rothwell J. Evidence favouring presynaptic inhibition between antagonist muscle afferents in the human forearm. *The Journal of Physiology.* 1987;391(1):71-83.
26. Pierrot-Deseilligny E, Burke D. *The circuitry of the human spinal cord: its role in motor control and movement disorders.* Cambridge University Press; 2005.
27. Hultborn H, Jankowska E, Lindström S. Recurrent inhibition of interneurons monosynaptically activated from group Ia afferents. *The Journal of Physiology.* 1971;215(3):613-636.
28. Lattari E, Velasques B, Paes F, et al. Corticomuscular coherence behavior in fine motor control of force: a critical review. *Rev Neurol.* 2010;51(10):610-623.
29. Porter R, Lemon R. *Corticospinal function and voluntary movement.* Oxford University Press, USA; 1993.
30. Petersen NT, Pyndt HS, Nielsen JB. Investigating human motor control by transcranial magnetic stimulation. *Exp Brain Res.* 2003;152(1):1-16.
31. Ushiyama J, Takahashi Y, Ushiba J. Muscle dependency of corticomuscular coherence in upper and lower limb muscles and training-related alterations in ballet dancers and weightlifters. *J Appl Physiol.* 2010;109(4):1086-1095.

32. Fetz E, Cheney P. Functional relations between primate motor cortex cells and muscles: fixed and flexible. *Motor areas of the cerebral cortex*. 1987:98-117.
33. Ushiyama J, Masakado Y, Fujiwara T, et al. Contraction level-related modulation of corticomuscular coherence differs between the tibialis anterior and soleus muscles in humans. *J Appl Physiol*. 2012;112(8):1258-1267.
34. Mima T, Simpkins N, Oluwatimilehin T, Hallett M. Force level modulates human cortical oscillatory activities. *Neurosci Lett*. 1999;275(2):77-80.
35. Kilner JM, Baker SN, Salenius S, Hari R, Lemon RN. Human cortical muscle coherence is directly related to specific motor parameters. *J Neurosci*. 2000;20(23):8838-8845.
36. Riddle CN, Baker SN. Digit displacement, not object compliance, underlies task dependent modulations in human corticomuscular coherence. *NeuroImage*. 2006;33(2):618-627.
37. Fisher R, Galea M, Brown P, Lemon R. Digital nerve anaesthesia decreases EMG-EMG coherence in a human precision grip task. *Exp Brain Res*. 2002;145(2):207-214.
38. Liv Hansen N, Bo Nielsen J. The effect of transcranial magnetic stimulation and peripheral nerve stimulation on corticomuscular coherence in humans. *The Journal of Physiology*. 2004;561(1):295-306.
39. McClelland VM, Cvetkovic Z, Mills KR. Modulation of corticomuscular coherence by peripheral stimuli. *Exp Brain Res*. 2012:1-18.
40. Pohja M, Salenius S. Modulation of cortex-muscle oscillatory interaction by ischaemia-induced deafferentation. *Neuroreport*. 2003;14(3):321-324.
41. Riddle CN, Baker SN. Manipulation of peripheral neural feedback loops alters human corticomuscular coherence. *The Journal of physiology*. 2005;566(2):625-639.
42. Johnson AN, Wheaton LA, Shinohara M. Attenuation of corticomuscular coherence with additional motor or non-motor task. *Clin Neurophysiol*. 2011;122(2):356-363.

43. Zheng Y, Gao L, Wang G, et al. The influence of unilateral contraction of hand muscles on the contralateral corticomuscular coherence during bimanual motor tasks. *Neuropsychologia*. 2016;85:199-207.
44. Kristeva R, Patino L, Omlor W. Beta-range cortical motor spectral power and corticomuscular coherence as a mechanism for effective corticospinal interaction during steady-state motor output. *NeuroImage*. 2007;36(3):785-792.
45. Ushiyama J, Yamada J, Liu M, Ushiba J. Individual difference in β -band corticomuscular coherence and its relation to force steadiness during isometric voluntary ankle dorsiflexion in healthy humans. *Clin Neurophysiol*. 2017;128(2):303-311.
46. Baweja HS, Kennedy DM, Vu J, Vaillancourt DE, Christou EA. Greater amount of visual feedback decreases force variability by reducing force oscillations from 0–1 and 3–7 Hz. *Eur J Appl Physiol*. 2010;108(5):935-943.
47. Slifkin AB, Vaillancourt DE, Newell KM. Intermittency in the control of continuous force production. *J Neurophysiol*. 2000;84(4):1708-1718.
48. Riddle CN, Baker MR, Baker SN. The effect of carbamazepine on human corticomuscular coherence. *NeuroImage*. 2004;22(1):333-340.
49. Matsuya R, Ushiyama J, Ushiba J. Inhibitory interneuron circuits at cortical and spinal levels are associated with individual differences in corticomuscular coherence during isometric voluntary contraction. *Sci Rep*. 2017;7.
50. Williams ER, Baker SN. Renshaw cell recurrent inhibition improves physiological tremor by reducing corticomuscular coupling at 10 Hz. *J Neurosci*. 2009;29(20):6616-6624.
51. Mehrkanoon S, Breakspear M, Boonstra TW. The reorganization of corticomuscular coherence during a transition between sensorimotor states. *NeuroImage*. 2014;100:692-702.
52. Cussons P, Matthews P, Muir R. Enhancement by agonist or antagonist muscle vibration of tremor at the elastically loaded human elbow. *The Journal of physiology*. 1980;302(1):443-461.

53. Budini F, McManus LM, Berchicci M, et al. Alpha band cortico-muscular coherence occurs in healthy individuals during mechanically-induced tremor. *PLoS One*. 2014;9(12):e115012.
54. Hansen S, Hansen N, Christensen L, Petersen N, Nielsen JB. Coupling of antagonistic ankle muscles during co-contraction in humans. *Exp Brain Res*. 2002;146(3):282-292.
55. Witham CL, Riddle CN, Baker MR, Baker SN. Contributions of descending and ascending pathways to corticomuscular coherence in humans. *The Journal of physiology*. 2011;589(15):3789-3800.
56. Liddell EGT, Sherrington CS. Recruitment and some other features of reflex inhibition. *Proceedings of the Royal Society of London Series B, Containing Papers of a Biological Character*. 1925;97(686):488-518.
57. Lloyd DP. Integrative pattern of excitation and inhibition in two-neuron reflex arcs. *J Neurophysiol*. 1946;9(6):439-444.
58. Clark DJ, Ting LH, Zajac FE, Neptune RR, Kautz SA. Merging of healthy motor modules predicts reduced locomotor performance and muscle coordination complexity post-stroke. *J Neurophysiol*. 2010;103(2):844-857.
59. Rodriguez KL, Roemmich RT, Cam B, Fregly BJ, Hass CJ. Persons with Parkinson's disease exhibit decreased neuromuscular complexity during gait. *Clin Neurophysiol*. 2013;124(7):1390-1397.
60. Lawrence JH, De Luca C. Myoelectric signal versus force relationship in different human muscles. *J Appl Physiol*. 1983;54(6):1653-1659.
61. Beck TW, Housh TJ, Johnson GO, et al. Mechanomyographic amplitude and mean power frequency versus torque relationships during isokinetic and isometric muscle actions of the biceps brachii. *J Electromyogr Kinesiol*. 2004;14(5):555-564.
62. Madeleine P, Bajaj P, Søgaard K, Arendt-Nielsen L. Mechanomyography and electromyography force relationships during concentric, isometric and eccentric contractions. *J Electromyogr Kinesiol*. 2001;11(2):113-121.

63. Shinohara M, Sogaard K. Mechanomyography for studying force fluctuations and muscle fatigue. *Exerc Sport Sci Rev.* 2006;34(2):59-64.
64. Salman M, Sabra KG, Shinohara M. Assessment of muscle stiffness using a continuously scanning laser-Doppler vibrometer. *Muscle Nerve.* 2014;50(1):133-135.
65. Shinohara M, Sabra K, Gennisson JL, Fink M, Tanter M. Real-time visualization of muscle stiffness distribution with ultrasound shear wave imaging during muscle contraction. *Muscle Nerve.* 2010;42(3):438-441.
66. Bercoff J, Chaffai S, Tanter M, et al. In vivo breast tumor detection using transient elastography. *Ultrasound Med Biol.* 2003;29(10):1387-1396.
67. Bercoff J, Tanter M, Fink M. Supersonic shear imaging: a new technique for soft tissue elasticity mapping. *IEEE Trans Ultrason, Ferroelect, Freq Control.* 2004;51(4):396-409.
68. Akagi R, Tanaka J, Shikiba T, Takahashi H. Muscle hardness of the triceps brachii before and after a resistance exercise session: A shear wave ultrasound elastography study. *Acta Radiol.* 2015;56(12):1487-1493.
69. Bouillard K, Nordez A, Hug F. Estimation of individual muscle force using elastography. *PLoS One.* 2011;6(12):e29261.
70. Kot BCW, Zhang ZJ, Lee AWC, Leung VYF, Fu SN. Elastic modulus of muscle and tendon with shear wave ultrasound elastography: variations with different technical settings. *PLoS One.* 2012;7(8):e44348.
71. Nordez A, Hug F. Muscle shear elastic modulus measured using supersonic shear imaging is highly related to muscle activity level. *J Appl Physiol.* 2010;108(5):1389-1394.
72. Lacourpaille L, Hug F, Bouillard K, Hogrel J-Y, Nordez A. Supersonic shear imaging provides a reliable measurement of resting muscle shear elastic modulus. *Physiol Meas.* 2012;33(3):N19.

73. Gallagher W, Ding M, Ueda J. Relaxed individual control of skeletal muscle forces via physical human–robot interaction. *Multibody Syst Dyn.* 2013;30(1):77-99.
74. Ueda J, Ming D, Krishnamoorthy V, Shinohara M, Ogasawara T. Individual muscle control using an exoskeleton robot for muscle function testing. *IEEE Trans Neural Syst Rehab Eng.* 2010;18(4):339-350.
75. Bernstein NA. The co-ordination and regulation of movements. 1967.
76. Latash ML. The bliss (not the problem) of motor abundance (not redundancy). *Exp Brain Res.* 2012;217(1):1-5.
77. Maher RM, Hayes DM, Shinohara M. Quantification of dry needling and posture effects on myofascial trigger points using ultrasound shear-wave elastography. *Arch Phys Med Rehabil.* 2013;94(11):2146-2150.
78. Taniguchi K, Shinohara M, Nozaki S, Katayose M. Acute decrease in the stiffness of resting muscle belly due to static stretching. *Scand J Med Sci Sports.* 2015;25(1):32-40.
79. Darby J, Li B, Costen N, Loram I, Hodson-Tole E. Estimating skeletal muscle fascicle curvature from b-mode ultrasound image sequences. *IEEE Trans Biomed Eng.* 2013;60(7):1935-1945.
80. Graf S, Garipey J, Massonneau M, et al. Experimental and clinical validation of arterial diameter waveform and intimal media thickness obtained from B-mode ultrasound image processing. *Ultrasound Med Biol.* 1999;25(9):1353-1363.
81. Loram ID, Maganaris CN, Lakie M. Use of ultrasound to make noninvasive in vivo measurement of continuous changes in human muscle contractile length. *J Appl Physiol.* 2006;100(4):1311-1323.
82. Peng Q, Jones RC, Constantinou CE. 2D Ultrasound image processing in identifying responses of urogenital structures to pelvic floor muscle activity. *Ann Biomed Eng.* 2006;34(3):477-493.

83. Yang M-S, Hu Y-J, Lin KC-R, Lin CC-L. Segmentation techniques for tissue differentiation in MRI of ophthalmology using fuzzy clustering algorithms. *Magn Reson Imaging*. 2002;20(2):173-179.
84. Brosnan T, Sun D-W. Improving quality inspection of food products by computer vision—a review. *J Food Eng*. 2004;61(1):3-16.
85. Du C-J, Sun D-W. Recent developments in the applications of image processing techniques for food quality evaluation. *Trends Food Sci Technol*. 2004;15(5):230-249.
86. Kim N-D, Amin V, Wilson D, Rouse G, Udpa S. Ultrasound image texture analysis for characterizing intramuscular fat content of live beef cattle. *Ultrason Imaging*. 1998;20(3):191-205.
87. Zhou Y, Zheng Y-P. Estimation of muscle fiber orientation in ultrasound images using revolving hough transform (RVHT). *Ultrasound Med Biol*. 2008;34(9):1474-1481.
88. Lapole T, Tindel J, Galy R, Nordez A. Contracting biceps brachii elastic properties can be reliably characterized using supersonic shear imaging. *Eur J Appl Physiol*. 2015;115(3):497-505.
89. Purslow PP. The structure and functional significance of variations in the connective tissue within muscle. *Comp Biochem Physiol, A: Mol Integr Physiol*. 2002;133(4):947-966.
90. Serres S, Milner T. Wrist muscle activation patterns and stiffness associated with stable and unstable mechanical loads. *Exp Brain Res*. 1991;86(2):451-458.
91. Radwin RG, Armstrong TJ, Chaffin DB. Power hand tool vibration effects on grip exertions. *Ergonomics*. 1987;30(5):833-855.
92. Rohmert W, Wos H, Norlander S, Helbig R. Effects of vibration on arm and shoulder muscles in three body postures. *Eur J Appl Physiol Occup Physiol*. 1989;59(4):243-248.

93. Shinohara M, Moritz CT, Pascoe MA, Enoka RM. Prolonged muscle vibration increases stretch reflex amplitude, motor unit discharge rate, and force fluctuations in a hand muscle. *J Appl Physiol*. 2005;99(5):1835-1842.
94. Krishnan C, Allen EJ, Williams GN. Effect of knee position on quadriceps muscle force steadiness and activation strategies. *Muscle Nerve*. 2011;43(4):563-573.
95. Brown M, Engberg I, Matthews P. The relative sensitivity to vibration of muscle receptors of the cat. *The Journal of Physiology*. 1967;192(3):773-800.
96. Burke D, Hagbarth K-E, Löfstedt L, Wallin BG. The responses of human muscle spindle endings to vibration of non-contracting muscles. *The Journal of physiology*. 1976;261(3):673-693.
97. Burke D, Hagbarth K-E, Löfstedt L, Wallin BG. The responses of human muscle spindle endings to vibration during isometric contraction. *The Journal of Physiology*. 1976;261(3):695-711.
98. Dimitriou M. Human muscle spindle sensitivity reflects the balance of activity between antagonistic muscles. *J Neurosci*. 2014;34(41):13644-13655.
99. Nielsen J, Sinkjær T, Toft E, Kagamihara Y. Segmental reflexes and ankle joint stiffness during co-contraction of antagonistic ankle muscles in man. *Exp Brain Res*. 1994;102(2):350-358.
100. Tihanyi TK, Horváth M, Fazekas G, Hortobágyi T, Tihanyi J. One session of whole body vibration increases voluntary muscle strength transiently in patients with stroke. *Clin Rehabil*. 2007;21(9):782-793.
101. van Nes IJ, Latour H, Schils F, Meijer R, van Kuijk A, Geurts AC. Long-term effects of 6-week whole-body vibration on balance recovery and activities of daily living in the postacute phase of stroke. *Stroke*. 2006;37(9):2331-2335.
102. Marconi B, Filippi GM, Koch G, et al. Long-term effects on cortical excitability and motor recovery induced by repeated muscle vibration in chronic stroke patients. *Neurorehab Neural Repair*. 2011;25(1):48-60.

103. Hsiao DN, S-F. Knee muscle isometric strength, voluntary activation and antagonist co-contraction in the first six months after stroke. *Disabil Rehabil.* 2001;23(9):379-386.
104. Hammond M, Fitts S, Kraft G, Nutter P, Trotter M, Robinson L. Co-contraction in the hemiparetic forearm: quantitative EMG evaluation. *Arch Phys Med Rehabil.* 1988;69(5):348-351.
105. Poon DM, Hui-Chan CW. Hyperactive stretch reflexes, co-contraction, and muscle weakness in children with cerebral palsy. *Dev Med Child Neurol.* 2009;51(2):128-135.
106. Katz R, Penicaud A, Rossi A. Reciprocal Ia inhibition between elbow flexors and extensors in the human. *The Journal of physiology.* 1991;437(1):269-286.
107. Yoshitake Y, Shinohara M. Low-frequency component of rectified EMG is temporally correlated with force and instantaneous rate of force fluctuations during steady contractions. *Muscle Nerve.* 2013;47(4):577-584.
108. Moritz CT, Barry BK, Pascoe MA, Enoka RM. Discharge rate variability influences the variation in force fluctuations across the working range of a hand muscle. *J Neurophysiol.* 2005;93(5):2449-2459.
109. Oldfield RC. The assessment and analysis of handedness: the Edinburgh inventory. *Neuropsychologia.* 1971;9(1):97-113.
110. Rickards C, Cody F. Proprioceptive control of wrist movements in Parkinson's disease. Reduced muscle vibration-induced errors. *Brain: a journal of neurology.* 1997;120(6):977-990.
111. Farina D, Negro F, Jiang N. Identification of common synaptic inputs to motor neurons from the rectified electromyogram. *The Journal of physiology.* 2013;591(10):2403-2418.
112. Halliday D, Rosenberg J, Amjad A, Breeze P, Conway B, Farmer S. A framework for the analysis of mixed time series/point process data—theory and application to the study of physiological tremor, single motor unit discharges and electromyograms. *Prog Biophys Mol Biol.* 1995;64(2):237-278.

113. Rosenberg J, Amjad A, Breeze P, Brillinger D, Halliday D. The Fourier approach to the identification of functional coupling between neuronal spike trains. *Prog Biophys Mol Biol.* 1989;53(1):1-31.
114. Baker S, Kilner J, Pinches E, Lemon R. The role of synchrony and oscillations in the motor output. *Exp Brain Res.* 1999;128(1):109-117.
115. Kristeva-Feige R, Fritsch C, Timmer J, Lücking C-H. Effects of attention and precision of exerted force on beta range EEG-EMG synchronization during a maintained motor contraction task. *Clin Neurophysiol.* 2002;113(1):124-131.
116. Masakado Y, Ushiba J, Tsutsumi N, et al. EEG-EMG coherence changes in postural tasks. *Electromyogr Clin Neurophysiol.* 2007;48(1):27-33.
117. Murnaghan CD, Squair JW, Chua R, Inglis JT, Carpenter MG. Cortical contributions to control of posture during unrestricted and restricted stance. *J Neurophysiol.* 2014;111(9):1920-1926.
118. Mustard B, Lee R. Relationship between EMG patterns and kinematic properties for flexion movements at the human wrist. *Exp Brain Res.* 1987;66(2):247-256.
119. Akazawa K, Milner TE, Stein RB. Modulation of reflex EMG and stiffness in response to stretch of human finger muscle. *J Neurophysiol.* 1983;49(1):16-27.
120. Johnson AN, Shinohara M. Corticomuscular coherence with and without additional task in the elderly. *J Appl Physiol.* 2012;112(6):970-981.
121. Baker MR, Baker SN. The effect of diazepam on motor cortical oscillations and corticomuscular coherence studied in man. *The Journal of physiology.* 2003;546(3):931-942.
122. Katz R, Mazzocchio R, Penicaud A, Rossi A. Distribution of recurrent inhibition in the human upper limb. *Acta Physiologica.* 1993;149(2):183-198.
123. Carroll TJ, Baldwin ER, Collins DF. Task dependent gain regulation of spinal circuits projecting to the human flexor carpi radialis. *Exp Brain Res.* 2005;161(3):299-306.

124. Hultborn H, Pierrot-Deseilligny E. Changes in recurrent inhibition during voluntary soleus contractions in man studied by an H-reflex technique. *The Journal of Physiology*. 1979;297(1):229-251.
125. Meunier S, Penicaud A, Pierrot-Deseilligny E, Rossi A. Monosynaptic Ia excitation and recurrent inhibition from quadriceps to ankle flexors and extensors in man. *The Journal of physiology*. 1990;423(1):661-675.
126. Lacquaniti F, Borghese N, Carrozzo M. Transient reversal of the stretch reflex in human arm muscles. *J Neurophysiol*. 1991;66(3):939-954.
127. Lewis GN, MacKinnon CD, Trumbower R, Perreault EJ. Co-contraction modifies the stretch reflex elicited in muscles shortened by a joint perturbation. *Exp Brain Res*. 2010;207(1-2):39-48.
128. Stein R, Oğuztöreli M. Tremor and other oscillations in neuromuscular systems. *Biol Cybern*. 1976;22(3):147-157.
129. Baudry S, Enoka RM. Influence of load type on presynaptic modulation of Ia afferent input onto two synergist muscles. *Exp Brain Res*. 2009;199(1):83-88.
130. Ushiyama J, Suzuki T, Masakado Y, et al. Between-subject variance in the magnitude of corticomuscular coherence during tonic isometric contraction of the tibialis anterior muscle in healthy young adults. *J Neurophysiol*. 2011;106(3):1379-1388.
131. Fang Y, Daly JJ, Sun J, et al. Functional corticomuscular connection during reaching is weakened following stroke. *Clin Neurophysiol*. 2009;120(5):994-1002.
132. Tecchio F, Melgari J, Zappasodi F, et al. Sensorimotor integration in focal task-specific hand dystonia: a magnetoencephalographic assessment. *Neuroscience*. 2008;154(2):563-571.
133. Lai M-I, Pan L-L, Kao C-L, Tsai M-W, Wei S-H, Chou L-W. The Effects of Neuromuscular Electrical Stimulation on Corticomuscular Coherence in Patients with Stroke. In: *Replace, Repair, Restore, Relieve—Bridging Clinical and Engineering Solutions in Neurorehabilitation*. Springer; 2014:493-500.